



Libraries and Learning Services

# University of Auckland Research Repository, ResearchSpace

## Copyright Statement

The digital copy of this thesis is protected by the Copyright Act 1994 (New Zealand).

This thesis may be consulted by you, provided you comply with the provisions of the Act and the following conditions of use:

- Any use you make of these documents or images must be for research or private study purposes only, and you may not make them available to any other person.
- Authors control the copyright of their thesis. You will recognize the author's right to be identified as the author of this thesis, and due acknowledgement will be made to the author where appropriate.
- You will obtain the author's permission before publishing any material from their thesis.

## General copyright and disclaimer

In addition to the above conditions, authors give their consent for the digital copy of their work to be used subject to the conditions specified on the [Library Thesis Consent Form](#) and [Deposit Licence](#).



THE UNIVERSITY OF AUCKLAND

# Capacitive Power Transfer with Advanced Compensation and Power Flow Control

---

*By*

**Liang Huang**

*A thesis submitted in partial fulfilment of the requirements*

*for the degree of*

***Doctor of Philosophy in Engineering***

*Department of Electrical and Computer Engineering,*

*The University of Auckland*

*October 2016*



## **Abstract**

In the past few decades, wireless/contactless power transfer technologies have become increasingly popular owing to their capability to deliver power to movable loads without direct electrical contacts between the primary transmitter and secondary pickups. Inductive Power Transfer (IPT) technology has been the most successful wireless power transfer solution, which has been commercialized in many domestic, industrial, and biomedical applications. However, because IPT is based on magnetic field coupling, it is unable to transfer power through metal barriers. In addition, the ferrite materials commonly used in IPT systems increase the system cost and size. Recently, Capacitive Power Transfer (CPT) has been proposed as an alternative wireless power transfer technology based on electric field coupling, which has the potential to transfer power through metal barriers, as well as other advantageous features such as low EMI and small volume. Some fundamental research on the CPT system has been conducted for understanding its working principle and improving its performance, but more advanced compensation and control methods are necessary to enhance its power transfer performance.

In this thesis, a general circuit model is developed to characterize the capacitive coupling interface of CPT with cross coupling. The model consists of an input capacitor, an output capacitor, and an ideal transformer with a turns ratio, which can be used to significantly simplify the design process of CPT systems. Furthermore, based on the charge balance principle, a new term named capacitive coupling coefficient has been defined to quantify the mutual coupling between the primary and secondary coupling plates. The proposed model and the defined term are based on rigorous mathematical derivation and also validated by experimental results.

Another significant contribution of this research is a development of a Z-impedance compensation network to cancel out the capacitive reactance of the capacitive coupling interface. The new compensation network can eliminate high voltage spikes suffered by conventional CPT systems with series inductor compensation when the secondary side plates are suddenly moved away. It also brings advantages such as short-circuit immunity and voltage boost capability. Based on thorough comparative study on three typical soft

switching converters, a half bridge resonant converter is selected to drive a practical CPT system with the proposed Z impedance compensation network. Simulations and practical results have demonstrated the Z-impedance network can effectively compensate for the effective reactance of the capacitive coupling interface with short-circuit and open-circuit immunity.

To achieve a controllable output power, a new power flow control method by switching the shunt capacitors of a CPT system is proposed. The system is designed to operate in a new sub-optimum mode of Class E converter, which is able to maintain soft-switching condition while controlling the output power according to the load requirements. Simulations and experimental results have indicated that the proposed control method can control the output power of CPT system with zero-voltage switching (ZVS) condition guaranteed.

## Acknowledgements

I would like to thank many people during my Ph.D. program. They have given so much unselfish help and valuable suggestions to enable me to finish this research. Without their help and company, the program would be a much harder and lonelier journey to me.

First and foremost, I would like to thank Dr. Aiguo Patrick Hu for offering me the opportunity to enter into the world of power electronics and for introducing me into a new and interesting field of Capacitive Power Transfer (CPT). He has given great guidance over the course of my study. His optimistic attitude and inspiring discussions have always been very helpful and supportive.

Next, I would also like to thank Dr. Akshya Kumar Swain for his great patience and kind help for reading my paper drafts and suggestions for my research.

Thirdly, I would like to express my gratitude to the University of Auckland and China Scholarship Council for offering me the doctoral scholarship to provide the financial support for my study.

In addition, I would like to express my many thanks to Mr. Howard Lu for his laboratory assistance. I am also very grateful to my friends and colleagues including Dr. Bob Wang, Dr. Chao Liu, Mr. Yuan Song, Ms. Yuan Liu, Mr. Zhenmin Li, Mr. Wentao Li, Mr. Xin Fan, Mr. Saranga Weerasinghe, Ms. Dulsha Abeywardana, Mr. Jianlong Tian, and other peers for their companionship and various help.

Last but not least, I would like to express my sincere gratitude to my parents, sisters, and brothers-in-law for their continuous support and understanding. Without their mental support and encouragement, the accomplishment of this program would be impossible.

Liang Huang

28 March 2016 Auckland

# Table of Contents

<i>Abstract</i> .....	<i>i</i>
<i>Acknowledgements</i> .....	<i>iii</i>
<i>Table of Contents</i> .....	<i>iv</i>
<i>Nomenclature</i> .....	<i>vii</i>
<i>List of Figures</i> .....	<i>xi</i>
<i>List of Tables</i> .....	<i>xvi</i>
<b>1 Introduction</b> .....	<b>1</b>
<b>1.1 Background of Wireless Power Transfer</b> .....	<b>1</b>
<b>1.2 Fundamentals of Capacitive Power Transfer (CPT)</b> .....	<b>3</b>
1.2.1 Basic Configuration and Operating Principle of CPT .....	5
1.2.2 Features .....	6
1.2.3 CPT Applications.....	9
<b>1.3 Challenges of CPT</b> .....	<b>14</b>
<b>1.4 Objectives and Scope of the Thesis</b> .....	<b>16</b>
<b>2 Literature Review of Compensation and Control Methods for CPT Systems</b> .....	<b>18</b>
<b>2.1 Introduction</b> .....	<b>18</b>
<b>2.2 Existing Compensation Methods for CPT</b> .....	<b>19</b>
2.2.1 Capacitive Coupling Interface .....	19
2.2.2 Series Inductor Tuning.....	24
2.2.3 High Order Compensation Methods .....	26
2.2.4 Active Compensation Methods.....	29
<b>2.3 Power Flow Control Methods</b> .....	<b>34</b>
2.3.1 Voltage Regulator .....	35
2.3.2 Modified Rectifier with Integrated Controller .....	36

2.3.3	Soft-switched Transformer.....	38
2.3.4	Multi-period Pulse-width Modulation.....	41
2.4	Summary.....	42
3	<b><i>Study of Soft-switching Resonant Power Converters for CPT Systems</i></b> .....	<b>44</b>
3.1	<b>Introduction.....</b>	<b>44</b>
3.2	<b>Autonomous Current-fed Push-pull Converter .....</b>	<b>45</b>
3.2.1	Circuit Description .....	45
3.2.2	Analysis of Operation .....	46
3.3	<b>Single-ended Class E Power Converters.....</b>	<b>48</b>
3.3.1	Circuit Description .....	48
3.3.2	Analysis of Operation .....	49
3.4	<b>Voltage-fed Half Bridge Converter .....</b>	<b>54</b>
3.4.1	Circuit Description .....	54
3.4.2	Analysis of Operation .....	55
3.5	<b>Comparison of the Three Resonant Converters.....</b>	<b>58</b>
3.5.1	Circuit Components .....	58
3.5.2	Effects of Coupling Capacitance.....	59
3.5.3	Control Schemes .....	61
3.6	<b>Summary.....</b>	<b>61</b>
4	<b><i>Modelling the Capacitive Coupling Interface.....</i></b>	<b>62</b>
4.1	<b>Introduction.....</b>	<b>62</b>
4.2	<b>Model Based on An Ideal Transformer .....</b>	<b>64</b>
4.2.1	Effects of Misalignment.....	67
4.2.2	Series Tuning Inductor Analysis .....	72
4.2.3	Simulations and Experimental Results.....	81
4.3	<b>Dynamic Model with State-space Description.....</b>	<b>85</b>



4.4	Defining the Mutual Coupling Coefficient.....	88
4.5	Summary.....	93
5	<i>High Order Compensation Networks for CPT</i> .....	96
5.1	Introduction.....	96
5.2	Proposed Z-Impedance Compensation Network for CPT .....	98
5.2.1	Modelling the Z-impedance Network.....	99
5.2.2	Simulations and Experimental Results .....	108
5.3	Modified Class E topology with Load Compensation.....	117
5.3.1	Modified Class E Topology and State-space modelling.....	117
5.3.2	Design of Load Transformation Network.....	121
5.3.3	Experimental results.....	122
5.4	Summary.....	125
6	<i>Power Flow Control of CPT Using Switched Capacitors</i> .....	127
6.1	Introduction.....	127
6.2	New Suboptimum Operation of Class E Converter .....	128
6.3	Power Flow Control Analysis.....	131
6.4	Simulations and Experimental Study.....	134
6.5	Summary.....	138
7	<i>Conclusions and Suggestions for Future Work</i> .....	139
7.1	General Conclusions .....	139
7.2	Publications from This Research.....	142
7.3	Suggestions for Future Work.....	143
	<i>Appendix</i> .....	145
	<i>References</i> .....	146

## Nomenclature

### Acronym

AC	-	Alternative current
AET	-	Acoustic energy transfer
CCM	-	Continuous conduction mode
CPT	-	Capacitive power transfer
DC	-	Direct current
DCM	-	Discontinuous current mode
DUT	-	Device under test
EMC	-	Electromagnetic compatibility
EMI	-	Electromagnetic interference
ESR	-	Equivalent series resistance
EV	-	Electric vehicle
GaN	-	Gallium nitride
IGBT	-	Insulated gate bipolar transistor
IPT	-	Inductive power transfer
KCL	-	Kirchhoff's Current Law
KVL	-	Kirchhoff's Voltage Law
LC	-	Inductor-capacitor connection
LCC	-	Inductor-capacitor-capacitor connection
LCL	-	Inductor-capacitor-inductor connection
LLC	-	Inductor-inductor-capacitor connection
MOSFET	-	Metal oxide silicon field effect transistor
PCB	-	Printed circuit board
PM	-	permanent magnet electric machine
PWM	-	Pulse-width modulation
Q	-	Quality factor
RF	-	Radio frequency
SiC	-	Silicon carbide
SMT	-	Surface mounting technology

ZCS	-	Zero current switching
ZVS	-	Zero voltage switching
VCO	-	Voltage controlled oscillator
WFSM	-	Wound field synchronous machine
2-D	-	Two dimensional
3-D	-	Three dimensional

### **Symbols**

$A$	-	Effective overlapping area between two plates
$C_C$	-	Equivalent capacitance of the capacitive coupling interface
$C_1$	-	Capacitor of the resonant tank N1
$C_1$	-	Shunt capacitor of Class E converter
$C_2$	-	Capacitor of the resonant tank N2
$C_{AB}$	-	Cross capacitance between primary side plates
$C_{Aa}$	-	Cross capacitance between primary side and secondary side plate
$C_{Ab}$	-	Cross capacitance between primary side and secondary side plate
$C_{Ba}$	-	Cross capacitance between primary side and secondary side plate
$C_{Bb}$	-	Cross capacitance between primary side and secondary side plate
$C_{ab}$	-	Cross capacitance between secondary side plate
$C_f$	-	Output filter capacitor
$C_Z$	-	Capacitor of the Z-impedance network
$d$	-	Distance between two plates
$d_{air}$	-	Distance of air gap
$d_d$	-	Thickness of the coating dielectric material
$f$	-	Operating frequency
$I_g$	-	DC input current
$I_L$	-	DC load current
$i_R$	-	Load tank current
$L_P$	-	Primary series tuning inductor

$L_S$	-	Secondary series tuning inductor
$L_1$	-	Inductor of the resonant tank N1
$L_2$	-	Inductor of the resonant tank N2
$L_C$	-	Equivalent controllable inductor
$L_{fa}$	-	Part of inductance to fully compensate for the coupling Capacitor
$L_{fb}$	-	Remaining inductance
$L_r$	-	Inductor of the resonant tank
$L_{mag}$	-	Magnetizing inductance
$L_Z$	-	Inductor of the Z-impedance network
$n$	-	Number of the negative capacitors
$n_1$	-	Turns ratio of the primary side transformer
$N_1$	-	Primary side resonant tank
$n_2$	-	Turns ratio of the secondary side transformer
$N_2$	-	Secondary side resonant tank
$P_{IN}$	-	Input power
$P_O$	-	Output power
$P_{OUT}$	-	Output power
$Q_L$	-	Quality factor of the load tank
$Q_S$	-	Quality factor of the series tank
$Q_2$	-	Quality factor of the tank N2
$R_{esr}$	-	Equivalent series resistance
$R$	-	Equivalent load resistance
$R_L$	-	Load resistance
$R_O$	-	Load resistance
$T$	-	Switching period
$t_{off}$	-	OFF time of switches
$\omega$	-	Angular switching frequency
$v_S$	-	Voltage at the switching node
$v_{sp}$	-	Peak value of the voltage at the switching node
$v_{ds}$	-	Voltage across the switch
$V_C$	-	Voltage across the coupling plates

$V_g$	-	DC input voltage
$V_O$	-	DC output voltage
$V_{O,max}$	-	Maximum output voltage
$V_{s1}$	-	Fundamental component of the output voltage of the inverter
$v_R$	-	Load voltage
$X_C$	-	Reactance of the coupling plates
$Z_L$	-	Impedance reflected to the primary side
$Z_{in}$	-	Input impedance seen by the inverter
$\epsilon_0$	-	Permittivity in vacuum
$\epsilon_r$	-	Dielectric constant
$\varphi$	-	Phase shift of the tank current

## List of Figures

Fig. 1-1: The diagram of set-up of wireless power transfer in 1921 [26].	2
Fig. 1-2: A typical IPT system.	3
Fig. 1-3: Basic configuration of a typical CPT system.	5
Fig. 1-4: (a) An IPT system and (b) a CPT system with a metal barrier existing in the coupling part.	6
Fig. 1-5: Equivalent circuit of the capacitive coupling when a metal slab is inserted in between.	8
Fig. 1-6: Illustration of capacitive charging and communication in 3D integrated circuit [33].	10
Fig. 1-7: Block diagram of biosignal instrumentation electronics using capacitive coupling.	11
Fig. 1-8: Capacitive charging docks from Murata [48].	11
Fig. 1-9: Powering the rotor using capacitive power transfer [37].	13
Fig. 1-10: A CPT EV charging system using aluminium foil as coupling plates [53].	14
Fig. 2-1 Possible configurations of the capacitive coupling interface.	19
Fig. 2-2: Photograph of the coupling plates structure based on aerodynamic fluid bearings [58].	20
Fig. 2-3: Coupling plates coated with dielectric material.	21
Fig. 2-4: Cross coupling in the capacitive coupling interface.	23
Fig. 2-5: A CPT system with series inductor tuning.	24
Fig. 2-6 Equivalent circuit of CPT with series inductor tuning	25
Fig. 2-7: Basic blocks of high order compensation network for CPT systems.	26
Fig. 2-8: Using transformers for transformation.	26
Fig. 2-9: Using L-C resonant tanks for transformation.	28
Fig. 2-10: Using a negative capacitor for compensation in a CPT system.	30
Fig. 2-11: Typical waveforms of a CPT system in DCM without compensation.	31

Fig. 2-12: Typical waveforms of a CPT system in DCM compensated by a negative capacitor. ....	33
Fig. 2-13: Secondary side of a CPT system with a voltage regulator. ....	35
Fig. 2-14: CPT system with integrated voltage rectification and power flow control. ....	36
Fig. 2-15: The output voltage waveform under the control of the modified rectifier. ....	37
Fig. 2-16: Output power versus frequency. ....	38
Fig. 2-17: The CPT system using soft-switched transformer control. ....	39
Fig. 2-18: The CPT system using soft-switched transformer control. ....	39
Fig. 2-19: The current waveforms of the soft-switched transformer. ....	40
Fig. 2-20: The normalized inductance $L_C/L_{mag}$ versus $\theta$ . ....	41
Fig. 2-21: The CPT system with multi-period pulse width modulation. ....	42
Fig. 3-1: Schematic diagram of a CPT system based on an autonomous current-fed push-pull converter. ....	45
Fig. 3-2: Selected voltage and current waveforms in the autonomous current-fed push-pull converter. ....	46
Fig. 3-3: Block diagram of single-ended power amplifier. ....	48
Fig. 3-4: Basic configuration of a CPT system based on a class E converter. ....	49
Fig. 3-5: Waveforms of $i_1(t)$ and $i_R(t)$ . ....	50
Fig. 3-6: A CPT system based on a half-bridge converter. ....	55
Fig. 3-7: The output power versus coupling capacitance for the three topologies. ....	60
Fig. 3-8: The efficiency versus coupling capacitance for the three topologies. ....	60
Fig. 4-1: (a) Well-aligned coupling plates, (b) Misaligned coupling plates ....	63
Fig. 4-2: Two scenarios of the capacitive coupling interface ....	64
Fig. 4-3: Redrawn diagram of the capacitive coupling interface with cross coupling ....	65
Fig. 4-4: The circuit model based on circuit transformation ....	67
Fig. 4-5: Misalignment of coupling plates ....	67
Fig. 4-6: Normalized turns ratio $n_E$ in relation to misalignment. ....	69

Fig. 4-7: Normalized input capacitance $C_{IN}/C_C$ versus misalignment .....	70
Fig. 4-8: Normalized output capacitance $C_{OUT}/C_C$ versus misalignment.....	71
Fig. 4-9: Primary side tuning .....	73
Fig. 4-10: Impedance transformation of primary side tuning .....	74
Fig. 4-11: Normalized primary side tuning inductance $L_P/(1/(\omega^2 C_C/2))$ versus misalignment .....	75
Fig. 4-12: Normalized output power at resonance for primary side tuning versus misalignment. ....	78
Fig. 4-13: Normalized output power $P_{O1}/(v_{IN,peak}^2/(2R))$ versus misalignment when $R_{Lp}/R=0.2$ , (a) $0<\alpha, \beta<0.4$ , (b) $0<\alpha, \beta<1$ . ....	78
Fig. 4-14: Secondary side tuning .....	79
Fig. 4-15: Impedance transformation of secondary side tuning.....	79
Fig. 4-16: The Prototype CPT system for cross coupling comparison. ....	81
Fig. 4-17: Experimental and simulated data plots of input voltage $v_{IN}$ and input current $i_L$ of CPT1. ....	82
Fig. 4-18: Experimental and simulated data plots of input voltage $v_{IN}$ and input current $i_L$ of CPT2. ....	83
Fig. 4-19: Experimental data plots of the normalized output power $P_{O1}/(v_{IN,peak}^2/(2R))$ versus misalignment ( $v_{IN,peak}^2/(2R) = 2 \text{ W}$ ). ....	84
Fig. 4-20: Output power versus load $R$ . ....	84
Fig. 4-21: An equivalent circuit of a CPT system with cross coupling. ....	85
Fig. 4-22: Capacitive coupling interface with cross coupling.....	89
Fig. 4-23: A dual model of the capacitive coupling interface. ....	90
Fig. 4-24: An equivalent model of the secondary side.....	91
Fig. 5-1: Demonstration of the sudden removal of the load in a CPT system. ....	97
Fig. 5-2: Proposed CPT system with LCC and Z-impedance compensation network.....	98
Fig. 5-3: Simplified circuit diagram of the CPT system with Z-impedance network.....	100
Fig. 5-4: The g-parameter description of the Z-impedance network. ....	100
Fig. 5-5: The equivalent circuit model of the Z-impedance network. ....	102



Fig. 5-6: Turns ratio $n_Z$ and normalized inductance $L_{eq}/L_Z (=C_{eq}/C_Z)$ versus $F$ .....	103
Fig. 5-7: The variations of turns ratio $n_Z$ and $C_Z/C_C$ versus $L_Z/(1/(\omega_s^2 C_C))$ .....	104
Fig. 5-8: Equivalent circuit of the proposed CPT system. ....	105
Fig. 5-9: The simplified circuit model of the proposed CPT system by reflecting components to the primary side through the ideal transformer. ....	106
Fig. 5-10: Normalized equivalent input capacitance $C_{eq}/C_C$ versus $L_Z/(1/(\omega_s^2 C_C))$ . ....	106
Fig. 5-11: Prototype of the proposed CPT system. ....	109
Fig. 5-12: Simulated waveforms of the output voltage of the inverter and the current into the LCC tank. ....	110
Fig. 5-13: Simulated waveforms of the input voltage of Z-impedance network and the current into it. ....	111
Fig. 5-14: Simulated waveforms of the input voltage of Z-impedance network $v_Z$ and the secondary side voltage. ....	111
Fig. 5-15: Simulated transient response of the voltage across the primary plates and the current through $L_f$ after the sudden shorting of the secondary plates. ....	112
Fig. 5-16: Simulated transient responses of the voltage across the primary plates after the sudden removal of secondary plates of the CPT system with (a) the single series inductor compensation and (b) the proposed Z-impedance compensation. ....	112
Fig. 5-17: Experimental waveforms of the output voltage of the inverter and the current into the LCC tank. ....	114
Fig. 5-18: Experimental waveforms of the input voltage of Z-impedance network and the current $i_Z$ into it with (a) 50 $\Omega$ AC load and (b) 50 $\Omega$ DC load. ....	114
Fig. 5-19: Experimental waveforms of the input voltage of Z-impedance network $v_Z$ and the secondary side voltage $n_Z v_Z$ . ....	115
Fig. 5-20: Transient response of the voltage across the primary plates and the current through $L_f$ after the sudden shorting of the secondary plates. ....	115
Fig. 5-21: Transient responses of the voltage across the primary plates after the sudden removal of secondary plates of the CPT system with (a) the single series inductor compensation and (b) the proposed Z-impedance compensation. ....	116
Fig. 5-22: Power distribution of the system. ....	116
Fig. 5-23: A CPT system based on a modified class E topology. ....	117
Fig. 5-24: Equivalent circuit of the proposed CPT system. ....	118

Fig. 5-25: Equivalent circuit when $S_1$ turns on. ....	118
Fig. 5-26: Equivalent circuit when $S_1$ turns off.....	120
Fig. 5-27: The equivalent circuit of the tank with $L_2$ represented by two split inductors $L_{2a}$ and $L_{2b}$ . ....	121
Fig. 5-28: Prototype of the proposed CPT system with load transformation.....	124
Fig. 5-29: The voltage across the switch and gate drive signal demonstrating ZVS. ....	124
Fig. 5-30: The currents through the capacitive coupling interface and the load.....	125
Fig. 6-1: Redrawn diagram of the CPT system based on Class E topology. ....	129
Fig. 6-2: Waveforms of the voltage $v_{C1}$ across the switch with different values of $C_1$ .....	130
Fig. 6-3: Waveforms of $i_1(t)$ , $i_R(t)$ , and $v_{C1}(t)$ .....	132
Fig. 6-4: The equivalent circuit of Class E converter using current pulse approximation. ....	133
Fig. 6-5: Controlling shunt capacitance with switches. ....	134
Fig. 6-6: Waveforms in the CPT in sub-optimum mode: the blue line is the voltage across the switch $v_{C1}$ , the red line is the gate drive signal, and the green line is tank current $i_R(t)$ . ....	136
Fig. 6-7: Output power with different shunt capacitances ranging from 50 pF to 250 pF in simulation. ....	136
Fig. 6-8: The voltage across the switch $v_{C1}(t)$ for different shunt capacitance ranging from 50 pF to 250 pF. ....	137
Fig. 6-9: Experimental waveform when CPT system works in sub-optimum mode. The yellow line is $v_{C1}(t)$ , the green line is gate signal, the blue line is the tank current, and the pink line is the output voltage. ....	137
Fig. 6-10: Experimental waveform when the shunt capacitance was increased to 220 pF. The yellow line is $v_{C1}(t)$ , the green line is gate signal, the blue line is the tank current, and the pink line is the output voltage. ....	138

## **List of Tables**

Table 1-1 Wireless Power Transfer Techniques .....	4
Table 3-1: Key component number for three topologies .....	58
Table 3-2: CPT system specifications.....	59
Table 3-3: Parameters of three topologies .....	59
Table 4-1: CPT system specification. ....	82
Table 4-2: Comparison between two CPT systems .....	93
Table 5-1: System parameters for CPT with Z impedance.....	109
Table 5-2: System parameters of CPT with load transformation .....	123
Table 6-1: System parameters of sub-optimum Class E.....	135

## Co-Authorship Form

Graduate Centre  
The ClockTower – East Wing  
22 Princes Street, Auckland  
Phone: +64 9 373 7599 ext 81321  
Fax: +64 9 373 7610  
Email: [postgraduate@auckland.ac.nz](mailto:postgraduate@auckland.ac.nz)  
[www.postgrad.auckland.ac.nz](http://www.postgrad.auckland.ac.nz)

This form is to accompany the submission of any PhD that contains published or unpublished co-authored work. **Please include one copy of this form for each co-authored work.** Completed forms should be included in all copies of your thesis submitted for examination and library deposit (including digital deposit), following your thesis Acknowledgements. Co-authored works may be included in a thesis if the candidate has written all or the majority of the text and had their contribution confirmed by all co-authors as not less than 65%.

Please indicate the chapter/section/pages of this thesis that are extracted from a co-authored work and give the title and publication details or details of submission of the co-authored work.

Chapter 5

Liang Huang, Aiguo Patrick Hu, Akshya K. Swain and Yugang Su. Z Impedance Compensation for Wireless Power Transfer Based on Electric Field Coupling, IEEE Trans on Power Electronics

Nature of contribution  
by PhD candidate

Majority of the work

Extent of contribution  
by PhD candidate (%)

90

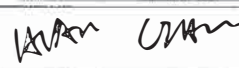



### CO-AUTHORS

Name	Nature of Contribution
Liang Huang	Majority of the work
Patrick Hu	Help with the idea and proofreading
Akshya Swain	Help with the idea and proofreading
Yugang Su	Help with the idea and proofreading

### Certification by Co-Authors

The undersigned hereby certify that:

- ❖ the above statement correctly reflects the nature and extent of the PhD candidate's contribution to this work, and the nature of the contribution of each of the co-authors; and
- ❖ that the candidate wrote all or the majority of the text.

Name	Signature	Date
Liang Huang		31/03/2016
Patrick Hu		31/03/16
Akshya Swain		31/3/2016
Yugang Su		31/03/2016

00 APR 2016

# Co-Authorship Form

Graduate Centre  
 The ClockTower – East Wing  
 22 Princes Street, Auckland  
 Phone: +64 9 373 7599 ext 81321  
 Fax: +64 9 373 7610  
 Email: [postgraduate@auckland.ac.nz](mailto:postgraduate@auckland.ac.nz)  
[www.postgrad.auckland.ac.nz](http://www.postgrad.auckland.ac.nz)

This form is to accompany the submission of any PhD that contains published or unpublished co-authored work. **Please include one copy of this form for each co-authored work.** Completed forms should be included in all copies of your thesis submitted for examination and library deposit (including digital deposit), following your thesis Acknowledgements. Co-authored works may be included in a thesis if the candidate has written all or the majority of the text and had their contribution confirmed by all co-authors as not less than 65%.

Please indicate the chapter/section/pages of this thesis that are extracted from a co-authored work and give the title and publication details or details of submission of the co-authored work.

Chapter 4

Liang Huang, Aiguo Patrick Hu, Akshya K. Swain and Yugang Su. Accurate steady-state modeling of capacitive-coupling interface of capacitive power transfer systems with cross-coupling. Wireless Power Transfer, available on CJO2016. doi:10.1017/wpt.2016.2.

Nature of contribution  
by PhD candidate

Majority of the text

Extent of contribution  
by PhD candidate (%)

90

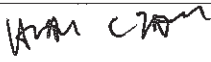
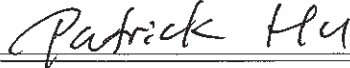



## CO-AUTHORS

Name	Nature of Contribution
Liang Huang	Majority of the work
Patrick Hu	Help with the idea and proofreading
Akshya Swain	Help with the idea and proofreading
Yugang Su	Help with the idea and proofreading

## Certification by Co-Authors

The undersigned hereby certify that:

- ❖ the above statement correctly reflects the nature and extent of the PhD candidate's contribution to this work, and the nature of the contribution of each of the co-authors; and
- ❖ that the candidate wrote all or the majority of the text.

Name	Signature	Date
Liang Huang		31/03/2016
		31/03/16
AKshya Swain		31/3/2016
Yugang Su		31/03/2016

## Co-Authorship Form

Graduate Centre  
 The ClockTower – East Wing  
 22 Princes Street, Auckland  
 Phone: +64 9 373 7599 ext 81321  
 Fax: +64 9 373 7610  
 Email: postgraduate@auckland.ac.nz  
 www.postgrad.auckland.ac.nz

This form is to accompany the submission of any PhD that contains published or unpublished co-authored work. **Please include one copy of this form for each co-authored work.** Completed forms should be included in all copies of your thesis submitted for examination and library deposit (including digital deposit), following your thesis Acknowledgements. Co-authored works may be included in a thesis if the candidate has written all or the majority of the text and had their contribution confirmed by all co-authors as not less than 65%.

Please indicate the chapter/section/pages of this thesis that are extracted from a co-authored work and give the title and publication details or details of submission of the co-authored work.

Chapter 4

L. Huang and A. P. Hu, "Defining the mutual coupling of capacitive power transfer for wireless power transfer," Electronics Letters, vol. 51, pp. 1806-1807, 2015.

Nature of contribution  
by PhD candidate

Majority of the text

Extent of contribution  
by PhD candidate (%)

90

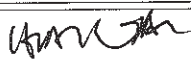

### CO-AUTHORS

Name	Nature of Contribution
Liang Huang	Majority of the text
Patrick Hu	Help with the idea and proofreading

### Certification by Co-Authors

The undersigned hereby certify that:

- ❖ the above statement correctly reflects the nature and extent of the PhD candidate's contribution to this work, and the nature of the contribution of each of the co-authors; and
- ❖ that the candidate wrote all or the majority of the text.

Name	Signature	Date
Liang Huang		31/03/2016
Patrick Hu		31/03/16



03 APR 2016

**Co-Authorship Form**

Graduate Centre  
 The ClockTower – East Wing  
 22 Princes Street, Auckland  
 Phone: +64 9 373 7599 ext 81321  
 Fax: +64 9 373 7610  
 Email: postgraduate@auckland.ac.nz  
 www.postgrad.auckland.ac.nz

This form is to accompany the submission of any PhD that contains published or unpublished co-authored work. **Please include one copy of this form for each co-authored work.** Completed forms should be included in all copies of your thesis submitted for examination and library deposit (including digital deposit), following your thesis Acknowledgements. Co-authored works may be included in a thesis if the candidate has written all or the majority of the text and had their contribution confirmed by all co-authors as not less than 65%.

Please indicate the chapter/section/pages of this thesis that are extracted from a co-authored work and give the title and publication details or details of submission of the co-authored work.

Chapter 3

L. Huang, A. P. Hu, and A. Swain, "A resonant compensation method for improving the performance of capacitively coupled power transfer system," in Energy Conversion Congress and Exposition (ECCE), 2014 IEEE, 2014, pp. 870-875.

Nature of contribution  
by PhD candidate

Majority of the text

Extent of contribution  
by PhD candidate (%)

90

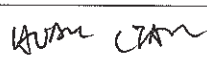


**CO-AUTHORS**

Name	Nature of Contribution
Liang Huang	Majority of the text
Patrick Hu	Help with the idea and proofreading
Akshya Swain	Help with the idea and proofreading

**Certification by Co-Authors**

The undersigned hereby certify that:

- ❖ the above statement correctly reflects the nature and extent of the PhD candidate's contribution to this work, and the nature of the contribution of each of the co-authors; and
- ❖ that the candidate wrote all or the majority of the text.

Name	Signature	Date
Liang Huang		31/03/2016
Patrick Hu		31/03/2016
AKshya Swain		31/03/2016

# Co-Authorship Form

Graduate Centre  
 The ClockTower – East Wing  
 22 Princes Street, Auckland  
 Phone: +64 9 373 7599 ext 81321  
 Fax: +64 9 373 7610  
 Email: postgraduate@auckland.ac.nz  
 www.postgrad.auckland.ac.nz

This form is to accompany the submission of any PhD that contains published or unpublished co-authored work. **Please include one copy of this form for each co-authored work.** Completed forms should be included in all copies of your thesis submitted for examination and library deposit (including digital deposit), following your thesis Acknowledgements. Co-authored works may be included in a thesis if the candidate has written all or the majority of the text and had their contribution confirmed by all co-authors as not less than 65%.

Please indicate the chapter/section/pages of this thesis that are extracted from a co-authored work and give the title and publication details or details of submission of the co-authored work.

Chapter 3

L. Huang, A. P. Hu, A. Swain, and D. Xin, "Comparison of two high frequency converters for capacitive power transfer," in Energy Conversion Congress and Exposition (ECCE), 2014 IEEE, 2014, pp. 5437-5443.

Nature of contribution  
by PhD candidate

Majority of the text

Extent of contribution  
by PhD candidate (%)

90

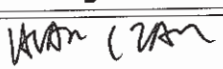
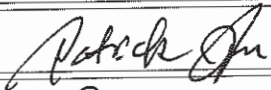
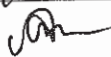

## CO-AUTHORS

Name	Nature of Contribution
Liang Huang	Majority of the text
Patrick Hu	Help with the idea and proofreading
Akshya Swain	Help with the idea and proofreading
Xin Dai	Help with the idea and proofreading

## Certification by Co-Authors

The undersigned hereby certify that:

- ❖ the above statement correctly reflects the nature and extent of the PhD candidate's contribution to this work, and the nature of the contribution of each of the co-authors; and
- ❖ that the candidate wrote all or the majority of the text.

Name	Signature	Date
Liang Huang		31/03/2016
Patrick Hu		31/03/16
Akshya Swain		31/03/2016
Xin Dai		31/03/2016



## Co-Authorship Form

Graduate Centre  
The ClockTower – East Wing  
22 Princes Street, Auckland  
Phone: +64 9 373 7599 ext 81321  
Fax: +64 9 373 7610  
Email: [postgraduate@auckland.ac.nz](mailto:postgraduate@auckland.ac.nz)  
[www.postgrad.auckland.ac.nz](http://www.postgrad.auckland.ac.nz)

This form is to accompany the submission of any PhD that contains published or unpublished co-authored work. **Please include one copy of this form for each co-authored work.** Completed forms should be included in all copies of your thesis submitted for examination and library deposit (including digital deposit), following your thesis Acknowledgements. Co-authored works may be included in a thesis if the candidate has written all or the majority of the text and had their contribution confirmed by all co-authors as not less than 65%.

Please indicate the chapter/section/pages of this thesis that are extracted from a co-authored work and give the title and publication details or details of submission of the co-authored work.

Chapter 1 Introduction

Publication: L. Huang, A. P. Hu, A. Swain, S. Kim, and Y. Ren, "An overview of capacitively coupled power transfer: A new contactless power transfer solution," in Industrial Electronics and Applications (ICIEA), 2013 8th IEEE Conference on, 2013, pp. 461-465.

Nature of contribution by PhD candidate	Majority of the text
---	----------------------

Extent of contribution by PhD candidate (%)	90
---	----

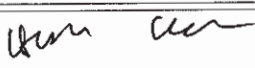



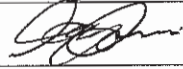
### CO-AUTHORS

Name	Nature of Contribution
Liang Huang	Majority of the text
Patrick Hu	Help with the idea and proofreading
Akshya Swain	Help with the idea and proofreading
Seho Kim	The diagram of the smartphone charging
Yijun Ren	The diagram of the smartphone charging

### Certification by Co-Authors

The undersigned hereby certify that:

- ❖ the above statement correctly reflects the nature and extent of the PhD candidate's contribution to this work, and the nature of the contribution of each of the co-authors; and
- ❖ that the candidate wrote all or the majority of the text.

Name	Signature	Date
Liang Huang		31/03/16
Patrick Hu		31/03/16
Akshya Swain		31/03/16
Seho Kim		31/03/16
Yijun Ren		31/03/16

# 1 Introduction

---

## 1.1 Background of Wireless Power Transfer

The idea of wireless power transfer can be traced back to the early work by Heinrich Hertz [1]. He conducted a series of experiments to demonstrate the existence of electromagnetic waves predicted by Maxwell's theory. A century ago the world-famous American inventor Nicolas Tesla, who was interested in the broad concept of resonance at that time, did amazingly great pioneering work on wireless high power transmission. He attempted to transfer a significant level of electrical energy without using cables [2-4]. In his proposed system, the active terminal of the transmitting device is subjected to such a high voltage potential with respect to the ground that it is capable to ionize the air molecules around it, which act as good conductors. Due to the extremely high voltage involved, this system currently has become a scientific demonstration of discharge sparks or serves for entertainment purposes, namely the Tesla coil. In 1921, inspired by the Tesla coil, an interesting experimental demonstration of wireless power transfer proved the feasibility of transmission of power across an air gap without galvanic contacts (illustrated in Fig. 1-1). Much later, in 1961, this concept was applied in a medical application which transferred electric energy through the skin to power an implanted pump [5]. In the 1980s, a research group at the University of California, Berkeley, charged the battery of an electric bus en route through coils buried beneath the road [6, 7]. A few years later, the power electronic group at the University of Auckland successfully commercialized a technology termed Inductive Power Transfer (IPT), which is based on the same principle, and successfully applied it to various industrial applications [8-25].

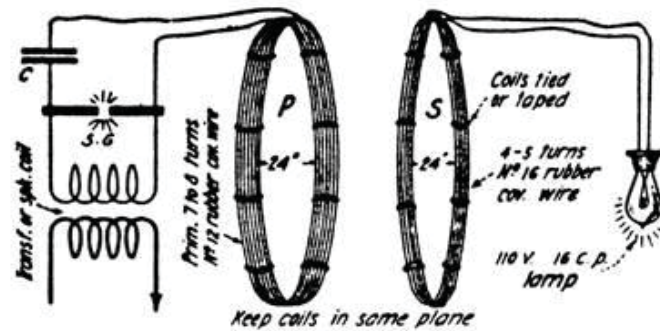


Fig. 1-1: The diagram of set-up of wireless power transfer in 1921 [26].

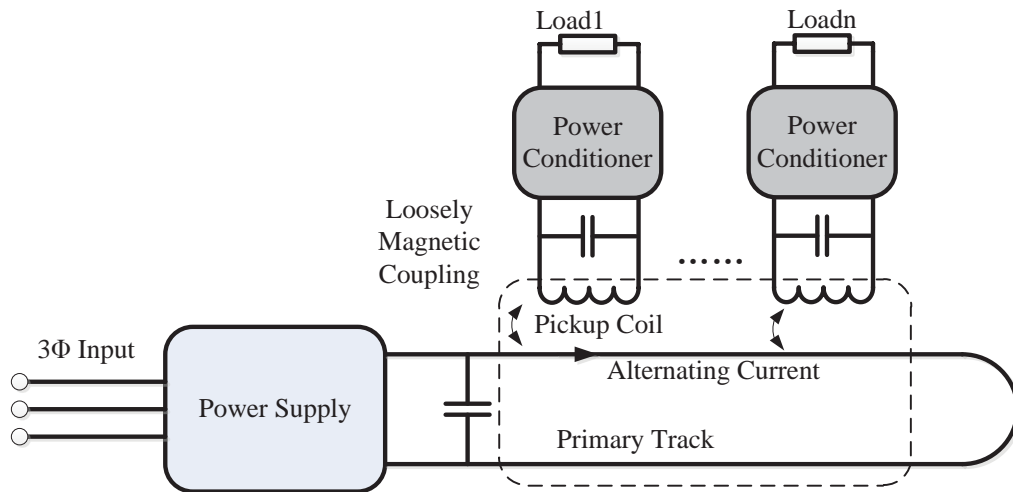
To date, several technologies have been investigated to achieve wireless power transfer. Table 1-1 briefly summarizes existing available techniques, some of which have already been applied in commercial products [8, 9, 20].

Among these wireless power transfer technologies, IPT is the dominant solution until now because of a better understanding of magnetic fields and widespread applications of this principle, for example, in transformers and motors. A typical IPT system consists of three main parts: a primary power supply, magnetic coupling coils, and secondary pickups, as shown in Fig. 1-2. The power converter generates an alternating current in the primary track, which induces a voltage in the secondary coils via magnetic coupling, thus delivering the required power to the load across an air gap. Compared with the conventional conduction method with wires, IPT is clean, spark-free, and impervious to dust and water. Furthermore, it offers a flexible configuration of multiple loads and requires lower maintenance [8].

Despite offering these unique advantages, IPT technology still has limitations on some special occasions due to its inherent operating principle. For example, it cannot transfer power across metal barriers, which is required in some situations such as machine tools or powering implanted medical devices with metallic shields. In consumer electronics applications, due to the small profiles of devices, IPT solutions require ferrite cores to enhance the magnetic coupling in order to increase the power transfer capability and power density, which add extra weight and cost to the system. In addition, the use of ferrites limits the highest operating frequency since core losses become significant during

high frequency operation, deteriorating the overall efficiency. Besides this, IPT systems require magnetic shielding in compliance with EMI/EMC regulations and health & safety requirements.

Aiming to overcome the aforementioned difficulties, Capacitive Power Transfer (CPT) technology has been proposed recently as a promising wireless power transfer technology offering unique features such as simple and flexible coupling designs, low EMI since most electric fields are confined within the coupling structure, and the ability to transfer power through metal barriers if the electric field is not fully shielded [27-29].



**Fig. 1-2: A typical IPT system.**

## **1.2 Fundamentals of Capacitive Power Transfer (CPT)**

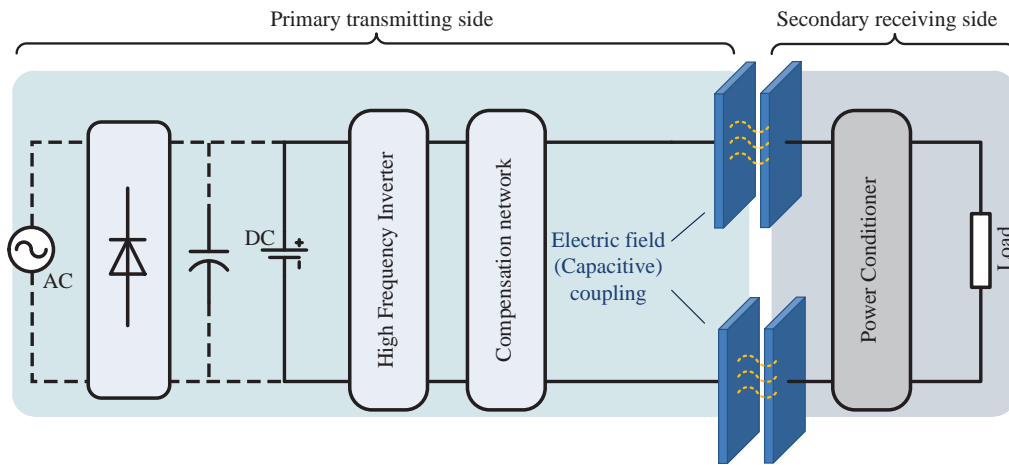
Capacitive Power Transfer (CPT) is a wireless/contactless power transfer technology based on the principle of electric field coupling (or capacitive coupling). At first CPT was considered to be impractical to deliver a usable amount of power due to the very

**Table 1-1 Wireless Power Transfer Techniques**

	<b>Near Field</b>		<b>Wave Propagation</b>		
<b>Types</b>	Electric Field	Magnetic Field	Acoustic Wave	Electromagnetic Wave	
<b>Typical Techniques</b>	Capacitive Power Transfer (CPT)	Inductive Power Transfer (IPT)	Acoustic Energy Transfer (AET)	Energy Harvesting	Microwave Power Transmission
<b>Power Levels</b>	mW~W	mW~kW	mW~W	$\mu$ W~mW	kW
<b>Transmission Range</b>	short	medium	medium	long	
<b>Typical Features</b>	<ul style="list-style-type: none"> <li>• Small volume</li> <li>• Low EMI</li> <li>• Ability to power through metal barriers</li> </ul>	<ul style="list-style-type: none"> <li>• Relatively mature technology</li> <li>• High power capability</li> </ul>	<ul style="list-style-type: none"> <li>• Ability to power through metal barriers [30]</li> <li>• Strong dependence on</li> </ul>	<ul style="list-style-type: none"> <li>• Long transmission distance [31]</li> </ul>	

low permittivity of air ( $\epsilon_0 \approx 8.8542 \times 10^{-12} \text{ C}^2 \cdot \text{N}^{-1} \cdot \text{m}^{-2}$ ) compared to its permeability ( $\mu_0 = 4\pi \times 10^{-7} \text{ N} \cdot \text{A}^{-2}$ ) [10]. For a long time, capacitive coupling has been mainly used for power isolation and signal transmission [32-35]. Although it involves power exchange, the power level is limited to a few tens or hundreds of milliwatts. However, with the fast development of semiconductor devices, the switching frequencies of power converters nowadays can approach hundreds of kHz or even several MHz levels, which enables CPT to transfer high power wirelessly.

### 1.2.1 Basic Configuration and Operating Principle of CPT



**Fig. 1-3: Basic configuration of a typical CPT system.**

A block diagram of a typical CPT system is shown in Fig. 1-3. It is composed of a DC source, a power converter that generates high-frequency voltage, an electric field (capacitive) coupling interface, and pickups. The DC source can be generated by rectifying a low frequency AC source, or it can come from a battery directly. Then a DC-AC inverter transforms the DC voltage/current to a high frequency AC voltage, driving the capacitive coupling interface. The capacitive coupling interface consists of two primary side conductive plates and two secondary side conductive plates – all of them should be insulated for safety. When the two pairs of plates are close to each other, they form two “capacitors” in series so that a closed loop is created for energy transfer. In most cases, the conductive plates of the capacitive coupling interface can be made of aluminium sheets, copper foils or other conductive materials. The plates can be of any shape rectangular,

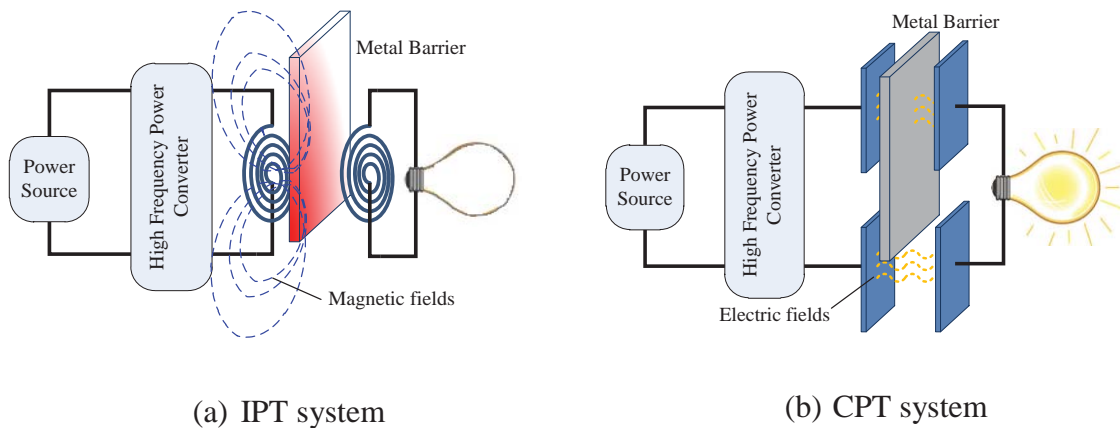
circular, and cylindrical, depending on specific applications. For instance, when designing the capacitive coupling interface for a smartphone charging platform, a planar rectangular shape is preferred. For rotatory applications like robot joints, a cylindrical or a multi-layer disk structure is preferred [36-39]. The secondary side plates are attached to the secondary pickup circuit, which usually involves combination of a rectifier and a filtering network for a DC load.

It can be seen that, compared to the IPT system, the most distinctive part of the CPT system is the coupling interface. As the only energy transfer channel, it can affect the overall performance of the system. The properties of dielectric materials have an important impact on the power density and efficiency. The alignment of plates determines the complexity of the CPT analysis. The large reactive impedance introduced by the capacitive coupling interface needs to be cancelled out by a proper compensation network, the design of which varies for different applications.

### 1.2.2 Features

Compared with IPT technology, CPT offers the following unique features:

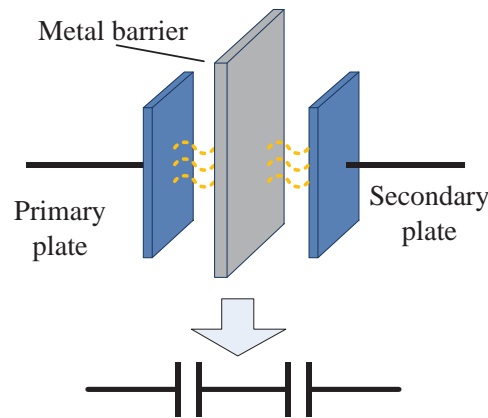
- Ability to transfer through metal barriers



**Fig. 1-4: (a) An IPT system and (b) a CPT system with a metal barrier existing in the coupling part.**

Due to the inherent working principle, IPT systems have the limitation that they cannot transfer power across metal objects. Fig. 1-4(a) shows that when a metallic slab is placed between the induction coils, it will weaken or block the magnetic coupling between the primary and secondary coils, thus reducing the power transfer capability significantly. For metallic materials such as iron and steel with high permeability (about 200), the magnetic field is rerouted or “blocked” away from the metallic slab. Besides this, the power losses related to hysteresis and eddy currents heat up these metals, presenting a safety issue to users. In addition, the generated heat increases the ambient temperature, which deteriorates the system operating performance. For copper and aluminium, which have high conductivity, they act as an intermediate coil that is short-circuited; this will also prevent the energy from being transferred to the secondary side [10]. They can be heated as well due to eddy currents. However, when a metallic slab is inserted between coupling plates in a CPT system as shown in Fig. 1-4(b), the electric fields can still penetrate through the metallic slab. Moreover, it can even help increase the power transfer capability. As shown in Fig. 1-5, the primary plate, the metallic slab, and the secondary plate form two capacitors in series. Without taking account of the thickness of the metal slab, the effective value of the two split capacitors should be equal to the original capacitance, meaning that the insertion of the slab has no effect on the power transfer. But in practical systems, the slab has physical thickness which has an equivalent effect of reducing the effective distance between the plates, thus yielding a larger coupling capacitance. It is noted that the ability of CPT systems to transfer power through metal barriers is achieved on the precondition that the metal slab does not fully cover the primary plates, which will shield the electric field completely.





**Fig. 1-5: Equivalent circuit of the capacitive coupling when a metal slab is inserted in between.**

- Simple coupling structure

The design and manufacturing of the capacitive coupling interface does not require as much complexity as IPT systems. In wireless power systems based on IPT solution, the design of the coupling coils is not a trivial task [6, 8, 40]. The inductive coupling coils usually have a spiral shape. To mitigate power losses caused by the skin effect and proximity effect at high frequency, Litz wires are widely used to wind the coils, and these increase the cost. In CPT systems, the coupling interface is made of planar conductive plates. They can be of any shape depending on specific applications. In addition, they can be very thin, such as aluminium foils or copper pad in a printed circuit board (PCB). Compared to IPT systems, the capacitive coupling of CPT systems is cost-effective and easy to manufacture.

- Low EMI emission

Electromagnetic interference (EMI) is an important issue to be dealt with and great care is required when designing electrical systems. For IPT systems, the magnetic fields emanating from the coupling coils need to be carefully shielded to avoid making nearby electronic circuits malfunction. Since the magnetic field lines tend to spread in all directions to form closed-loops, the shielding design is not a trivial task. Unlike magnetic fields in IPT systems existing in closed-loops, the electric field is mostly confined between the coupling plates since the distance between primary and secondary plates is quite small

in most CPT applications. Therefore, harmonic radiation and EMI are significantly reduced, which can lessen the burden of EMI shielding design, thus making CPT systems more cost-effective.

- Light weight and small volume

In some space-confined applications, IPT systems require extra ferrites to enhance the magnetic coupling between primary and secondary side coils, which add cost and increase the size of the system. The use of ferrites also limits the operating frequency due to core losses. However, in CPT systems, the coupling plates can be made very thin (such as aluminium foil) and small. Moreover, the operating frequency is chosen to be much higher than IPT systems, which serves the purpose of reducing the reactive impedance and the dissipation (a higher operating frequency leads to a smaller loss tangent). Higher operating frequencies can also scale down the sizes of reactive components in the circuit, which help to further reduce the weight and size of the entire system.

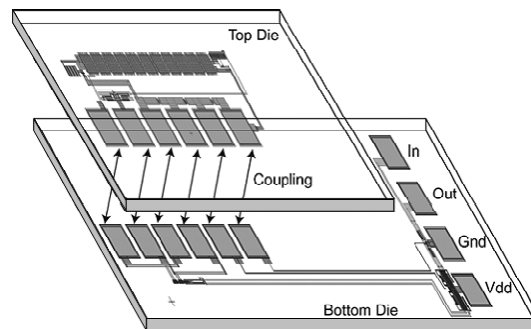
### 1.2.3 CPT Applications

Owing to its unique features, CPT can be applied in various applications, ranging from a low power level of a few mW to a high power of up to several kW. Following are details of some applications and discussion about them.

- 3D integrated chips

3D integrated circuits emerge as a viable technology for information processing that can bring advantageous features such as locality of reference and short interconnects for information processing systems including high-throughput sensor arrays and large scale parallel computer architectures [41]. The methods of implementing interconnects have been investigated extensively [42, 43]. Using capacitive vias to transfer power and signal between isolated chips can achieve high interconnect density, turning out to be a more competent way since this avoids physical connections that impose mechanical and cost limitations on the number and density of data transfer to the package [33]. Fig. 1-6 illustrates the arrangement of the first inter-chip non-galvanic capacitive coupling to provide both power and signal exchange between two dies. The transmitter is in the bottom die and the receiver circuit is in the top die. The power exchange is achieved using

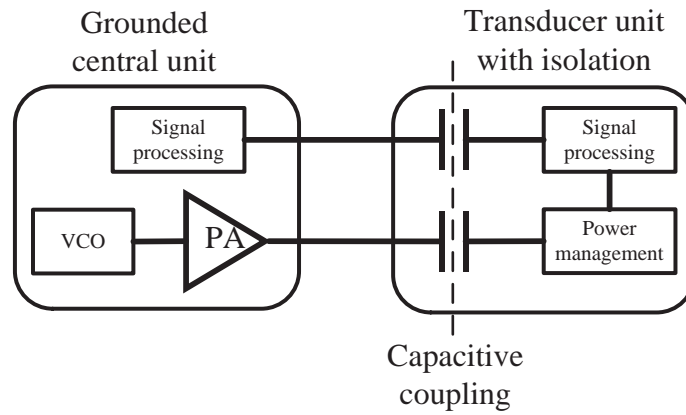
a charge pump that delivers the power to the top die through capacitively coupled pads. These pads occupy an area of  $90 \times 90 \mu\text{m}^2$  with a separation of  $10 \mu\text{m}$  filled with transparent varnish; each pair of coupling pads produces a capacitance of 8 fF. In the prototype system a 3.3 V power supply from 1 kHz to 15 MHz produces a 9 mA output current in the receiver circuit that is used to drive the device under test (DUT). Compared to the inductive via method, the capacitive via method can be implemented with much smaller area, which is a desirable feature in integrated circuits.



**Fig. 1-6: Illustration of capacitive charging and communication in 3D integrated circuit [33].**

- Powering biomedical devices

Biomedical devices has been playing an increasingly important role in people's lives. Considerable effort has been put into their design to address health-related issues and to alleviate the suffering of patients. IPT has been researched to provide power and signal communication through skin [44-47]. However, this method is still under investigation due to the concern about the heat generated by the coils and the issue of the effects of EMI on the human body. Capacitive power transfer has been applied in a biosignal instrumentation system to achieve power and signal isolation with an isolation capacitance of about 1.6 pF [34]. Fig. 1-7 illustrates the power stage which comprises of a voltage-controlled oscillator (VCO) operating at 1.98 GHz and a power amplifier, and which can provide a power exchange up to 600 mW to the isolated electronics. In this application, capacitive coupling serves the purpose of isolation inclusive of data and power transfer as well.



**Fig. 1-7: Block diagram of biosignal instrumentation electronics using capacitive coupling.**

- Charging consumer electronics



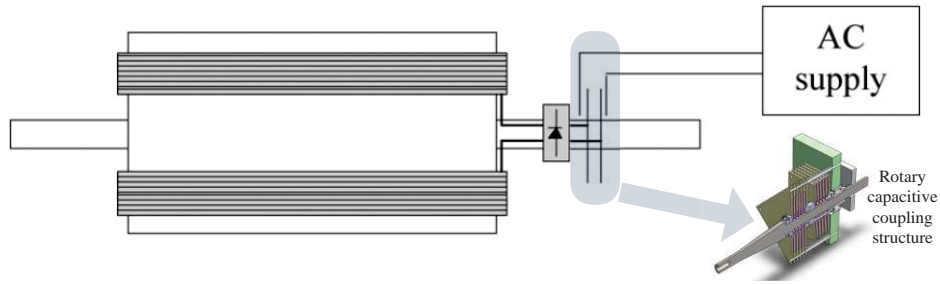
**Fig. 1-8: Capacitive charging docks from Murata [48].**

Wireless charging has been an attractive feature for consumer electronics devices. Many hi-tech giants have been making efforts to integrate this function into their products. Recently, Apple has started to offer wireless charging for the Apple watch, which adopted the Qi standard as a replacement to its Lightning ports and cable [49]. However, CPT provides another potential method for wireless charging of consumer electronics. The first commercialized CPT product was developed by Murata Semiconductor Manufacturing, which has developed its capacitive charging dock for smartphones and digital reading devices (shown in Fig. 1-8). A prototype CPT system targeted to produce an output power of 10 W exhibits 70% efficiency at an operating frequency of ~500 kHz. The voltage

across capacitive coupling plates can approach 500 V to 2 kV, but the current through it can be very small, reducing the risk of overheating. Due to the high operating voltage, reliable insulating materials are required for safe operation.

- Power supply for rotors

The permanent magnet electric machine (PM) dominates in the industrial driving systems due to its high performance such as high torque density and efficiency. The demand for rare earth materials imposes limitations on its development since this kind of rare resource will be exhausted in the near future. The wound field synchronous machine (WFSM) is an alternative solution, which holds comparable characteristics to PM. However, the WFSM requires a current delivery to the rotor. To eliminate the need for periodic replacement of the mechanical slip ring due to friction via carbon brushed contacts, the contactless method based on transformer principle to supply power has successfully demonstrated high system efficiency with lower lifetime cost [21]. However, design of the transformer-based method requires a closed magnetic path using ferrites and windings. These special transformers operating at high frequency (a few tens of kHz) present significant parasitics such as stray capacitance and leakage inductance, which have to be taken into consideration in design [37]. Featured with simple coupling design and low cost, capacitive power transfer provides an alternative solution. Utilizing a coupling structure similar to a radio tuning capacitor, the capacitive way of transferring power to the rotor has proved to be feasible [50]. A high frequency inverter operating at 626 kHz drives the rotary capacitive coupling structure, which has been demonstrated to deliver a 500 mA field current with 94% efficiency. This shows that CPT is a competent way of replacing the mechanical slip-ring method.



**Fig. 1-9: Powering the rotor using capacitive power transfer [37].**

- Electric vehicle charging

Although earlier CPT systems mainly targeted low power applications, recent development of CPT demonstrates its feasibility to transfer high power using coupling plates [51-54]. Fig. 1-10 shows a 1 kW prototype electric vehicle (EV) charging system using CPT. In the charging stage, the electric vehicle is pulled into the charging dock, which consists of a foam-based charging bumper and the primary side transmitter. The foam is used to minimize the air gap between primary and secondary side coupling plates to increase the coupling capacitance. In this way, the measured coupling capacitance ranges between 9.5 nF and 10 nF. The primary side circuit is based on a split buck-boost converter, in which the capacitive coupling interface serves as the intermediate energy storage element. The system is operated at the switching frequency of 540 kHz with overall efficiency exceeding 90% due to the low conduction loss brought by the high-voltage and low-current feature of the CPT system. As can be seen, this type of CPT EV charging system requires very close non-galvanic “contact” between coupling plates, which cannot compete with the flexibility offered by IPT solution. However, another CPT EV charging system with a large air gap between coupling plates has also been reported [51, 55]. The coupling distance is 150 mm, with the coupling capacitance calculated to be 36.7 pF. The whole system can deliver a 2.4 kW output power with 90.9% efficiency at 1 MHz operating frequency.

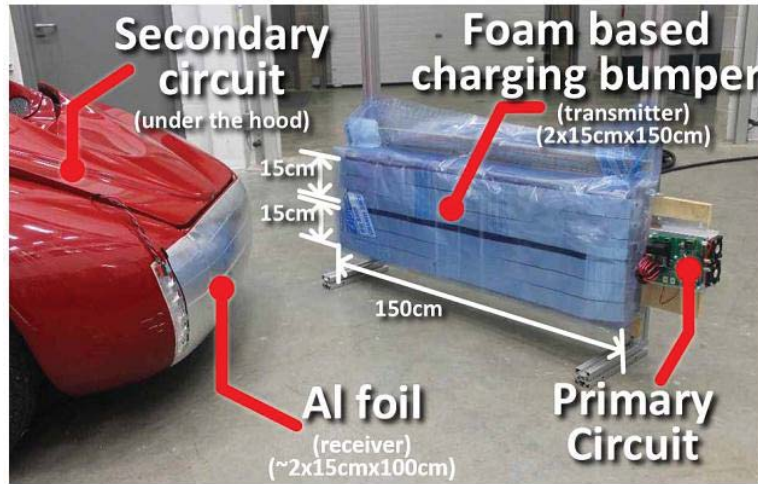


Fig. 1-10: A CPT EV charging system using aluminium foil as coupling plates [53].

### 1.3 Challenges of CPT

Despite the desired features offered by CPT, some theoretical and practical difficulties need to be overcome for its further development. They involve various aspects, such as the selection of primary side converters, the modelling of the capacitive coupling interface, and the design of proper compensation networks and power flow controllers.

#### *A. High frequency issues*

High frequency operation is preferred in CPT systems, which ranges from a few hundred kHz to a few MHz. Some CPT systems are even driven at 100 MHz [56]. This feature justifies the need for consideration of all aspects of high frequency issues, including the generation of high frequency voltage and switching losses due to turn-on/turn-off transients of switching devices. High frequency power converters, which can generate high quality AC voltage with high efficiency, might be suitable for CPT; this needs to be investigated. Since one of CPT's unique features is small size, the chosen topology should be simple to implement and able to maintain high frequency. The count number of components used in the converter should be small so overall volume of the system is reduced. The characteristics of CPT systems based on these converters need to be



discussed and compared to provide useful guidance for the best choice in specific applications. Switching devices suited for high operation are needed. The insulated gate bipolar transistor (IGBT) has high voltage and current ratings, but its switching speed is relatively slow, and is used in converters at an operating frequency of up to tens of kHz. Other types of semiconductor switches based on new materials such as gallium nitride (GaN) and silicon carbide (SiC) have been developed recently and are suitable for high frequency with reduced switching losses, but they are quite costly and require delicate and special driver circuits to work reliably. Another possibility is metal oxide semiconductor field effect transistors (MOSFETs), which can switch at an operating frequency of up to MHz without much sacrifice of efficiency; also its manufacturing technology is quite mature. A synthesized consideration of performance and cost makes MOSFETs the ideal choice for switching devices on CPT systems. Other aspects related to high frequency include the choice of inductor core materials, which should have low losses at high frequency. The winding wires and physical layout of the circuits should be optimized for high frequencies.

### ***B. Capacitive coupling variations***

The coupling plates of CPT systems suffer from misalignment, which complicates the modelling of the CPT system. When misalignment between coupling plates occurs, two additional capacitors are formed. If the terminal plates on the same side are very close, another two parasitic capacitors need to be taken into account. Therefore, a composite network consisting of six capacitors has to be used to characterize the capacitive coupling interface. Direct use of this composite circuit network into the system model increases the complexity of the system analysis and compensation design. To address this difficulty, a circuit-intuitive model of the capacitive coupling interface is necessary to provide easy insight into the structure of the CPT systems and simplify the compensation design and analysis. Additionally, for easy evaluation and comparison of CPT systems with different coupling configurations, a quantitative term for characterization of different coupling conditions is required, which should have physical meaning and be easy to measure.

### ***C. Practical operation transients***

Flexible movement of the load to be powered by CPT systems brings more transient events than the conventional method using cable. For example, when it is used in a



smartphone charging application, the user may suddenly remove the smartphone, leading to a no-load or open-circuit operating condition. The issues brought by this feature should be addressed properly, which requires novel compensation networks. In previous CPT systems, the single series tuning inductor has been widely used to compensate for the capacitive reactance introduced by the capacitive coupling interface due to its simplicity of implementation and cost effectiveness. However, it will impose a health hazard on operation when the secondary side plates are removed since the current through the inductor will be interrupted, generating extremely high voltage spikes. If the voltage exceeds the breakdown voltage of the dielectric materials used, this dangerous high voltage could not only destroy the components in the circuit, but could also fail the insulation function of the coupling plates.

### **1.4 Objectives and Scope of the Thesis**

To address the existing problems of the CPT system for its further development, this research aims to develop advanced compensation and power flow control methods to improve the system power transfer performance. Different types of resonant power converters suited for high frequency electric field generation will be studied and compared. Additionally, a general model to characterise the capacitive coupling interface of CPT systems will be derived to facilitate the system analysis.

The main body of the thesis is structured as follows:

Chapter 1 introduces the development of wireless power transfer, basic structure and working principle of CPT systems, and lists the challenges of CPT systems.

Chapter 2 provides an overview of existing compensation and power flow control methods in CPT systems. A brief discussion on their advantages and disadvantages is also given.

Chapter 3 studies three soft-switching resonant power converters suitable for high frequency operation in CPT systems, which are an autonomous current-fed push-pull converter, a class E converter, and a voltage-fed half-bridge converter. Their working principles and design procedures are provided. Their characteristics such as control and sensitivity to coupling variations are compared and discussed.

Chapter 4 establishes a new model of the capacitive coupling interface, which includes the effect of cross coupling. Analysis of the compensation method using a series inductor is conducted based on the new model. Furthermore, a new term to quantify mutual coupling between coupling plates is derived based on the charge balance principle.

Chapter 5 proposes a novel compensation network using a Z-impedance network to solve the high spike voltage issue suffered by the conventional compensation method using a single series inductor. An equivalent circuit model is established to analyze its compensation functionality. Additional benefits such as short-circuit immunity and voltage boost capability are also demonstrated.

Chapter 6 develops a novel power flow control method based on a switched shunt capacitor bank while maintaining high efficiency. The CPT system is built on the class E converter topology, and works in a new sub-optimum mode and can regulate the output power by changing the effective shunt capacitance.

Chapter 7 summarizes the work of this research, and provides suggestions for future research on CPT systems.

## **2 Literature Review of Compensation and Control Methods for CPT Systems**

---

### **2.1 Introduction**

CPT technology has gained increasing interest from industrial and academic fields owing to its unique features. Like IPT technology, CPT systems require compensation networks and control strategies to increase the power transfer capacity and to meet the requirements of the load regardless of operation variations and component uncertainties. The compensation design is focused on the large impedance introduced by the small coupling capacitance, which differs from application to application. A series tuning inductor can serve this purpose. In other applications, where the single series tuning inductor cannot be used or the value of the inductor required is so large that it is impractical to implement at high frequency operation, other composite compensation networks need to be employed. The power flow controllers are essential in any power converters. It can be a simple linear voltage regulator. When other advanced features such as robustness to more system variations are desired, novel and advanced controllers are needed to meet the design requirements.

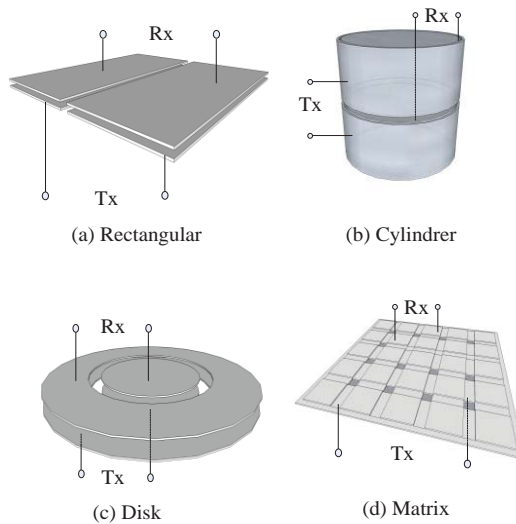
This chapter will examine existing compensation methods and power flow controllers that have been employed in CPT systems with different electric field coupling configurations. Firstly, the general characteristics of the capacitive coupling interface, which is unique to CPT systems, will be provided. Then a general principle of compensation will be described, followed by state-of-art compensation methods. After that, the control methods

in CPT systems will be described, and their working principles will be explained, followed by a brief discussion about their disadvantages and drawbacks.

## 2.2 Existing Compensation Methods for CPT

### 2.2.1 Capacitive Coupling Interface

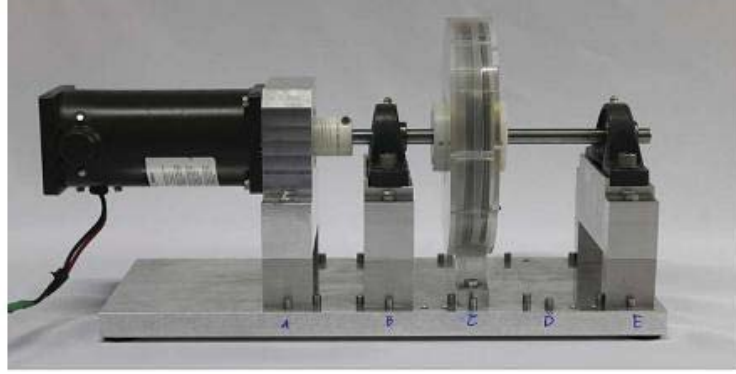
The capacitive coupling interface is the key part of a CPT system. It typically consists of four metallic plates made from copper or aluminium foil, coated with dielectric materials for insulation. Two plates are connected to the primary side converter, referred to as the primary side plates. The other two are connected to the secondary side receiver circuit, referred to as the secondary side plates. During the period of powering the load, the primary side and the secondary side plates face each other, forming two parallel plate capacitors, through which the high frequency alternating current can flow. The shape of the coupling structure is dependent on specific applications. The disk or cylinder type can be used in rotary application [29]. The rectangular type is suitable for smart phone or laptop charging platform [38, 57]. Fig. 2-1 shows some possible configurations of the capacitive coupling interface.



**Fig. 2-1 Possible configurations of the capacitive coupling interface.**

It is noted that some special coupling designs are proposed to maximize the coupling capacitance [58]. For example, a modified aerodynamic fluid bearing used to eliminate the

air between plates is shown in Fig. 2-2, which can increase the coupling capacitance up to ten times through the dynamic performance of the bearings.



**Fig. 2-2: Photograph of the coupling plates structure based on aerodynamic fluid bearings [58].**

In the simplest case, the capacitance of a pair of coupling plates can be calculated by

$$C = \frac{A\epsilon_r\epsilon_0}{d} \quad (2-1)$$

where  $A$  is the effective overlapping area between the two plates,  $\epsilon_r$  is the dielectric constant of the dielectric material filled between plates,  $\epsilon_0$  is the permittivity in vacuum (about  $8.85 \times 10^{-12} \text{ C}^2\cdot\text{N}^{-1}\cdot\text{m}^{-2}$ ), and  $d$  is the distance between the two plates.

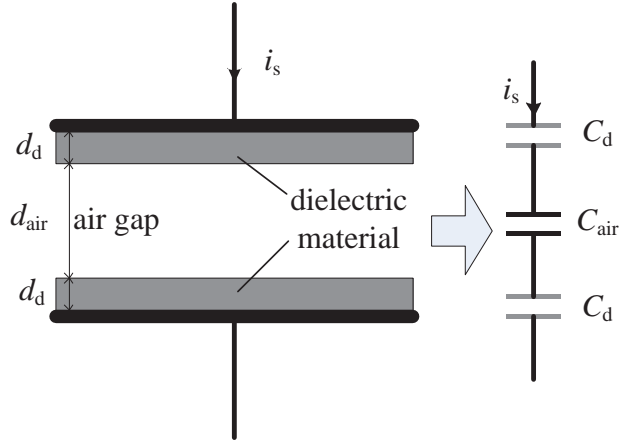
For example, with two  $100 \text{ mm} \times 100 \text{ mm}$  coupling plates separated by a  $0.2 \text{ mm}$  air gap, the formed effective coupling capacitance is about  $440 \text{ pF}$ . In this case, the two coupling plates are closely spaced, the wireless feature of which cannot be discerned with eyes. If the air gap is increased to  $2 \text{ mm}$ , the formed coupling capacitance falls to  $44 \text{ pF}$ , which is very small, making the compensation design a challenging task.

#### *A) Effects of Dielectric Materials*

In CPT systems, coupling plates are coated with dielectric insulation material to ensure safe operation. A pair of coupling plates insulated with dielectric material is depicted in Fig. 2-3. The thickness of the dielectric coating is  $d_d$ . The air gap between the plates is  $d_{\text{air}}$ .

It can be seen as a series combination of three capacitors [59]. Their equivalent capacitance  $C_C$  can be obtained by

$$C_C = \frac{2C_d C_{air}}{C_d + 2C_{air}} \quad (2-2)$$



**Fig. 2-3: Coupling plates coated with dielectric material.**

In terms of the geometric parameters, it can also be expressed as

$$C_C = \epsilon_0 \frac{A}{d_{air} + \frac{2d_d}{\epsilon_r}} \quad (2-3)$$

From (2-3), the second term in the denominator accounts for the effect of the dielectric layer on the total capacitance. The thickness of the dielectric material increases the distance between the plates and reduces the coupling capacitance. Although materials with a high dielectric constant can alleviate the effect of capacitance reduction, the impact of the air gap dominates the formed capacitance. Therefore, to increase the coupling capacitance, soft dielectric materials and special coating methods are used to reduce the air gap [53, 60].

Although dielectric materials with high dielectric constant are helpful to increase coupling capacitance, dielectric properties such as loss tangent and dielectric strength need to be taken into consideration in design.

The term loss tangent  $\tan\delta$  is used to characterize the dissipative property of a dielectric material [61]; it can be described using lumped circuit components, which is

$$\tan\delta = \frac{R_{esr}}{X_C} = 2\pi f C_C R_{esr} \quad (2-4)$$

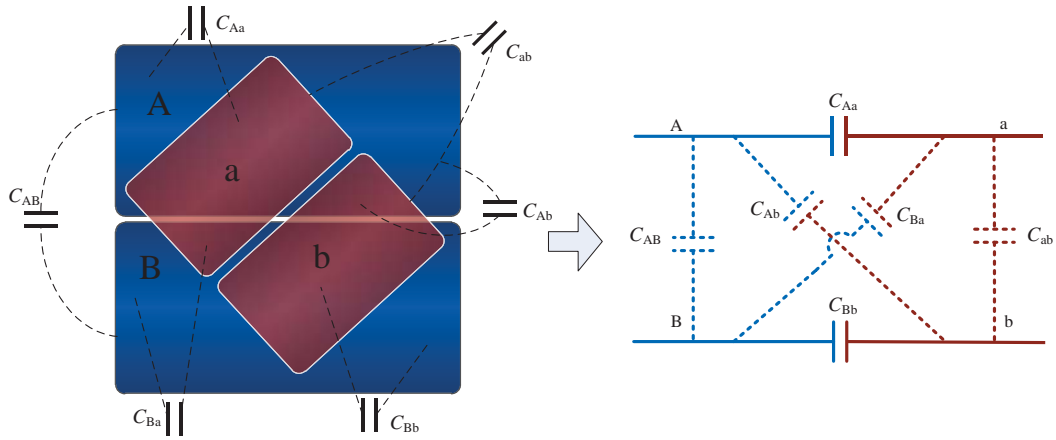
where  $X_C=1/(\omega C_C)$ ,  $f$  is the operating frequency, and  $R_{esr}$  is the equivalent series resistance.

It can be seen from (2-4) that a high operating frequency contributes to the reduction of the loss from dielectric materials (since  $\tan\delta$  is usually constant, a higher frequency leads to a lower  $R_{esr}$ ), which is one of reasons why CPT systems prefer high frequency.

Dielectric strength is another factor to be considered when choosing dielectric materials. When the voltage imposed across the coupling plates exceeds the dielectric strength of the dielectric material, it will lose its insulation property, which presents a safety hazard. To ensure safe operation, the voltage across the coupling plates cannot exceed the dielectric strength of the dielectric materials. Referring to Fig. 2-3, the safe condition for the coupling plates is

$$E_d > \varepsilon_r \varepsilon_0 2\pi f A i_T \quad (2-5)$$

where  $E_d$  is the dielectric breakdown electric field,  $i_T$  is the current flowing through the coupling plates.

***B) Effects of misalignment***

**Fig. 2-4: Cross coupling in the capacitive coupling interface.**

In the situation where one of the primary side plates overlap with both secondary side plates, cross coupling occurs in the capacitive coupling interface, as illustrated in Fig. 2-4. Considering the parasitic capacitance due to the proximity of plates on the same side, four additional capacitors are formed in the capacitive coupling interface. The cross coupling significantly increases the complexity of analysis. It will make the calculation of the accurate series tuning inductor tedious and mathematical results intractable [62].



### 2.2.2 Series Inductor Tuning

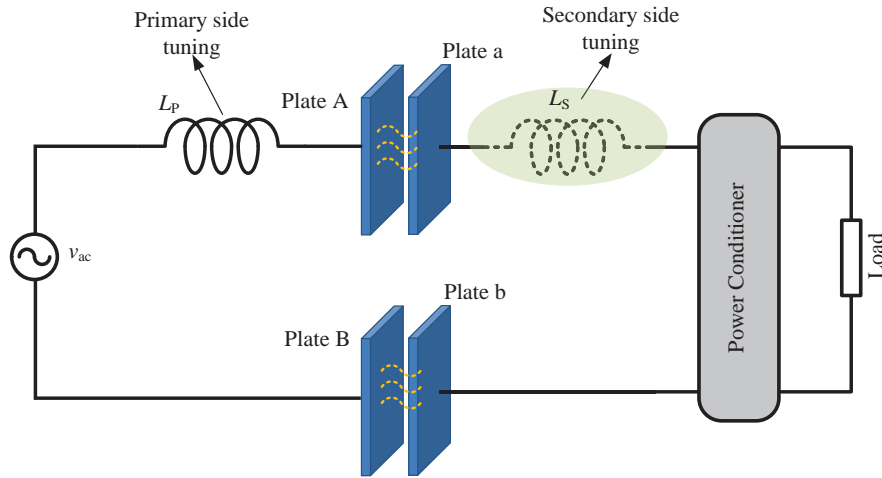
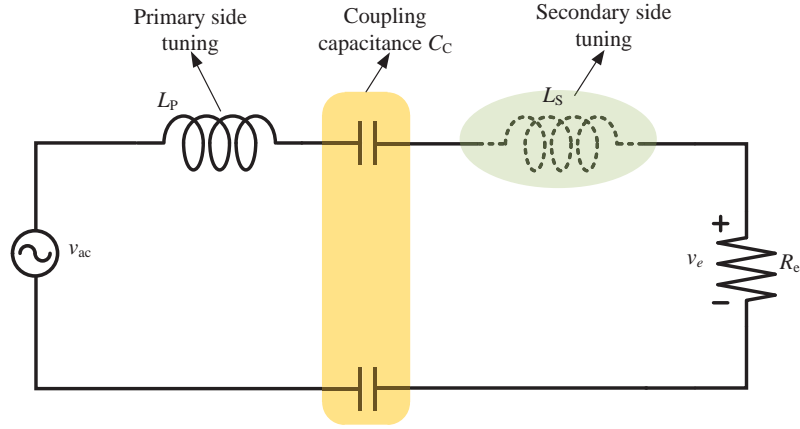


Fig. 2-5: A CPT system with series inductor tuning.

The most common and straightforward method to compensate for the capacitive reactance caused by the capacitive coupling is to connect an inductor in series with the capacitive coupling interface. As shown in Fig. 2-5, the series tuning inductor can be placed on the primary side converter, or the secondary side highlighted within the oval shape. The position of the inductor makes no difference when there is no cross coupling between coupling plates. Because the inductor is usually bulky, it is beneficial to put the inductor on the primary side since it can reduce the size of the pickup circuit, which is a desirable feature for small-volume applications. Fig. 2-6 shows an equivalent circuit of a CPT system with series tuning.  $v_{ac}$  is the high frequency AC input voltage source,  $R_e$  is the equivalent ac resistance,  $C_C$  is the total effective coupling capacitance of the two pairs of coupling plates, and  $L_P$  or  $L_S$  is the series tuning inductor. Without considering cross capacitance,  $L_P$  and  $L_S$  should be equal since their tuning effects are equivalent:

$$L_P = L_S = \frac{1}{\omega^2 C_C} \quad (2-6)$$

where  $\omega = 2\pi f$ , the angular switching frequency of the system.



**Fig. 2-6 Equivalent circuit of CPT with series inductor tuning**

The quality factor  $Q_s$  of the system is:

$$Q_s = \frac{\omega L_P}{R} = \frac{1}{\omega C_C R} \quad (2-7)$$

The peak value of the voltage across the coupling plates  $v_C$  is:

$$V_C = Q_s V_o \quad (2-8)$$

where  $V_o$  is the peak value of the voltage across the equivalent AC load, which is then fed into the rectifier.

In an ideal situation where primary and secondary side plates are aligned without causing cross coupling, the position of the inductor does not make any difference to the characteristics of the system. However, in real-world CPT applications, parasitic cross capacitances among coupling plates usually exist in the capacitive coupling interface due to various reasons such as misalignment of coupling plates. Thus the position of the series tuning inductor will make a difference [62].

### 2.2.3 High Order Compensation Methods

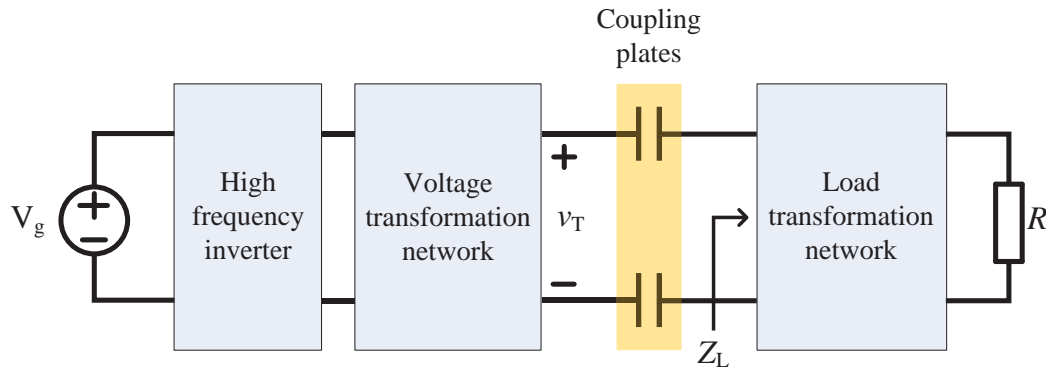


Fig. 2-7: Basic blocks of high order compensation network for CPT systems.

Fig. 2-7 shows a block diagram of a CPT system with a high order compensation network. In this method, a voltage transformation network steps up the output voltage from the high frequency inverter. The load transformation network combined with the load  $R$  presents an “amplified” impedance, which should be at least comparable to the capacitive reactance of the capacitive coupling interface.

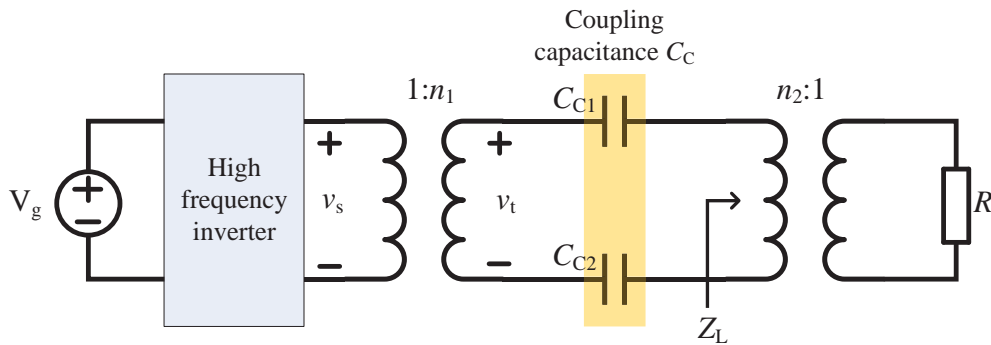


Fig. 2-8: Using transformers for transformation.

Two methods can be used to perform the transformation of the voltage and load. One is using high frequency transformers, as shown in Fig. 2-8 [63]. An additional benefit of this method includes electrical isolation, which is an inherent property of transformers. The voltage transformation network is a step-up transformer with a turns ratio  $n_1$ . The load

transformation network is a step-down transformer with a turns ratio  $n_2$ . The output voltage of the switching network is  $v_s$ . Then the voltage driving the coupling plates is

$$v_t = n_1 v_s \quad (2-9)$$

The impedance reflected to the primary side of the step-down transformer is

$$Z_L = n_2^2 R \quad (2-10)$$

Therefore, the output power received by the load is

$$P_o = \frac{1}{2} \frac{n_1^2 n_2^2 v_{sp}^2 R}{\left( \frac{1}{\omega C_c} \right)^2 + n_2^4 R^2} \quad (2-11)$$

where  $v_{sp}$  is the peak value of the output voltage of the inverter  $v_s$ . If  $v_s$  is a non-sinusoidal waveform,  $v_{sp}$  is the peak value of its fundamental component.

The other method for transformation is using resonant L-C networks. Compared to the transformation network using transformers, it lacks electrical isolation and requires more components. However, in extra high frequency applications, this method is free of concern about the core loss from transformers, which impose a limit to the highest frequency. If the operating frequency is high enough, the air core inductor can be used as the resonant component. Besides, The size of capacitors can be scaled to be very small at higher frequencies [56]. Fig. 2-9 shows a CPT system based on transformation networks using L-C resonant tanks.

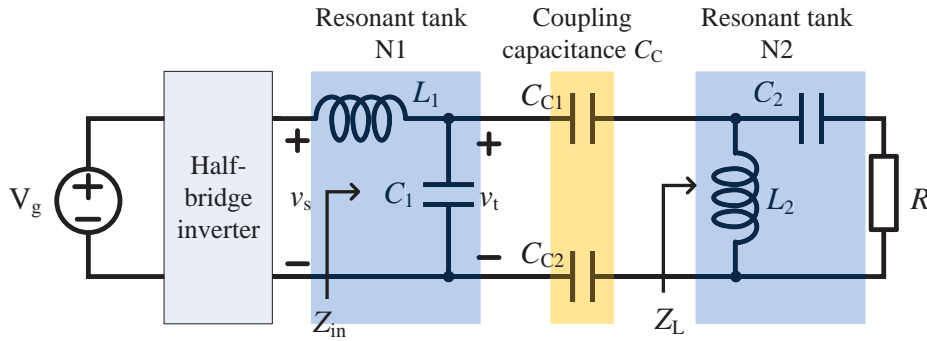


Fig. 2-9: Using L-C resonant tanks for transformation.

The half-bridge inverter is used as the switching network. A resonant tank N1 consisting of  $L_1$  and  $C_1$  is used to boost the input voltage. A resonant tank N2 consisting of  $L_2$  and  $C_2$  is used to “amplify” the load resistance. The quality factor of the resonant tank N2 is

$$Q_2 = \frac{1}{\omega C_2 R} \quad (2-12)$$

The impedance  $Z_L$  presented by the resonant tank N2 is

$$\begin{aligned} Z_L &= \frac{j\omega L_2 \left( \frac{1}{j\omega C_2} + R \right)}{j\omega L_2 + \frac{1}{j\omega C_2} + R} \\ &= \frac{C_2^2 L_2^2 R \omega^4}{C_2^2 R^2 \omega^2 + (C_2 L_2 \omega^2 - 1)^2} + j \frac{\omega L_2 - C_2 L_2^2 \omega^3 + C_2^2 L_2 R^2 \omega^3}{C_2^2 R^2 \omega^2 + (C_2 L_2 \omega^2 - 1)^2} \end{aligned} \quad (2-13)$$

The impedance  $Z_{in}$  seen by the half-bridge inverter is

$$\begin{aligned} Z_{in} &= j\omega L_1 + \frac{1}{j\omega C_1} \parallel \left( \frac{1}{j\omega C_c} + Z_L \right) \\ &= \frac{R_1}{C_1^2 \omega^2 \left( R_1^2 + \left( X_1 - \frac{1}{\omega C_1} \right)^2 \right)} + j \left( \omega L_1 - \frac{\omega C_1 R_1^2 + \omega C_1 X_1^2 - X_1}{C_1^2 \omega^2 \left( R_1^2 + \left( X_1 - \frac{1}{\omega C_1} \right)^2 \right)} \right) \end{aligned} \quad (2-14)$$

where  $R_1$  and  $X_1$  are the real and imaginary parts of the sum of impedances  $1/(j\omega C_C) + Z_L$ , respectively.

Because the components of the resonant tanks are decided such that  $Z_{in}$  exhibits a pure resistance, the output power  $P_O$  is given by

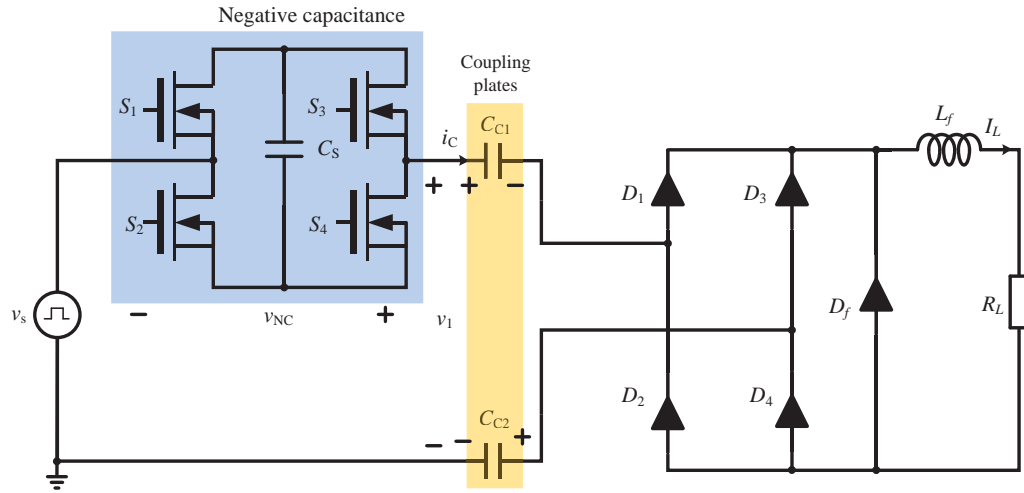
$$P_O = \frac{V_{s1}^2}{2\text{Re}(Z_{in})} \quad (2-15)$$

where  $V_{s1}$  is the peak value of the fundamental component of output voltage of the switching inverter  $v_s$ .

Although this method avoids the use of the series tuning inductor, it requires more reactive components to constitute transformation networks. The capacitor in the transformation network that drives the capacitive coupling interface has to endure extremely high voltage and suffers from short-circuit fault if the coupling plates on the same side are shorted due to the wearing out of the dielectric materials.

#### 2.2.4 Active Compensation Methods

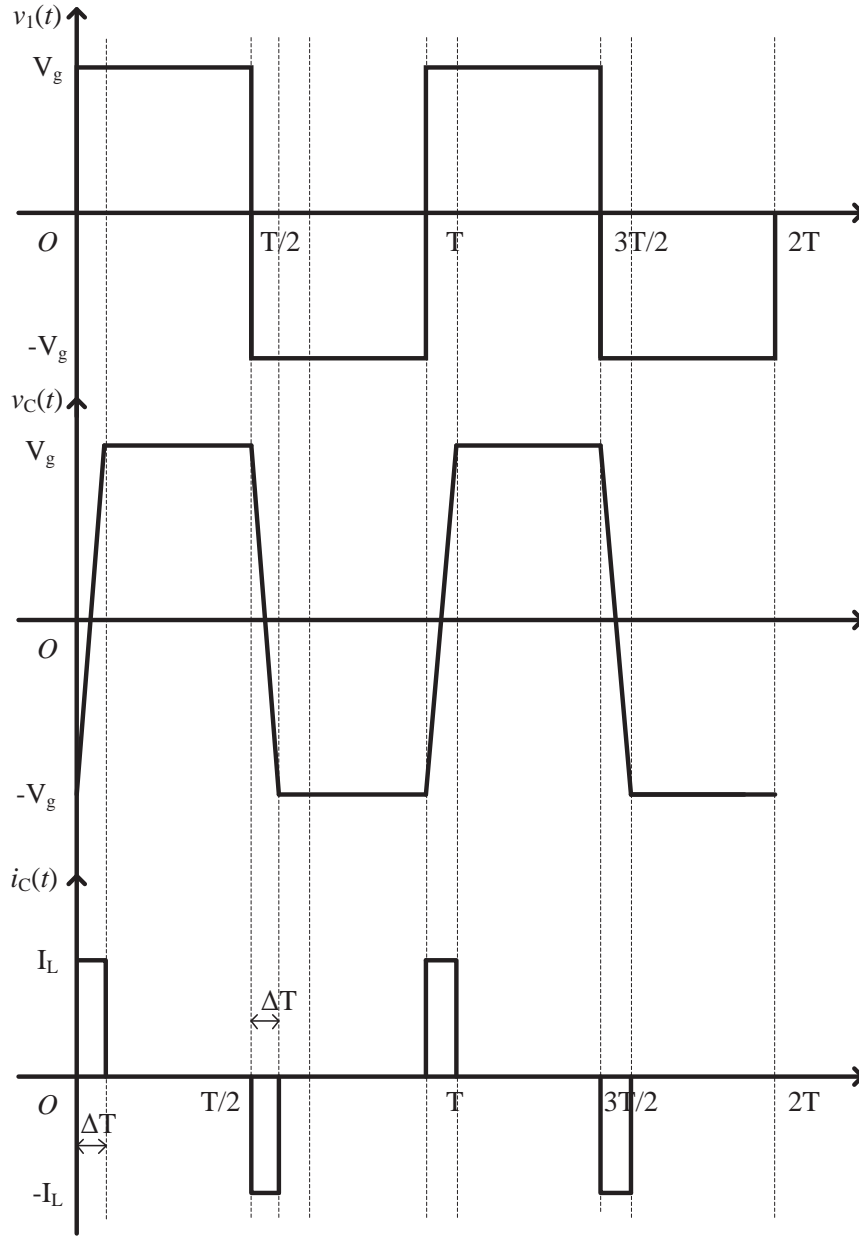
A switched capacitor network is used to compensate the reactance of the capacitive coupling interface as shown in Fig. 2-10 [64, 65]. The connection of  $C_S$  with the circuit is controlled by a full-bridge topology, which is called active negative capacitance. Compared with the conventional compensation method using inductors, the performance of this method is not affected by frequency variation since its working principle is not based on resonance.



**Fig. 2-10: Using a negative capacitor for compensation in a CPT system.**

This method is based on the operation conditions that the load current is constant and the CPT system is working in discontinuous current mode (DCM), which is different from the aforementioned compensation methods. The square waveform  $v_s$  is produced by a full-bridge inverter with a peak value of  $V_g$ .  $I_L$  is the constant load current because of the large output filter inductor  $L_f$ .  $v_1$  is the voltage across the primary side plates, and  $v_C$  is the sum of the two voltages across  $C_{C1}$  and  $C_{C2}$ . When the diodes are conducting, the load current flows through the coupling plates, charging the coupling capacitances. When the diodes are turned off, there is no current drawn from the source  $v_s$ , and the load current is freewheeled by the diode  $D_f$ .

Without the negative capacitance, the voltage across the primary side plates  $v_1$  is equal to  $v_s$ , which is a square waveform with a switching period  $T$ . Fig. 2-11 shows the typical waveforms of  $v_1$ ,  $v_C$ , and  $i_C$ . When  $v_1$  is in the positive half cycle, the diodes  $D_1$  and  $D_4$  are forward-biased and start to conduct. During this conduction period  $\Delta T$ ,  $i_C = I_L$ . The constant current  $I_L$  is charging  $C_{C1}$  and  $C_{C2}$  until the voltage  $v_C$  is equal to  $V_g$ . Then the diodes turn off and no current is drawn from the source. Similarly, when  $v_1$  is in the negative half cycle, the diodes  $D_2$  and  $D_3$  are forward-biased and start to conduct. During the conduction period  $\Delta T$ ,  $i_C = -I_L$ . The constant current  $I_L$  is charging  $C_{C1}$  and  $C_{C2}$  reversely until the voltage  $v_C$  is equal to  $-V_g$ . Then the diodes turn off and no current is drawn from the source.



**Fig. 2-11: Typical waveforms of a CPT system in DCM without compensation.**

By knowledge of the voltage and current waveforms, the use of the voltage-current relationship of a capacitor gives

$$C_c \frac{\Delta V}{\Delta T} = I_L \quad (2-16)$$



where  $C_C$  is the total effective capacitance of the two pairs of coupling plates,  $\Delta T$  is the conduction period,  $\Delta V = 2V_g$ , which is the change of the voltage  $v_C$  during time period  $\Delta T$ .

From (2-16),  $\Delta T$  can be obtained as

$$\Delta T = \frac{2C_C V_g}{I_L} \quad (2-17)$$

It is noted that when  $\Delta T \geq T/2$ , the CPT system works in continuous conduction mode (CCM). When  $\Delta T < T/2$ , the CPT system works in DCM.

Assuming 100% efficiency, the average input power is equal to the output power, which gives

$$\frac{1}{T} \int_0^T v_s(t) i_C(t) dt = I_L^2 R_L \quad (2-18)$$

From (2-17) and (2-18), the load current  $I_L$  can be obtained as

$$I_L = 2V_g \sqrt{\frac{C_C}{R_L T}} \quad (2-19)$$

The insertion of negative capacitance can increase the conduction time in each half cycle. The typical waveforms of the CPT system using one negative capacitor are shown in Fig. 2-12. It is shown that one negative capacitor increases one more conduction time in a half period. Because the CPT system operates in DCM, the following condition should be satisfied when choosing the number of the negative capacitance:

$$\Delta T(n+1) \leq \frac{T}{2} \quad (2-20)$$

where  $n$  is the number of negative capacitors.

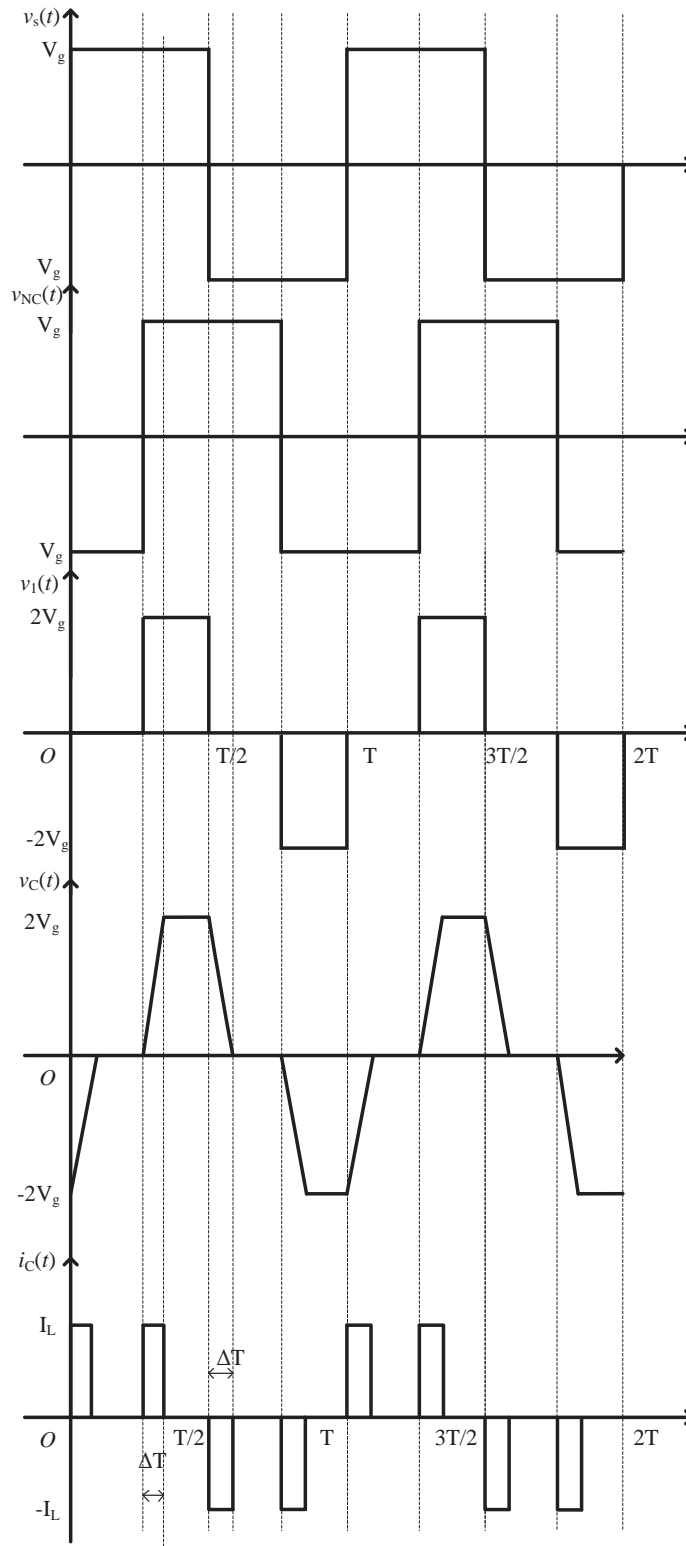


Fig. 2-12: Typical waveforms of a CPT system in DCM compensated by a negative capacitor.

Similarly, the load current compensated by  $n$  negative capacitors is

$$I_L = 2V_g \sqrt{n+1} \sqrt{\frac{C_c}{R_L T}} \quad (2-21)$$

Although this method eliminates the use of inductors, which can decrease the size and weight, it needs to use four extra switches for each negative capacitor, involving complicated control circuitry and cost.

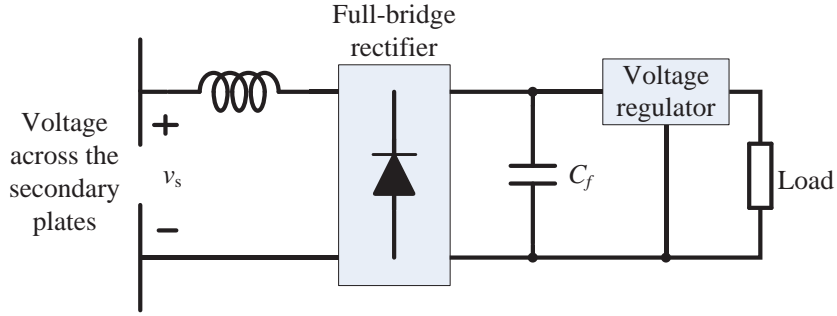
### 2.3 Power Flow Control Methods

Control is essential in any practical power supply in order to regulate the output power according to the requirements of the load, regardless of circuit parameter variations and load changes. As a contactless/wireless power transfer solution, CPT systems have to address similar regulation problems, which are particularly caused by capacitive coupling variations. In practical applications, the input voltage fluctuates due to the variations of the line voltage. In the charging process, misalignment between the coupling plates can occur. Additionally, the load may also change in operation. All these application conditions require a control method to be integrated into the system to meet the requirements of the load.

In order to address this problem, several control methods have been proposed [27, 66, 67]; all these control methods can be divided into two categories based on the position of the controller. One class of controllers is implemented on the primary side, which can be referred to as the primary side control. The other is implemented on the secondary side, which can be referred to as the secondary side control. To minimise the size of the secondary circuit, the controller on the secondary side is much simpler and easier for implementation than the one on the primary side. This feature is particularly important in some space-confined applications, like charging implanted biomedical devices. While for the primary side control, a more advanced and complicated controller can be used to make the system more stable and robust.

### 2.3.1 Voltage Regulator

Fig. 2-13 shows a CPT system with the series tuning inductor on the secondary side. The output voltage is regulated by a simple linear voltage regulator [27]. The working principle of a linear voltage regulator is similar to a voltage divider, except that it functions as a variable resistor controlled by a feedback circuit.



**Fig. 2-13: Secondary side of a CPT system with a voltage regulator.**

A full-bridge rectifier combined with an output filter capacitor  $C_f$  is used to produce a DC output voltage. Then a voltage regulator regulates the rectified and smoothed DC output to a DC voltage of a desired value. Because the linear voltage regulator is inherently a step-down converter, the output voltage from the full-bridge rectifier must be larger than the required DC level of the load. Under normal working conditions, the secondary side tuning inductor is fine-tuned to fully compensate for the coupling capacitance so as to yield maximum output power. If the working conditions change, such as variations of the coupling capacitance, change of the operating frequency, and fluctuation of the input voltage, the output voltage of the series tank will be reduced, which will prevent the voltage regulator from regulating the output voltage at the required level. To make the linear voltage regulator work properly, the designed average output voltage from the rectifier should be greater than the desired DC output voltage. Despite the simplicity and low cost of the linear voltage regulator, this control method has low efficiency and is not particularly robust. It can only work in a narrow range of working conditions, making it only suitable for a simple system without few system variations.

### 2.3.2 Modified Rectifier with Integrated Controller

Fig. 2-14 shows a simple regulation method which integrates the voltage rectification and the power flow control. The modified full-bridge rectifier consists of two upper leg controllable switching devices (MOSFET or IGBT) and two lower leg diodes. The controller switches the two upper transistors to implement rectification and power regulation according to the feedback voltage and current into the rectifier.

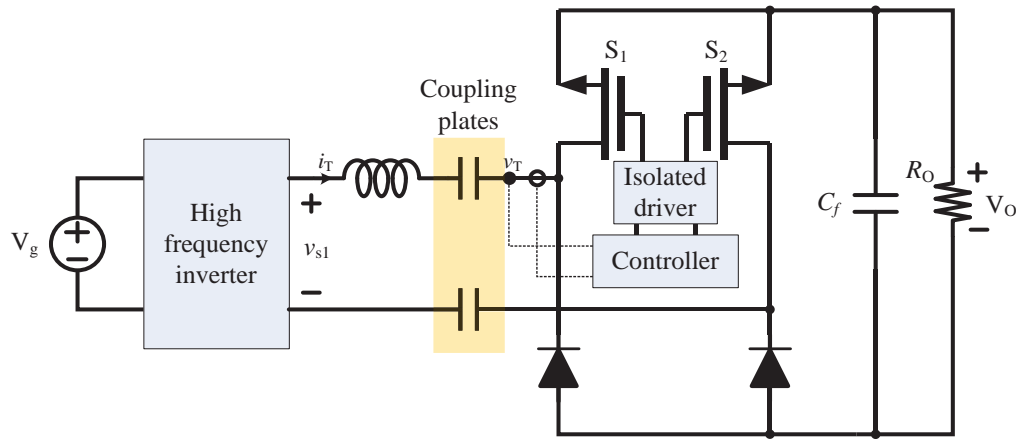


Fig. 2-14: CPT system with integrated voltage rectification and power flow control.

The output voltage  $V_O$  is compared with the two reference voltages  $V_{\text{ref}}^+$  and  $V_{\text{ref}}^-$  to determine the behaviour of the controller, which executes a hysteresis control law. When  $V_O$  is between  $V_{\text{ref}}^+$  and  $V_{\text{ref}}^-$ , the two switches  $S_1$  and  $S_2$  both perform the function of diodes. If  $V_O$  is greater than  $V_{\text{ref}}^+$ , both upper switches will be turned off to reduce the output voltage. During this period, the output voltage is supplied by the output capacitor  $C_f$ . The output voltage  $v_O$  can be expressed as

$$v_O = V_O(t_{\text{off}}) e^{-\frac{t}{R_O C_f}} \quad (2-22)$$

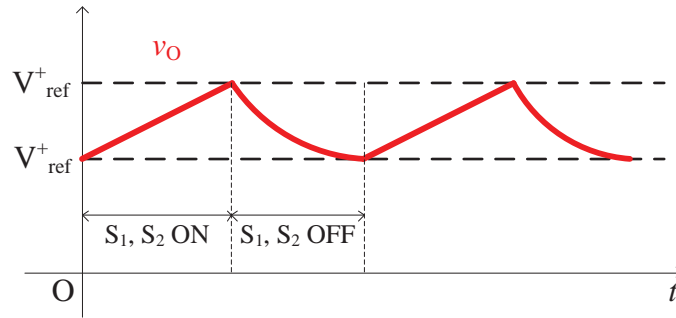
where  $V_O(t_{\text{off}})$  is the output voltage at the time when both transistors are turned off.

Under normal conditions, the maximum output voltage  $V_{O,\text{max}}$  is achieved at resonance, and can be obtained from an analysis of a DC-DC series resonant converter, which is

$$V_{O,\max} = \frac{\pi}{4} v_{s1p} \quad (2-23)$$

where  $v_{s1p}$  is the peak value of the fundamental component of the output voltage  $v_{s1}$  of the inverter.

Another feature of this control method is that it can achieve zero current switching (ZCS) during the turn-off transition of the switches, thus reducing switching loss. The direction of the current  $i_T$  into the rectifier is detected to determine which switch is turned off first. When  $i_T > 0$ , indicating the current  $i_T$  flows from the left to the right (as shown in Fig. 2-14),  $S_2$  should be turned off since the current is flowing through  $S_1$ . When  $i_T < 0$ , indicating the current  $i_T$  flows from the right to the left,  $S_1$  should be turned off first since the current is flowing through  $S_2$ . When the current  $i_T = 0$ ,  $S_2$  is then turned off. The control law is illustrated in Fig. 2-15.

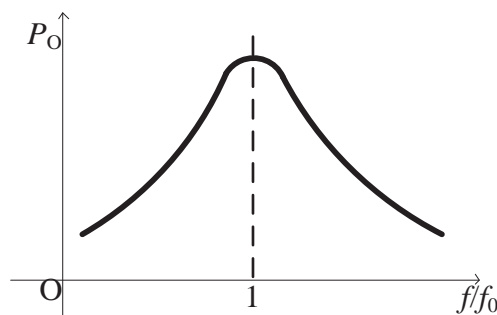


**Fig. 2-15: The output voltage waveform under the control of the modified rectifier.**

Although simple to implement, this control method also presents some drawbacks. It only works under the condition that the operating frequency and coupling capacitance are constant. When the operating frequency changes, the available maximum output voltage will be reduced. If the maximum voltage falls below the lower limit  $V_{\text{ref}}^-$ , the controller will always keep both switches on, attempting to make the output voltage increase. Since it can never reach the lower limit  $V_{\text{ref}}^-$ , the controller will fail to regulate the output voltage. With variations of the coupling capacitance, the maximum output voltage obtained will also be reduced, making the controller ineffective. Thus, this controller lacks robustness and is only effective under load change.

### 2.3.3 Soft-switched Transformer

The output voltage regulation of a resonant converter can be achieved by adjusting the ratio of its operating frequency to the resonant frequency [68, 69]. This method is also referred to as the tuning/detuning control method in IPT [70, 71]. Its working principle is based on the relationship between the output power and the ratio of both frequencies, which resembles a bell shape as shown in Fig. 2-16. When the operating frequency  $f$  is close to the resonant frequency  $f_0$ , the output  $P_O$  will increase. The control of the frequency ratio is realized by changing either the switching frequency of the converter or the resonant frequency of the resonant tank.



**Fig. 2-16: Output power versus frequency.**

One of the tuning/detuning control methods is implemented via a switched-transformer with a 1:1 turns ratio. Fig. 2-17 illustrates the schematic diagram of a CPT system based on this method. The secondary winding of the transformer  $T_C$  is connected in series with the capacitive coupling interface. The primary winding is switched by two switching devices  $S_1$  and  $S_2$ , which constitute an AC switch to control the transformer in such a way that it behaves as a variable inductor  $L_C$  (as shown in Fig. 2-18).  $L_{\text{mag}}$  denotes the magnetizing inductance, and the AC switch  $S_L$ .

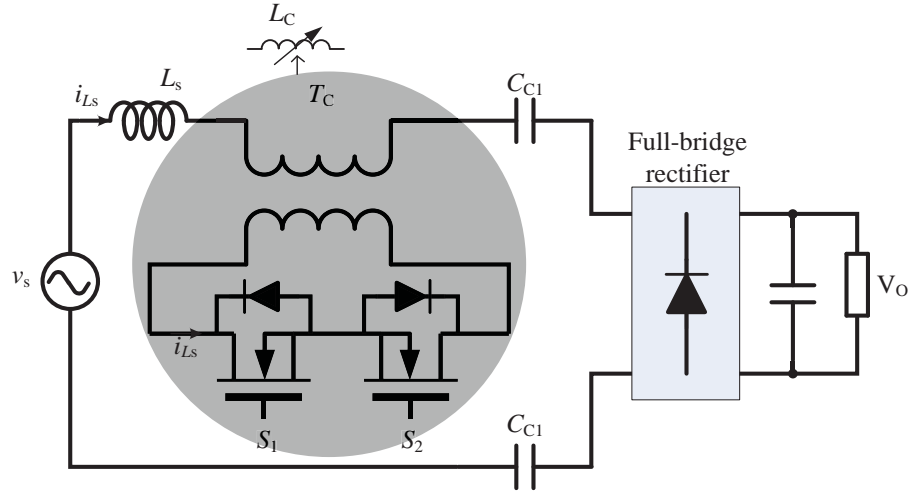


Fig. 2-17: The CPT system using soft-switched transformer control.

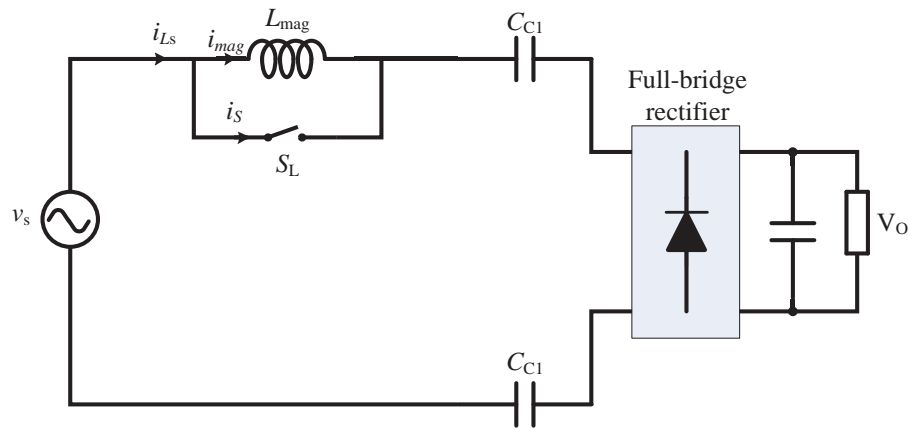


Fig. 2-18: The CPT system using soft-switched transformer control.

When the switch  $S_L$  is closed, the magnetizing inductance of the transformer  $L_{mag}$  will be shorted, which means the current through  $L_{mag}$  is clipped to a constant value, as shown in Fig. 2-19.

The flux linkage balance between the switched transformer and the equivalent inductor gives



$$\int_0^\pi L_{mag} i_{mag} d(\omega t) = \int_0^\pi L_C i_{Ls} d(\omega t) \quad (2-24)$$

From the above equation, the normalized inductor  $L_C$  with respect to  $L_{mag}$  can be obtained as

$$\frac{L_C}{L_{mag}} = 1 - \cos \theta + (0.5\pi - \theta) \sin \theta \quad (2-25)$$

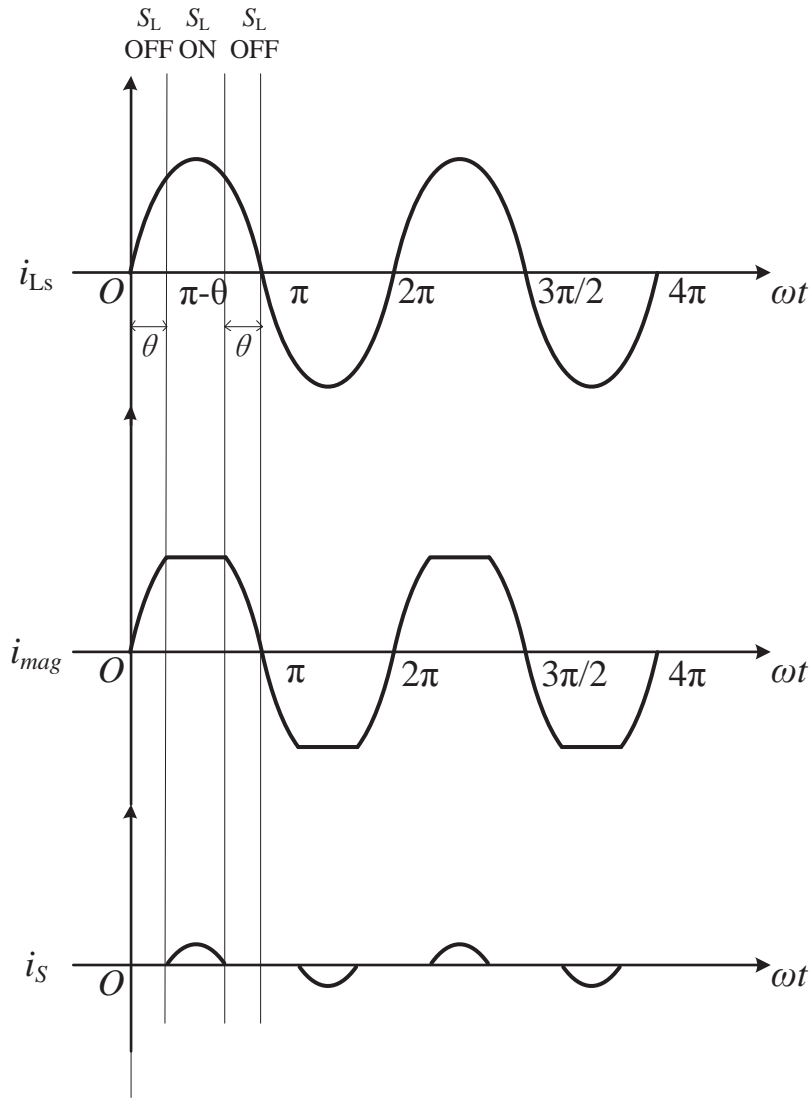
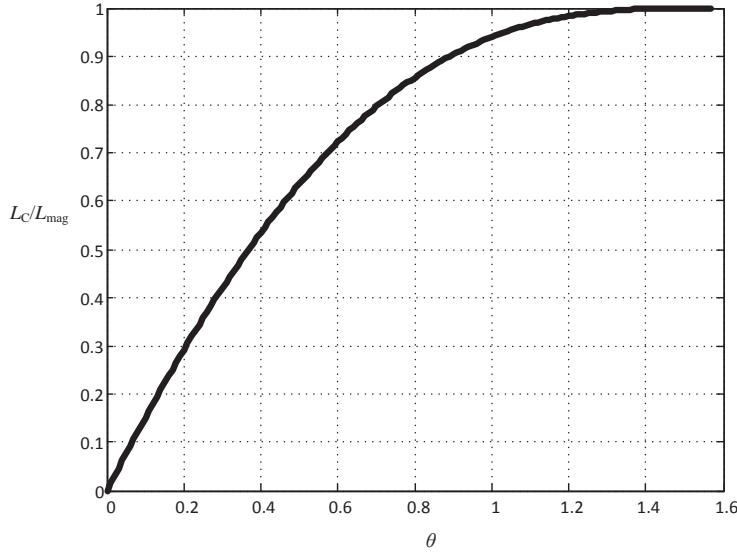


Fig. 2-19: The current waveforms of the soft-switched transformer.

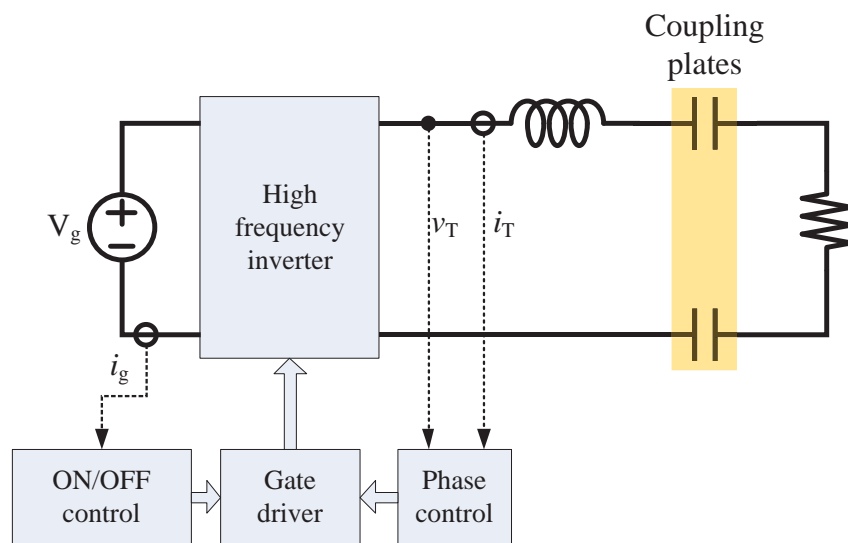


**Fig. 2-20: The normalized inductance  $L_C/L_{\text{mag}}$  versus  $\theta$ .**

Fig. 2-20 shows the curve of variation of  $L_C/L_{\text{mag}}$  with the phase shift  $\theta$ . As can be seen, the equivalent inductance  $L_C$  ranges between zero and the magnetizing inductance  $L_{\text{mag}}$ . At the normal operating point,  $L_C$  should be set to half the value of the magnetizing inductance.

#### 2.3.4 Multi-period Pulse-width Modulation

A combination of frequency and duty cycle control has been used in a CPT system, which can regulate the output power while maintaining high efficiency [72, 73]. The system contains an automatic frequency controller and a duty cycle controller. The frequency controller adjusts the frequency to maintain the phase difference between the tank voltage and current, which is essential to for the system to maintain ZVS condition. The duty cycle controller changes the ON time of switches to control the input power supplied by the source according to the load requirements. The schematic diagram of the system is illustrated in Fig. 2-21. The phase control detects the tank voltage and current, and compares their phase angles. The frequency can be shifted up/down according to the sign of the phase difference, which keeps the phase angle at a fixed value. The ON/OFF control monitors the average value of the input current, which is then compared with a reference value. When it goes above the



**Fig. 2-21: The CPT system with multi-period pulse width modulation.**

reference value, the ON/OFF controller switches off the transistors to block the input power. When it goes below the threshold value, the ON/OFF controller switches the transistors ON to allow the input energy to flow into the tank. Therefore, the output power is effectively regulated. However, the drawback of this method is the variation of the operation frequency requires more complicated filter design to meet EMI requirements.

## 2.4 Summary

An overview of existing compensation methods and power flow controls is given in this chapter. Their pros and cons were discussed and reviewed.

Regarding compensation design of CPT systems, the method using a single series inductor is the most widely used compensation network in CPT systems due to its simplicity and low cost. However, this method suffers from the open-circuit fault when the secondary side coupling plates are removed suddenly, which is a common scenario in CPT charging applications. The open-circuit will interrupt the current flowing through the series compensating inductor, which generates ultra-high voltage spikes exhibiting safety hazards such as causing failure of the insulating materials coated on the coupling plates. The compensation method based on transformation networks eliminates the use of the series tuning inductor, but it requires a significant number of reactive components, which

will increase the size and cost of system. In addition, the capacitors in the transformation network have to endure high voltages, which will cause failure of the system if the coupling plates on the same side are shorted accidentally. Another compensation method uses a switched capacitor to imitate a negative capacitor to increase the power transfer capability, which requires additional control circuitry. The switching frequency of the full-bridge, which controls the negative capacitor, needs to be higher than the switching frequency of the main converter. At high frequency CPT applications, this method faces switching timing issue caused by the negative capacitor.

To maintain a constant output voltage of a CPT system, a power flow controller is always necessary to regulate the system effectively regardless of the circuit component tolerance, the load change and coupling variations. The simplest way is to use a voltage regulator on the secondary load side. However, this method suffers from low efficiency. A novel control method, which integrates the power flow controller into the secondary side rectifier, can regulate the output with increased efficiency. However, it is unable to provide effective control when the input energy into the rectifier cannot provide enough power to sustain the output voltage required by the load, such as when the input voltage is reduced or the coupling condition varies to the extent that the received power by the secondary side is diminished. Two frequency control methods are also proposed to control the output power. One is based on a variable inductor, which is not suitable for high frequency operation since the core losses of the variable inductor deteriorate the entire system efficiency. The multi-period pulse-width method changes the operating frequency, which will bring EMI/EMC problem and increase the complexity of the filter design since a range of frequencies are involved.

## **3 Study of Soft-switching Resonant Power Converters for CPT Systems**

---

### **3.1 Introduction**

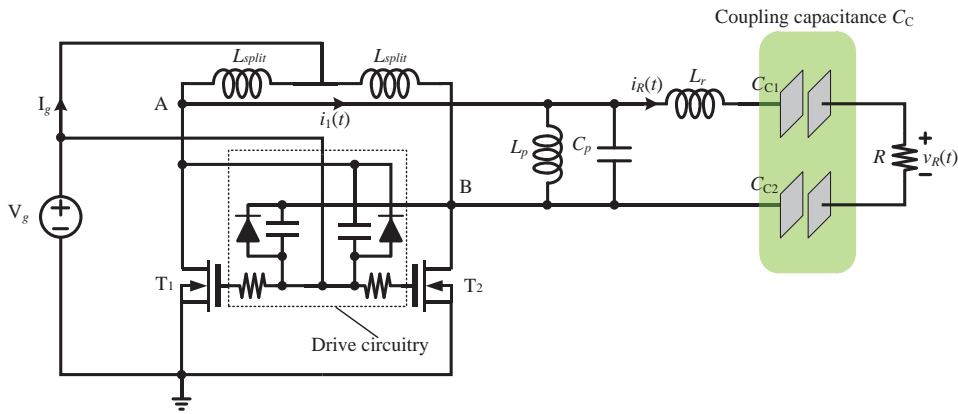
Similar to IPT systems which require suitable power converters to generate high quality sinusoidal current to drive the coupling coils, CPT systems need power converters suited to generate high quality sinusoidal voltage to drive the coupling plates to transfer power without electrical contacts. However, the operating frequencies of CPT systems ( $\sim$ MHz) are much higher than IPT systems ( $\sim$ kHz). The operating frequencies of IPT systems are limited to a relatively low due to the increased core losses and conduction loss caused by the hysteresis effect of ferrite materials and the skin effect of the wires used extensively for coil windings. On the contrary, in CPT systems, high operating frequencies can reduce the equivalent series resistance of the coupling capacitance formed by coupling plates coated with dielectric materials. Furthermore, high operating frequencies can reduce the impedance introduced by the coupling capacitance, which means the tuning inductors for compensation can be very small, making it possible to use air core inductors without core losses. Considering these benefits brought by high frequencies, it is advantageous and preferable to select power converters suitable for operation at high frequencies.

This chapter investigates three power converters suitable for high frequency operation, which are used as the primary side converters for CPT systems. The basic configurations and working principles of these converters are described. Advantages and disadvantages of CPT systems based on the three topologies are discussed and comparison among them

regarding coupling misalignment, circuit component selection, and applicable control schemes is provided.

## 3.2 Autonomous Current-fed Push-pull Converter

### 3.2.1 Circuit Description



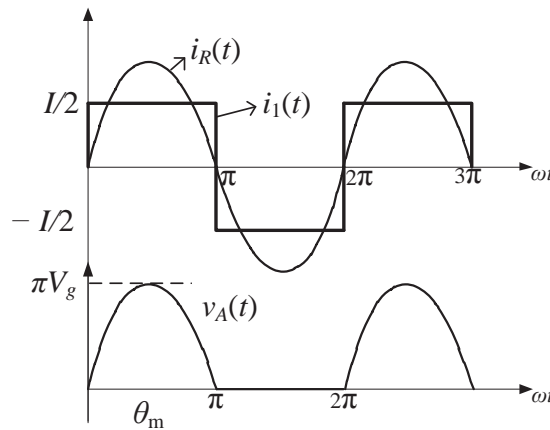
**Fig. 3-1: Schematic diagram of a CPT system based on an autonomous current-fed push-pull converter.**

The autonomous current-fed push-pull converter is suitable for high frequency operation due to its internal driver circuitry which maintain ZVS condition automatically. Fig. 3-1 shows a CPT system based on this converter. As can be seen, the gate drive signals come from the main resonant tank instead of external driver controllers. At steady state, the internal drive circuitry dictates the two switching devices switch automatically under ZVS condition with a complementary 180 degree conduction. The avoidance of using external driver controllers makes this converter cost-effective and simple to implement. Two large inductors ( $L_{split}$ ) serve the purpose of splitting the input DC current  $I_g$  into two equal parts, which drive the resonant tank by repetitively switching the two transistors. Another feature of the converter is that it can realize automatic start-up. When the converter is powered up, the current through the two phase-splitting inductors begins to rise. One transistor will reach ON state faster than the other due to the manufacturing tolerances in real transistors. Assuming that the transistor  $T_1$  is switched on first, the voltage at point A is going to be close to the ground reference, which will aid the turn-off transition of the transistor  $T_2$  because the gate-to-source voltage of  $T_2$  is closer to zero. This positive feedback can speed

up the turn-off transition of  $T_1$ . A similar process occurs when the transistor  $T_2$  is being turned on when the tank resonant response swing the voltage at point B to ground reference.

### 3.2.2 Analysis of Operation

As shown in Fig. 3-1, the phase-splitting inductors  $L_{\text{split}}$  divide the input DC current  $I_g$  into two identical dc current  $I_g/2$ . Both transistors are switched alternatively under ZVS condition without detection circuits and external controller. It is noted that in a CPT system based on the autonomous current-fed push-pull converter, two cascaded resonant tanks exist. One is the parallel resonant tank as in the conventional current-fed push-pull converter. The other is a series resonant tank consisting of a tuning inductor and the capacitive coupling interface. From the perspective of two cascaded resonant tank configuration, it can be seen that the output of the parallel resonant drives the series tank.



**Fig. 3-2: Selected voltage and current waveforms in the autonomous current-fed push-pull converter.**

Typical current and voltage waveforms are depicted in Fig. 3-2. The sinusoidal approximation method is used to derive equations governing the characteristics of the converter at steady state. A high quality factor of the tank is assumed, so the load current  $i_R(t)$ , which also flows through the series tank, is expressed as

$$i_R(t) = I_R \sin(\omega t + \varphi) \quad (3-1)$$

where  $I_R$  is the peak amplitude of the load current,  $\varphi$  is the phase shift respective to current  $i_1(t)$ .

Then the output voltage  $v_R(t)$  can be expressed as

$$v_R(t) = I_R R \sin(\omega t + \varphi) \quad (3-2)$$

The voltage across the capacitor  $C_R$  in the parallel tank is imposed on the transistor that is turned off in each half period. For example, when the transistor  $T_1$  is OFF and  $T_2$  ON, the voltage across  $T_1$   $v_A(t)$  is equal to the output  $v_R(t)$ ; when  $T_1$  is ON and  $T_2$  OFF,  $v_A(t)$  is shorted to the ground. Since the transistor is turned on at zero voltage crossing,  $v_A(T/2)$  should be equal to zero, that is

$$v_A\left(\frac{T}{2}\right) = v_R\left(\frac{T}{2}\right) = I_R R \sin(\pi + \varphi) = 0 \quad (3-3)$$

which indicates that the phase shift angle  $\varphi$  equals zero.

Due to the filtering of resonant tanks with high quality factors, the fundamental component of  $i_1(t)$  should be equal to the load current  $i_R(t)$ , which gives

$$I_R = \frac{4}{\pi} \cdot \frac{I_g}{2} = \frac{2}{\pi} I_g \quad (3-4)$$

Because the converter is operating under ZVS condition, thus eliminating switching losses, 100% efficiency can be assumed without much sacrifice of accuracy. Equating the input power with the output power yields

$$V_g I_g = \frac{1}{2} I_R^2 R \quad (3-5)$$

From (3-4) and (3-5), the relationship between the output voltage and input DC voltage can be obtained:

$$\frac{V_R}{V_g} = \pi \quad (3-6)$$

The equivalent resistance seen by the input DC voltage  $V_g$  is



$$\frac{V_g}{I_g} = \frac{2}{\pi^2} R \quad (3-7)$$

The calculation of device stresses in the autonomous current-fed push-pull converter is quite straightforward. The maximum voltage across the transistor is the peak voltage across the parallel resonant tank, which is

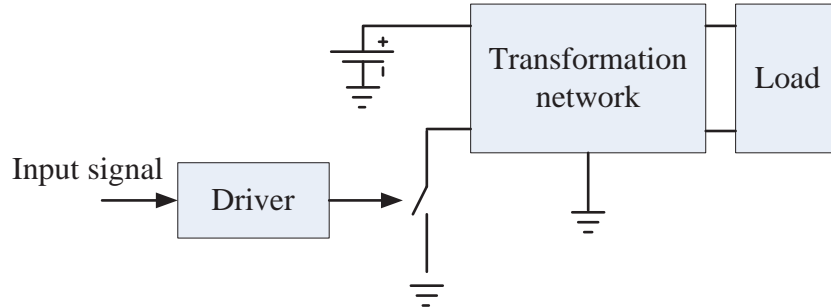
$$v_{ds,\max} = \pi V_g \quad (3-8)$$

The current through the transistor is almost constant, that is

$$i_{ds,\max} = \frac{I_g}{2} \quad (3-9)$$

### 3.3 Single-ended Class E Power Converters

#### 3.3.1 Circuit Description



**Fig. 3-3: Block diagram of single-ended power amplifier.**

Single-ended power amplifiers are designed to improve efficiency at high operating frequencies up to tens of MHz [74]. Fig. 3-3 shows the block diagram of a single-ended switching-mode amplifier. Using a single switch element avoids the dead-time issues suffered by converters that employ a pair or multiple pairs of switches. In the family of single-ended amplifiers, the class E power amplifier is widely adopted by the radio frequency industry [75-82]. The circuit components of a class E converter are arranged in such a way that the switching device is turned on under zero voltage switching (ZVS) condition to achieve a very high efficiency, yielding negligible switching losses and EMI.

Fig. 3-4 shows a CPT system based on a class E converter. As can be seen, the capacitive coupling interface of a CPT system ( $C_{C1}$  and  $C_{C2}$ ) functions as two tank capacitors in series. To achieve the optimum operation, the duty cycle of the switching signal is set to 0.5 [83]. The voltage source, in series with a large inductor  $L_1$ , behaves as a DC current source. When the switch is turned on, the constant current  $I_g$  is shorted and no external energy is fed into the resonant tank, which consists of  $L_r$ ,  $C_{C1}$ , and  $C_{C2}$ . This tank can be called a free oscillation tank. When the switch is turned off, the external energy flows into the resonant tank consisting of  $C_1$ ,  $L_r$ ,  $C_{C1}$ , and  $C_{C2}$ . This tank can be called an energy injection tank. Both resonant tanks are damped by the load resistance  $R$ . If a DC output voltage is required,  $R$  represents the equivalent AC resistance seen from the rectifier. The quality factor of the resonant tank should be high enough to generate pure sinusoidal current waveforms.

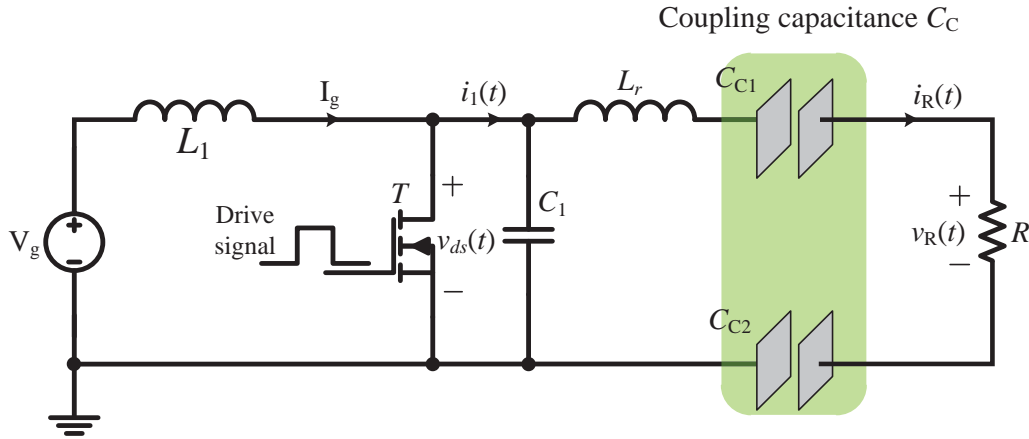


Fig. 3-4: Basic configuration of a CPT system based on a class E converter.

### 3.3.2 Analysis of Operation

To evaluate the steady-state characteristics of the CPT system based on a class E topology, the sinusoidal approximation is also used to derive key equations of the system. This means the derived results are under the assumption that the quality factor of the tank is sufficiently high and the system is working in continuous conduction mode. At steady state, the repetitive switching generates a series of current pulses with a duty cycle of 0.5, which is designated as  $i_1(t)$  in Fig. 3-4.

Waveforms of the current  $i_1(t)$  and the tank current  $i_R(t)$  are illustrated in Fig. 3-5. It is noted that  $i_1(t)$  is an imaginary current inclusive of the currents through the output capacitance of the transistor and the capacitor in parallel with it, both of which are included into  $C_1$ .

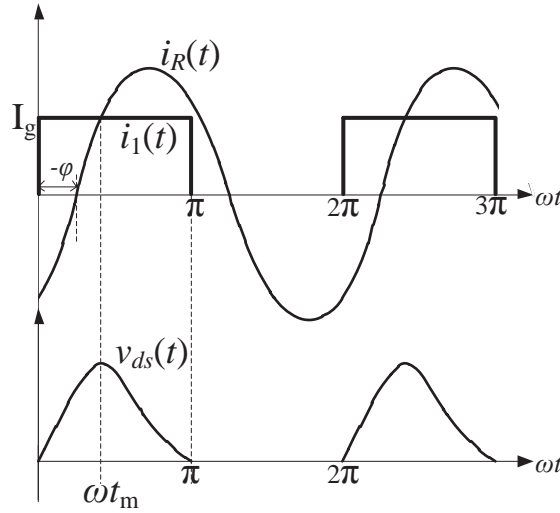


Fig. 3-5: Waveforms of  $i_1(t)$  and  $i_R(t)$ .

The current through the tank inductor  $L_r$  is assumed to be sinusoidal, expressed as

$$i_R(t) = I_R \sin(\omega t + \varphi) \quad (3-10)$$

where  $I_R$  is the load current amplitude,  $\varphi$  is the phase shift relative to the fundamental component of the current  $i_1(t)$  of a square waveform.

The input current through  $L_1$  is approximated as a DC current of constant value  $I_g$ , so the voltage across the transistor is given by

$$v_{ds}(t) = \frac{1}{C_1} \int_0^t (I_g - i_R(\tau)) d\tau \quad (3-11)$$

Substituting (3-10) into (3-11) gives

$$\begin{aligned}
 v_{ds}(t) &= \frac{1}{C_1} \int_0^t (I_g - I_R \sin(\omega\tau + \varphi)) d\tau \\
 &= \frac{1}{\omega C_1} \int_0^t (I_g - I_R \sin(\omega\tau + \varphi)) d\omega\tau \\
 &= \frac{1}{\omega C_1} [\omega t I_g - I_R (\cos \varphi - \cos(\omega t + \varphi))]
 \end{aligned} \tag{3-12}$$

Because at steady-state operation there is no average DC voltage drop across the choke  $L_1$  over a period, the DC component of  $v_{ds}(t)$  should be equal to the input DC voltage  $V_g$ , which is

$$\begin{aligned}
 V_g &= \frac{1}{2\pi} \int_0^{2\pi} v_{ds}(\theta) d\theta \\
 &= \frac{1}{\omega C_1} \left[ \frac{\pi}{4} I_g - \left( \frac{\cos \varphi}{2} + \frac{1}{\pi} \sin \varphi \right) I_R \right]
 \end{aligned} \tag{3-13}$$

where  $\theta = \omega t$ .

From (3-13),  $C_1$  can be expressed as

$$C_1 = \frac{1}{\omega V_g} \left( \frac{\pi}{4} I_g - \left( \frac{\cos \varphi}{2} + \frac{1}{\pi} \sin \varphi \right) I_R \right) \tag{3-14}$$

For a given coupling capacitance  $C_c$ , the quality factor  $Q_L$  of the energy injection tank is given by

$$Q_L = \frac{C_c + C_1}{\omega C_c C_1 R} \tag{3-15}$$

The tank inductor  $L_r$  can be obtained as

$$L_r = \frac{Q_L R}{\omega} \tag{3-16}$$

The high efficiency operation of the class E converter is achieved by satisfying two conditions. One is the ZVS condition requiring that when the switch is turned on,  $v_{ds}(t)$  should be zero at  $t=T/2$ , so

$$v_{ds}\left(\frac{T}{2}\right)=0 \quad (3-17)$$

The other is at the instant of  $t=T/2$ , the derivative of  $v_{ds}(t)$  should be equal to zero, that is

$$\left.\frac{dv_{ds}(t)}{dt}\right|_{t=\frac{T}{2}}=0 \quad (3-18)$$

These two conditions correspond to the two relationships below

$$\begin{cases} I_g = \frac{2 \cos \varphi I_R}{\pi} \\ I_g = -I_R \sin \varphi \end{cases} \quad (3-19)$$

which yields

$$\tan \varphi = -\frac{2}{\pi} \quad (3-20)$$

From (3-20), the phase shift  $\varphi$  can be obtained:

$$\varphi = -0.56691(\text{in radians}) \quad (3-21)$$

Assuming 100% efficiency, the input power is given by

$$P_{IN} = V_g I_g \quad (3-22)$$

The average output power received by the load is given by

$$P_{OUT} = \frac{I_R^2}{2} R \quad (3-23)$$

Combining (3-22), (3-23), and (3-19) gives

$$\frac{V_R}{V_g} = \frac{4 \cos \varphi}{\pi} = 1.076 \quad (3-24)$$

$$\frac{V_g}{I_g} = \frac{\pi^2}{8 \cos^2 \varphi} R = 1.7337 R \quad (3-25)$$

where  $V_R$  is the peak amplitude of the output voltage  $v_R(t)$  across  $R$ .

From (3-14), (3-19), and (3-25),  $C_1$  can be calculated:

$$C_1 = -\frac{2 \sin(2\varphi)}{\omega \pi^2 R} \quad (3-26)$$

From (3-24) and (3-25), it can be seen that the conversion ratio of the output voltage to the input voltage is slightly larger than one, meaning that class E topology has almost no voltage boost capability. The DC equivalent resistance presented by the tank to the DC power supply is 1.7337 times larger than the tank AC resistance  $R$ .

Before evaluating the device stress at steady-state operation, the time instants when the maximum voltage and current imposed on the transistor need to be determined. The directions of the voltages and currents are indicated in Fig. 3-4. When the switch is turned off, the difference between the input DC current  $I_g$  and the tank current  $i_R(t)$  will flow into the shunt capacitor  $C_1$ , which produces a voltage drop  $v_{ds}(t)$  across the switch. When  $I_g$  is larger than  $i_R(t)$ ,  $v_{ds}(t)$  keeps increasing until they are equal, then starts to fall down because the current into  $C_1$  becomes negative and starts discharging the capacitor. Therefore, the peak voltage across the switch occurs at  $t_m$  when  $I_g$  is equal to the load current  $i_R(t)$ , which gives

$$I_g = i_R(t_m) = I_R \sin(\omega t_m + \varphi) \quad (3-27)$$

$t_m$  can be obtained by substituting (3-19) into (3-27) as

$$t_m = \frac{1}{\omega} \left( \arcsin\left(\frac{2}{\pi} \cos \varphi\right) - \varphi \right) \quad (3-28)$$

From (3-12) and (3-28), the peak voltage across the transistor can be obtained:

$$\begin{aligned} v_{ds,\max} &= V_g \frac{\left(\frac{2}{\pi} \omega t_m - 1\right) \cos \varphi + \cos(\omega t_m + \varphi)}{-\frac{1}{\pi} \sin \varphi} \\ &= 3.562 V_g \end{aligned} \quad (3-29)$$

The peak current through the transistor occurs when the tank current swings to the negative peak value, which is

$$\begin{aligned} i_{s,\max} &= I_g + I_R = \left(1 - \frac{1}{\sin \varphi}\right) I_g \\ &= 2.862 I_g \end{aligned} \quad (3-30)$$

## 3.4 Voltage-fed Half Bridge Converter

### 3.4.1 Circuit Description

The voltage-fed resonant converters based on bridge topology have two main categories: one is a full-bridge topology, and the other a half-bridge topology. One major difference between the two is the output voltage waveforms generated. The full-bridge topology generates a full square waveform with a positive peak value of  $V_g$  and a negative peak value of  $-V_g$ , while the half-bridge topology generates a half square waveform with a peak value of  $V_g$ . Although the CPT system based on the half-bridge topology produces an output voltage with a smaller magnitude due to the filtering of the resonant tank, it requires fewer switches and simpler gate drivers. Considering the simplicity and cost-effectiveness of CPT systems, the half-bridge topology is more suitable for CPT systems at high frequencies. Fig. 3-6 shows a CPT system based on a half-bridge topology. Two switches  $S_1$  and  $S_2$  are turned on/off alternatively, with a dead time inserted between the ON signals for the two switches to prevent shoot-through failure. The inductor  $L_r$  and the capacitive coupling interface form a series resonant tank, which can filter out the DC component of the voltage  $v_s$  at the switching node. If a DC output voltage is required, a full-bridge rectifier combined with a capacitive filter can be used.

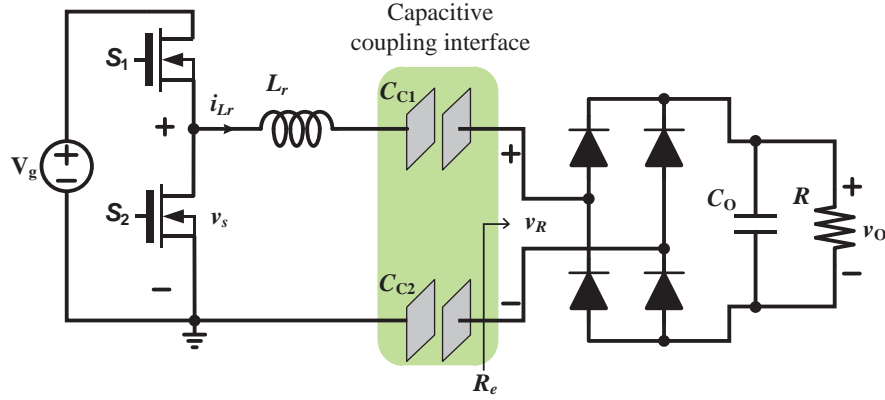


Fig. 3-6: A CPT system based on a half-bridge converter.

### 3.4.2 Analysis of Operation

The analysis of the system is also based on the sinusoidal approximation, which assumes the quality factor  $Q$  of the series resonant tank is high enough to have a good filtering effect. Then the tank current can be seen as a purely sinusoidal waveform.

Given a load resistance  $R$ , which can also represent the equivalent resistance exhibited by the rectifier, the operating frequency  $f$  is given by

$$f = \frac{1}{2\pi Q C_C R} \quad (3-31)$$

In practical systems, the value of  $L_r$  is chosen to be slightly bigger than the value at resonance with  $C_C$ , which makes the series resonant tank present an inductive impedance to the half-bridge inverter. Thus, the inductor can be divided into two parts. One part is used for the resonance with the capacitive coupling interface; the other part contributes to the lagging current required to achieve ZVS condition.

The part of  $L_r$  which is at resonance with  $C_C$  is calculated by

$$L_{ra} = \frac{1}{\omega C_C} \quad (3-32)$$

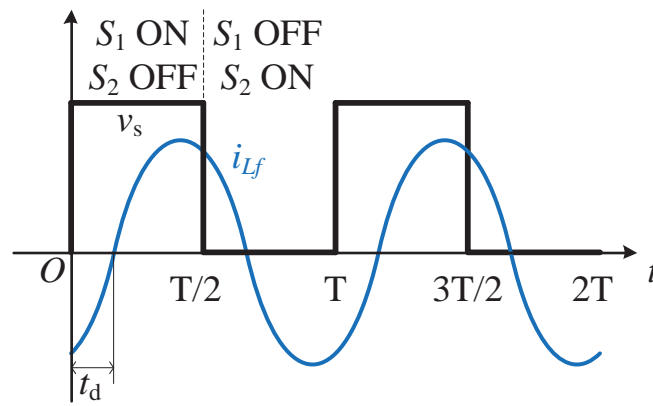


Assuming the time by which the tank current is lagging the switching node voltage  $v_s$  of the inverter is  $t_d$ , the part of  $L_r$  which contributes to this lagging can be calculated by

$$L_{rb} = \frac{R \arctan(\omega t_d)}{\omega} \quad (3-33)$$

Then the tank inductor is the sum of the two parts, which is

$$L_r = L_{ra} + L_{rb} \quad (3-34)$$



The input power can be obtained by

$$P_{IN} = \frac{1}{\pi} V_g I_{L_r} \cos(\omega t_d) \quad (3-35)$$

where  $I_{L_r}$  is the peak value of the current flowing through the tank.

The current through the tank can be expressed as

$$\mathbf{I}_{L_r} = \frac{\mathbf{V}_s}{R + jR \tan(\omega t_d)} \quad (3-36)$$

The output power received by the load is

$$\begin{aligned}
 P_O &= \frac{1}{2} \|\mathbf{I}_{L_f}\|^2 R \\
 &= \frac{1}{\pi} \frac{V_g I_{L_f}}{\sqrt{1 + (\tan(\omega t_d))^2}}
 \end{aligned} \tag{3-37}$$

The ratio of the fundamental component of the voltage  $v_R$  into the rectifier to the fundamental component of the switching node voltage of the half-bridge inverter is

$$\frac{v_{R1}}{v_{s1}} = \frac{I_{L_r} R}{\frac{2}{\pi} V_g} = \frac{1}{\sqrt{1 + (\tan(\omega t_d))^2}} \tag{3-38}$$

Since  $v_{R1}=4V_O/\pi$ ,  $v_{s1}=2V_g/\pi$ , the ratio between the output voltage  $V_O$  and the input voltage  $V_g$  is

$$\frac{V_O}{V_g} = \frac{1}{2\sqrt{1 + (\tan(\omega t_d))^2}} \tag{3-39}$$

The maximum voltage stress  $v_{ds,\max}$  across the switch occurs when the switch is turned off, which is

$$v_{ds,\max} = V_g \tag{3-40}$$

The maximum current stress  $i_{ds,\max}$  through the switch is the peak value of the tank current, which is

$$i_{ds,\max} = \frac{2}{\pi} \frac{V_g}{R \sqrt{1 + \tan^2(\omega t_d)}} \tag{3-41}$$

As can be seen, the half-bridge topology has a low voltage boost ratio. However, the switch is subject to a relatively low voltage stress.

### 3.5 Comparison of the Three Resonant Converters

#### 3.5.1 Circuit Components

The class E topology, the autonomous push-pull topology, and half-bridge topology all require resonant tanks to realize DC-AC conversion and ZVS switching. The CPT system based on the autonomous push-pull topology requires two resonant tanks. One is a parallel tank and the other a series tank to compensate for the capacitive coupling interface. The CPT system based on the class E topology requires one inductor and one capacitor to form resonant tanks along with the capacitive coupling interface. The CPT system based on the half-bridge topology requires one inductor to constitute a resonant tank with the capacitive coupling interface. The key circuit components are listed in Table 3-1. As can be seen, the half-bridge topology requires the least number of reactive components.

**Table 3-1: Key component number for three topologies**

Number of components	Autonomous topology	Class E topology	Half-bridge topology
<b>Inductor</b>	4	2	1
<b>Capacitor</b>	3	1	0
<b>Switching device</b>	2	1	2

Table 3-2 shows the specifications of CPT systems based on the three converters. All the CPT systems use the same coupling structure with a total effective coupling capacitance of  $C_C$ . Design equations of other parameters for the three converters are listed in Table 3-3. It shows that to deliver the same amount of power, the class E topology requires the highest input voltage and a slightly larger resonant inductor. However, in the autonomous topology, the circuit has two resonant tanks with an internal drive circuitry. This requires more circuit elements than the class E topology, which increases the system volume. The half-bridge topology needs to consider the dead-time issue as any other converters based on bridge topology, which limits the upper boundary of the switching frequencies.

Table 3-2: CPT system specifications

Parameter	Value
Input voltage $V_g$	20 V
Operating frequency $f$	2 MHz
Load Resistance $R$	50 $\Omega$
Total coupling capacitance $C_c$	225 pF

Table 3-3: Parameters of three topologies

Parameter	Class E topology	Autonomous topology	Half-bridge topology
Input voltage $V_g$	$\sqrt{1.7337RP_{in}}$	$\sqrt{0.2026RP_{in}}$	$\sqrt{4RP_{in}}$
Series resonant inductor $L_r$	$\frac{1.1525R}{\omega} + \frac{QR}{\omega}$	$\frac{QR}{\omega}$	$\frac{QR}{\omega}$
Voltage stress across transistor	$3.562\sqrt{1.7337RP_{in}}$	$\pi\sqrt{0.2026RP_{in}}$	$2\sqrt{RP_{in}}$
Maximum current through transistor	$2.862\frac{\sqrt{P_{in}}}{3.562\sqrt{1.7337R}}$	$\frac{1}{2}\frac{\sqrt{P_{in}}}{\pi\sqrt{0.2026R}}$	$\frac{\pi}{2}\frac{\sqrt{P_{in}}}{\sqrt{R}}$

### 3.5.2 Effects of Coupling Capacitance

In practical CPT systems, due to misalignment between the two pairs of the coupling plates and variation of the characteristics of dielectric materials coated on them, the coupling capacitance will change during operation. Fig. 3-7 and Fig. 3-8 show the effects of coupling variation on the converter output power and efficiency. From Fig. 3-7, the output power of the CPT systems based on the three topologies dropped when coupling capacitance decreased. When the coupling capacitance increased, only the CPT system based on the autonomous push-pull topology can work properly since it can automatically adjust operating frequency to achieve soft switching. The other two cannot maintain ZVS

condition, which generates noise to make system unstable. Fig. 3-8 shows that all three topologies can sustain reasonably high efficiency under the variation of coupling capacitance as long as the resonant tank presents an inductive impedance. As can be seen, the class E topology can achieve the highest efficiency among the three.

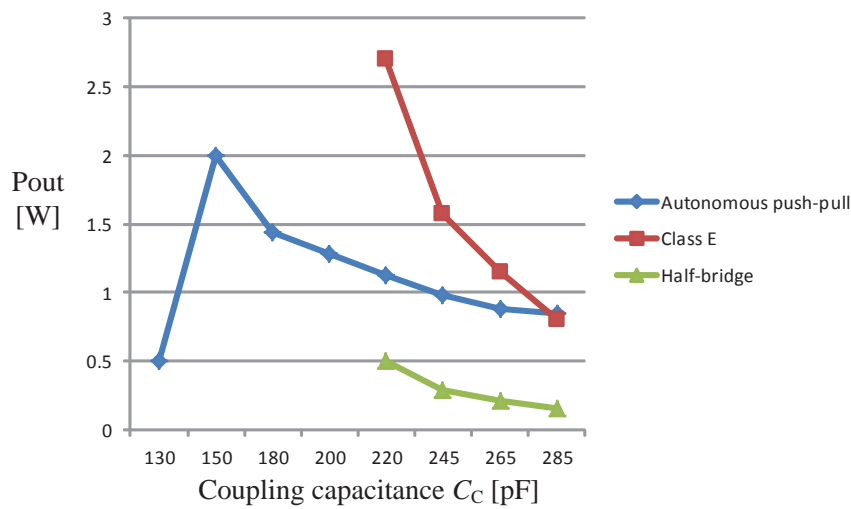


Fig. 3-7: The output power versus coupling capacitance for the three topologies.

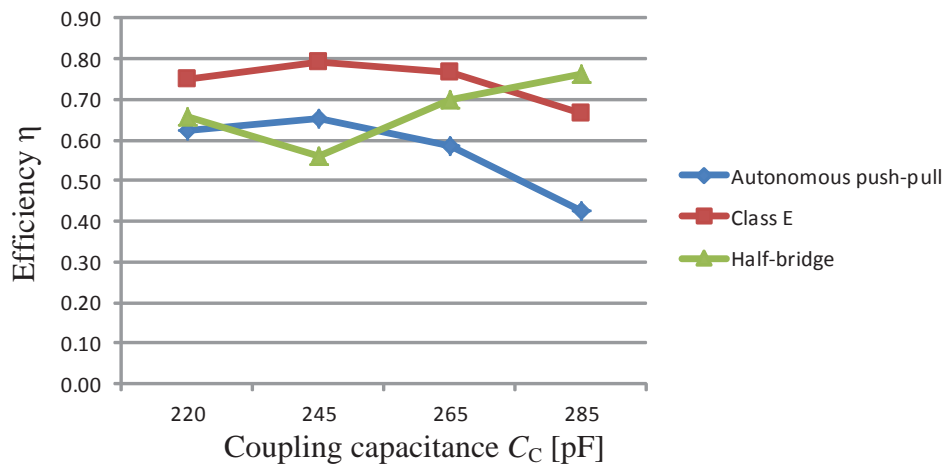


Fig. 3-8: The efficiency versus coupling capacitance for the three topologies.

### 3.5.3 Control Schemes

The output power changes when the load or coupling capacitance varies. It is necessary to have a controller to maintain a constant output voltage for most applications. The main advantage of the autonomous topology is that it requires no external drive circuit and the operating frequency is dictated by the parallel resonant tank. But the problem with this topology is that it offers no control of the operating frequency. If the values of the tank elements change, the operating frequency would change correspondingly. However, the amplitude control for the autonomous topology is possible. A DC-DC converter can be added at the input of the converter to provide amplitude control. Compared with the autonomous topology, the class E and half-bridge topologies offer more flexibility of control. Both frequency and amplitude control schemes can be implemented by duty cycle control within a certain range.

### 3.6 Summary

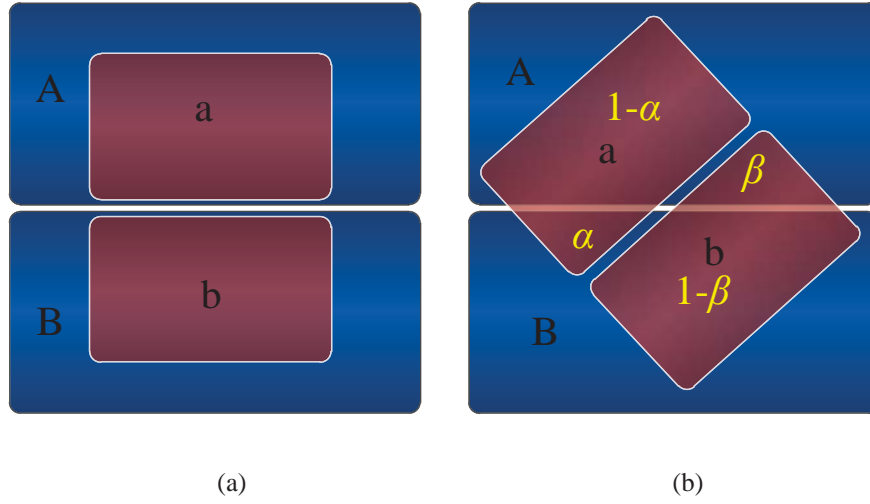
This chapter has compared the performance of CPT systems based on autonomous push-pull, Class E, and half-bridge topologies. The working principles of the three converter topologies were briefly discussed and detailed analyses undertaken. It was found that the Class E converter topology could produce higher power within a specified range of the coupling capacitance. But when the coupling capacitance deviated from the designed value, the efficiency quickly dropped. The autonomous converter can maintain a relatively high efficiency within a wider range of the variations of the coupling capacitance, since the operating frequency is adjusted automatically according to the change of the resonant tank. However, its output power drops more quickly at lower coupling capacitance. This means a trade-off between the output power and system power efficiency has to be made in selecting the power converter for a CPT system.

## 4 Modelling the Capacitive Coupling Interface

---

### 4.1 Introduction

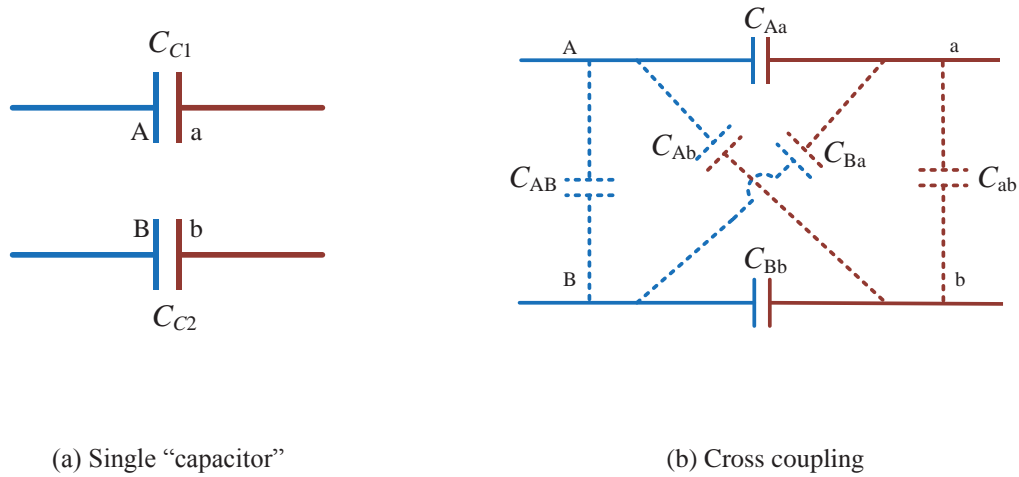
The capacitive coupling interface is the core part of a CPT system. It is the sole energy channel of power transfer between the primary and pickup sides. A good understanding of the coupling interface and its effect on the system performance plays an important role in a proper analysis and design of a CPT system, necessitating an appropriate model of the capacitive coupling. In most CPT literature, the capacitive coupling interface is simply modelled as a pair of capacitors in series [37, 73, 84-86], assuming the two pairs of plates are well aligned as shown in Fig. 4-1 (a). However, in real-world CPT applications, misalignment would occur in CPT systems with the most commonly used two-pair-plates configuration, in which one plate on the secondary side will overlap both plates on the primary side causing cross coupling problem as illustrated in Fig. 4-1 (b). Although some novel coupling structure designs are proposed to achieve position independence, cross coupling problem between coupling plates still exists [67, 72, 87]. Therefore, an appropriate model to characterize the cross coupling in CPT systems is necessary for the accurate analysis and evaluation of a general CPT system.



**Fig. 4-1: (a) Well-aligned coupling plates, (b) Misaligned coupling plates**

The simplest model of the capacitive coupling interface is shown in Fig. 4-2(a), which can be simplified as a single capacitor which is a series combination of two coupling capacitor  $C_{C1}$  and  $C_{C2}$ . This model is only valid under the ideal coupling condition where the coupling plates are so well aligned that no cross coupling occurs, which is impractical for most CPT applications. An accurate model that accounts for all the cross coupling effects is shown in Fig. 4-2 (b). The two capacitors  $C_{Aa}$  and  $C_{Bb}$  represent the two main coupling capacitances designed as the energy transfer channel.  $C_{Ab}$  and  $C_{Ba}$  represent the cross coupling effect due to misalignment.  $C_{AB}$  and  $C_{ab}$  represent the cross coupling occurring at the input and output terminals of the capacitive coupling interface. It is noted that in the space-confined applications, the effect of  $C_{AB}$  and  $C_{ab}$  can be significant. However, this circuit model contains six capacitors, and using it to analyse the CPT system directly will result in complex manipulation of the mathematical equations. For instance, the determination of the accurate value of the tuning inductor with this model can be tedious, and derived results can be intractable [62].





**Fig. 4-2: Two scenarios of the capacitive coupling interface**

To address these difficulties, this chapter proposes two new accurate models for the capacitive coupling interface with cross coupling effect taken into account. One is derived by equivalent circuit transformation and the other is based on the charge balance principle. Based on the latter model, a new term named capacitive coupling coefficient  $k_E$  is introduced to provide a quantitative measure of the coupling condition of a typical CPT system. Both models can be integrated easily with the remaining lumped circuit models of CPT systems.

## 4.2 Model Based on an Ideal Transformer

For ease of analysis, the circuit diagram in Fig. 4-2 (b) is redrawn in Fig. 4-3. Apart from the direct main coupling capacitances  $C_{Aa}$  and  $C_{Bb}$ ,  $C_{AB}$ ,  $C_{ab}$ ,  $C_{Ab}$ , and  $C_{Ba}$  denote the four cross-coupling capacitances among the four coupling plates, respectively. The primary side plates A and B are referred to as port A-B, while the secondary side plates a and b are referred to as port a-b.

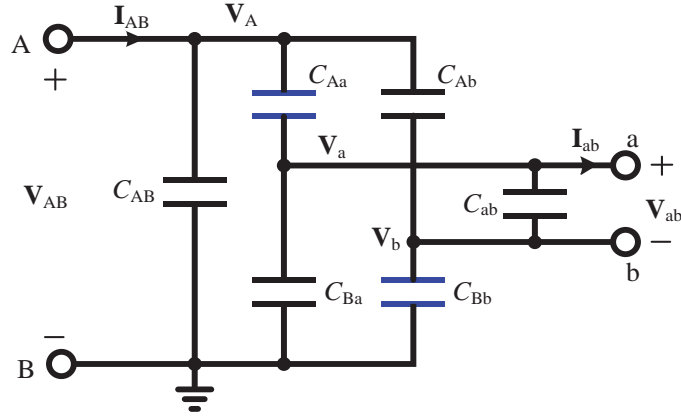


Fig. 4-3: Redrawn diagram of the capacitive coupling interface with cross coupling

$V_A$ ,  $V_a$ , and  $V_b$  denote the voltage in phasor form at node A, a, and b with respect to the node B as the ground.  $I_{AB}$  is the current flowing into port A-B, while  $I_{ab}$  is the current out of port a-b. Under steady-state condition, a nodal analysis based on KCL gives the following equations:

$$\begin{cases} j\omega C_{AB} V_A + j\omega C_{Aa} (V_A - V_a) + j\omega C_{Ab} (V_A - V_b) = I_{AB} \\ j\omega C_{Aa} (V_A - V_a) - j\omega C_{Ba} V_a - j\omega C_{ab} (V_a - V_b) = I_{ab} \\ j\omega C_{Bb} V_b - j\omega C_{Ab} (V_A - V_b) - j\omega C_{ab} (V_a - V_b) = I_{ab} \end{cases} \quad (4-1)$$

Based on equations above,  $I_{AB}$  and  $V_{ab}$  can be expressed in terms of  $V_A$  and  $I_{ab}$  as:

$$I_{AB} = j\omega \left( C_{AB} + C_1 + \frac{C_{ab} C_2}{C_{ab} + C_2} k_E^2 \right) V_A + \frac{k_E C_2}{C_{ab} + C_2} I_{ab} \quad (4-2)$$

$$V_{ab} = \frac{k_E C_2}{C_{ab} + C_2} V_A - \frac{1}{j\omega (C_{ab} + C_2)} I_{ab} \quad (4-3)$$

where

$$C_1 = \frac{C_{Aa} C_{Ba}}{C_{Aa} + C_{Ba}} + \frac{C_{Ab} C_{Bb}}{C_{Ab} + C_{Bb}} \quad (4-4)$$

$$C_2 = \frac{1}{\frac{1}{C_{Aa} + C_{Ba}} + \frac{1}{C_{Ab} + C_{Bb}}} \quad (4-5)$$

$$k_E = \frac{C_{Aa}}{C_{Aa} + C_{Ba}} - \frac{C_{Ab}}{C_{Ab} + C_{Bb}} \quad (4-6)$$

Based on (4-2) and (4-3), an equivalent circuit model of the capacitive coupling interface can be established as illustrated in Fig. 4-4. The model consists of three key components:

The first one is an equivalent ideal transformer that couples the primary and secondary side, with a turns ratio  $n_E$ :

$$n_E = \frac{k_E C_2}{C_{ab} + C_2} \quad (4-7)$$

which is dependent on the alignment of coupling plates, indicating the coupling condition in some sense.

The second and third are the input capacitance  $C_{IN}$ , and the output capacitance  $C_{OUT}$ , which can be determined by, respectively

$$C_{IN} = C_{AB} + C_1 + \frac{C_{ab} C_2}{C_{ab} + C_2} k_E^2 \quad (4-8)$$

$$C_{OUT} = C_{ab} + C_2 \quad (4-9)$$

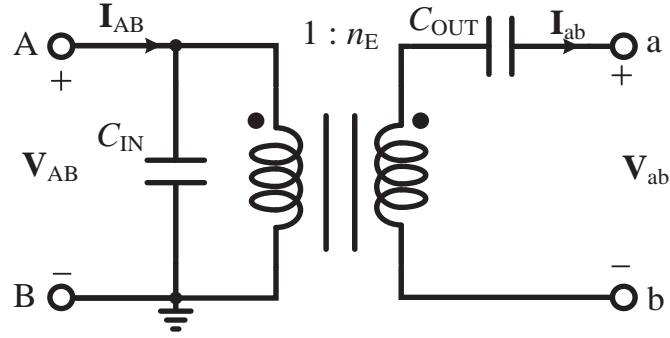


Fig. 4-4: The circuit model based on circuit transformation

#### 4.2.1 Effects of Misalignment

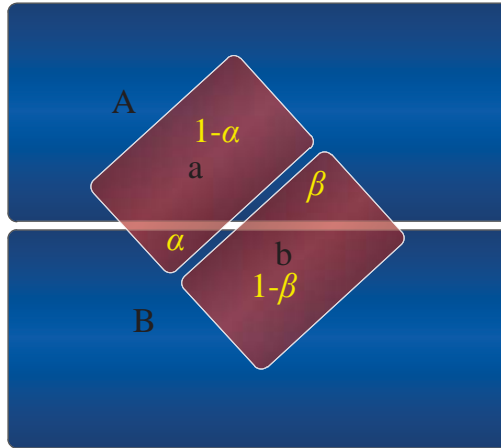


Fig. 4-5: Misalignment of coupling plates

According to (4-7), the ideal transformer is inherently a step-down transformer. It has a maximum turns ratio of 1:1 without cross coupling. When cross coupling is taken into consideration, the maximum turns ratio is  $C_2/(C_{ab}+C_2)$ . Besides, unlike conventional transformers always with a positive turns ratio, the turns ratio of the ideal transformer in the proposed model can be negative, which means that the direction of the coupled voltage on the secondary side is reversed (180 degrees out of phase). In such a case, the cross coupling has changed to such an extent that the cross capacitances ( $C_{Ba}$  and  $C_{Ab}$ ) become larger than the designed main capacitances ( $C_{Aa}$  and  $C_{Bb}$ ). From (4-8) and (4-9), the input

capacitance  $C_{IN}$  and the output capacitance  $C_{OUT}$  are also affected by the cross coupling capacitances.

To provide a quantitative analysis of how misalignment affects the three components, following assumptions are made without losing generality:

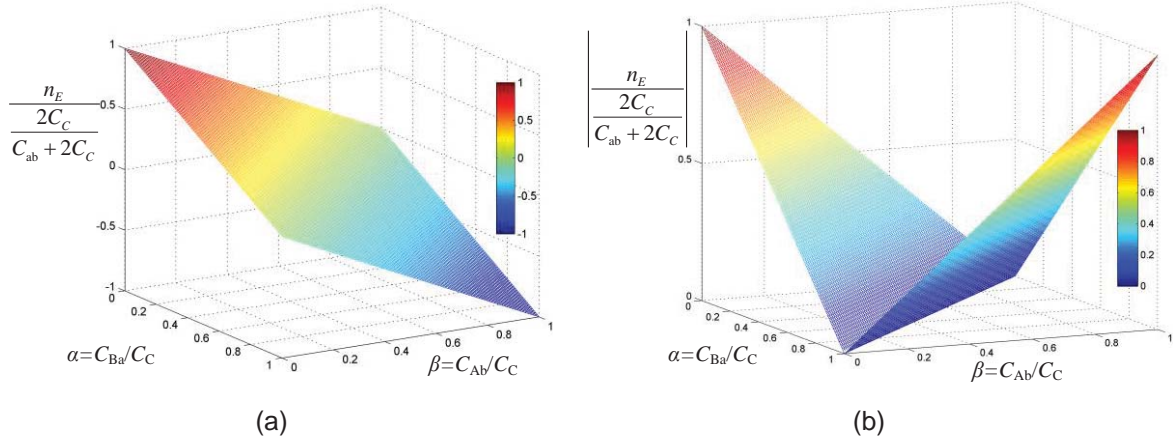
- 1) The size of the primary side plates A and B is much larger than that of the secondary side plates a and b so that the secondary side plates are always be placed within the boundary of the primary side plates.
- 2) The gap between primary side plates A and B are negligible so that uncoupled part between both primary and secondary side plates does not exist.
- 3) The main capacitance  $C_C$  formed between each pair of plates (plate A coupled to a or plate B coupled to b) is the same when misalignment does not occur.

When misalignment happens, for instance, some part of one secondary plate a is coupled to plate A and the other part of plate a is coupled to plate B as shown in Fig. 4-5. Define  $\alpha$ ,  $\beta$  as the portion of plate a coupled to plate B and plate b coupled to plate A, respectively. So the cross coupling capacitances  $C_{Ba}=\alpha C_C$ ,  $C_{Ab}=\beta C_C$ , while the main coupling capacitances  $C_{Aa}=(1-\alpha)C_C$ ,  $C_{Bb}=(1-\beta)C_C$ . At different situations of misalignment, three special cases are summarized below:

- a) When  $\alpha=1$  and  $\beta=0$ , it means plate a and plate b are all totally coupled with plate B, while plate A is left uncoupled.
- b) When  $\alpha=0$  and  $\beta=1$ , it means plate a and plate b are all totally coupled with plate A, while plate B is left uncoupled.
- c) When  $\alpha=0.5$  and  $\beta=0.5$ , it means half of plate a is coupled with plate A and the other half is coupled with plate B, so does plate b.

Therefore, in terms of  $C_C$ ,  $\alpha$ , and  $\beta$ ,  $n_E$  can be expressed as:

$$n_E = \frac{C_C}{2C_{ab} + C_C} (1 - \alpha - \beta) \quad (4-10)$$



**Fig. 4-6: Normalized turns ratio  $n_E$  in relation to misalignment**

Fig. 4-6 shows the variation of normalized turns ratio  $n_E$  with misalignment. In the ideal situation where coupling plates are well aligned, i.e.,  $\alpha=\beta=0$ , the ideal transformer has the maximum turns ratio. In the worst situation where plates are misaligned such that  $\alpha+\beta=1$ , the transformer has the minimum turns ratio of zero. In the situation where plate a is completely coupled with plate B and plate b to plate A, which means  $\alpha=\beta=1$ , it is equivalent to the situation in which  $\alpha=\beta=0$ , except for the reverse direction of the coupled voltage on the secondary side in the former case.

Similarly, the input and output capacitances  $C_{IN}$  and  $C_{OUT}$  can be expressed as

$$C_{IN} = C_{AB} + (\alpha + \beta - \alpha^2 - \beta^2)C_C + \frac{2C_{ab}C_C}{2C_{ab} + C_C}(1 - \alpha - \beta)^2 \quad (4-11)$$

$$C_{OUT} = C_{ab} + \frac{C_C}{2} \quad (4-12)$$

In most practical CPT systems, capacitances  $C_{AB}$  and  $C_{ab}$  formed between plates on the same side are small relative to the main coupling capacitances  $C_C$ . The effects of  $C_{AB}$  and  $C_{ab}$  are not considered for clarity, so  $n_E$ ,  $C_{IN}$ , and  $C_{OUT}$  can be simplified as, respectively:

$$n_E = 1 - \alpha - \beta \quad (4-13)$$

$$C_{IN} = (\alpha + \beta - \alpha^2 - \beta^2)C_C \quad (4-14)$$

$$C_{\text{OUT}} = \frac{C_{\text{C}}}{2} \quad (4-15)$$

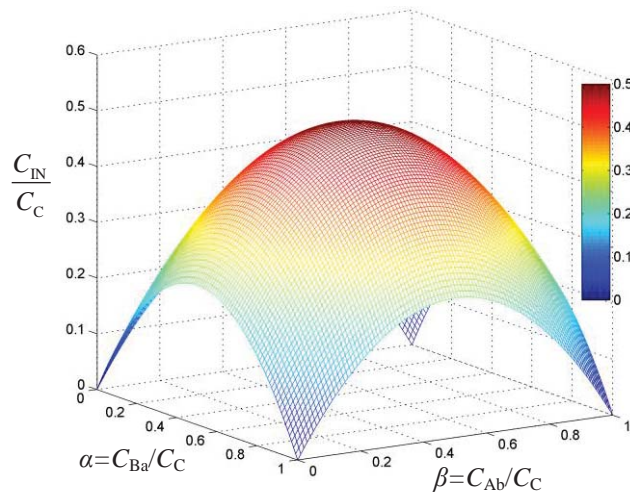
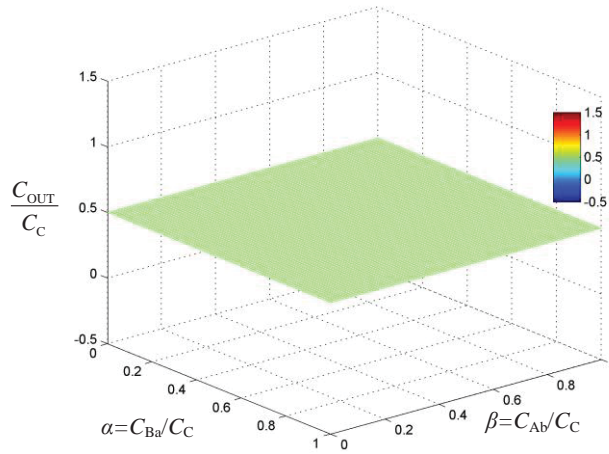


Fig. 4-7: Normalized input capacitance  $C_{\text{IN}}/C_{\text{C}}$  versus misalignment



**Fig. 4-8: Normalized output capacitance  $C_{OUT}/C_C$  versus misalignment**

In Fig. 4-7 and Fig. 4-8, ignoring  $C_{AB}$  and  $C_{ab}$ , the normalized input and output capacitances  $C_{IN}/C_C$  and  $C_{OUT}/C_C$  are plotted as the functions of misalignment, respectively. As can be seen from Fig. 4-7, under the best alignment condition ( $\alpha=\beta=0$ ), input capacitance  $C_{IN}$  becomes zero.  $C_{IN}$  reaches the maximum value under the coupling condition ( $\alpha=\beta=0.5$ ) in which half of a secondary side plate is coupled to one primary side plate and the other half coupled to another primary side plate, where no power is coupled to the secondary side. Fig. 4-8 shows that the output capacitance  $C_{OUT}$  maintains a constant value of  $C_C/2$  regardless of variations of misalignment, which is equal to the series combination of the two main coupling capacitances.

The three parameters in the proposed model interconnect with each other, describing the characteristics of the capacitive coupling interface collectively. The ideal transformer in the model reflects the coupling condition between primary and secondary coupling plates. Unlike actual transformer, its turns ratio can never exceed unity, meaning that it is unity or step-down transformer inherently. Besides, it can become zero under the worst case of coupling. In the best coupling situation, the two pairs of coupling plates are well aligned with each other without cross coupling, yielding a unity of  $n_E$ . For the worst case of coupling, the effect of cross coupling cancels the main coupling capacitances, yielding a zero turns ratio, and no power can be transferred to the secondary side. Unlike the input



capacitance  $C_{IN}$  that varies with the alignment condition, the output capacitance  $C_{OUT}$  keeps unchanged regardless of coupling conditions.

It should be noted that the analysis of the effect of misalignment on the model is based on the assumption that the distances between primary and secondary coupling plates keep unchanged. For those CPT systems in which the coupling distances change during operation, another varying factor can be introduced to take account of the coupling distance variation.

The three parameters of the proposed model can be determined easily by experiments.  $C_{IN}$  can be measured at the input port A-B when the output port a-b is open-circuit.  $C_{OUT}$  can be measured at the port a-b when the input port A-B is shorted. The capacitive turn ratio  $n_E$  can be obtained by applying an AC voltage at the input port A-B and measuring the ratio of the output open-circuit voltage to the input voltage.

The proposed model can provide a circuit-intuitive guideline for the selection of driving inverters and tuning circuits. It can be inferred that a voltage-fed inverter is not suitable for driving the capacitive coupling interface directly since a capacitor  $C_{IN}$  presents at the input port of the interface. Thus, a primary side series tuning inductor is always necessary when a voltage-fed inverter is used if less noise is required.

### 4.2.2 Series Tuning Inductor Analysis

The proposed model can be used for the calculation of series tuning inductor and analysis of its tuning effect in CPT systems. The inductor can be placed in two different positions, either before the capacitive coupling interface (referred to as primary side tuning) or after it (referred to as secondary side tuning). A comprehensive comparison of effects of the two tuning positions has been made using conventional AC circuit analysis [62]. However, the process and results are tedious and intractable, which is not design-oriented. As can be seen in the following, the analysis based on the proposed model is much simplified and can provide design guidance and more insights into the system in a circuit-intuitive way.

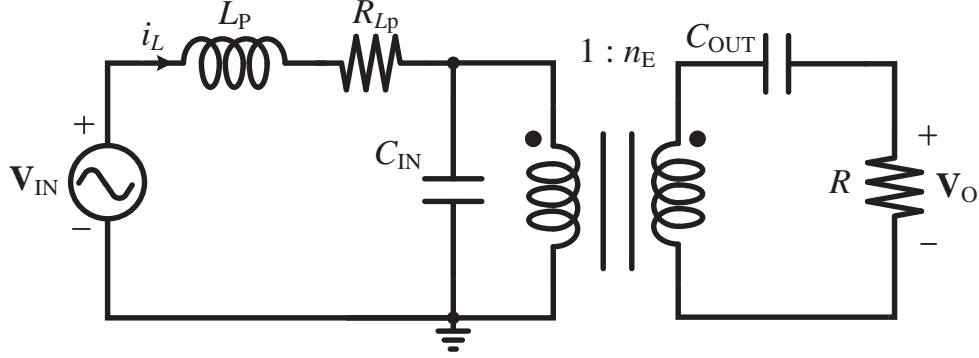
A) *Primary Side Tuning*

Fig. 4-9: Primary side tuning

In Fig. 4-9, a series tuning inductor  $L_P$  with an equivalent series resistance  $R_{L_P}$  is placed on the primary side to achieve full resonance.  $V_{IN}$  is the AC input voltage source at an operating frequency of  $f_s$ ,  $R$  is the AC load or the equivalent resistance presented by the rectifier with a DC load. With the proposed model, the secondary side circuit can be reflected to the primary side through the ideal transformer, as shown in Fig. 4-10. Then the CPT system can be transformed to a second order system. The current through the primary tuning inductor  $i_L$  is

$$\mathbf{I}_L = \frac{\mathbf{V}_{IN}}{j\omega L_P + R_{L_P} + \frac{R_1}{1 + j\omega(C_{IN} + C_{OUT1})R_1}} \quad (4-16)$$

where

$$\omega = 2\pi f_s \quad (4-17)$$

$$C_{OUT1} = \frac{Q_s^2}{1 + Q_s^2} n_E^2 C_{OUT} \quad (4-18)$$

$$R_1 = (1 + Q_s^2) \frac{R}{n_E^2} \quad (4-19)$$

$$Q_s = \frac{1}{\omega C_{OUT} R} \quad (4-20)$$

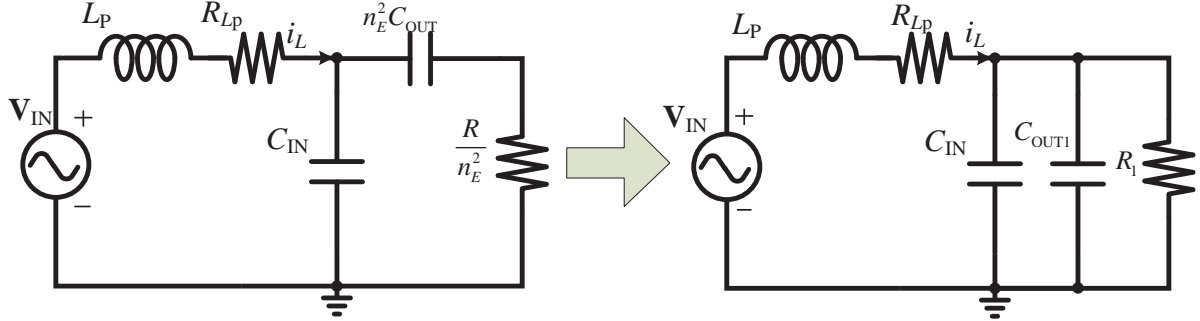


Fig. 4-10: Impedance transformation of primary side tuning

The required tuning inductor  $L_P$  can be calculated by setting the imaginary part of  $\mathbf{I}_L$  to be zero:

$$L_P = \frac{1}{\omega^2 (C_{IN} + C_{OUT1})} \frac{Q_1^2}{1 + Q_1^2} \quad (4-21)$$

where

$$Q_1 = \omega R_1 (C_{IN} + C_{OUT1}) \quad (4-22)$$

The value of the tuning inductor to achieve resonance changes with the coupling condition since  $C_{IN}$  and  $C_{OUT}$  are functions of misalignment. In terms of  $\alpha$  and  $\beta$ ,  $L_P$  can be expressed as

$$\begin{aligned} L_P &= \frac{1}{\omega^2 \frac{C_C}{2}} \frac{1}{2(\alpha + \beta - \alpha^2 - \beta^2) + \frac{Q_s^2}{1 + Q_s^2} (1 - \alpha - \beta)^2} \frac{Q_1^2}{1 + Q_1^2} \\ &\approx \frac{1}{\omega^2 \frac{C_C}{2}} \frac{1}{1 - (\alpha - \beta)^2}. \end{aligned} \quad (4-23)$$

While  $Q_1$  can be expressed in terms of  $Q_s$ ,  $\alpha$  and  $\beta$ :

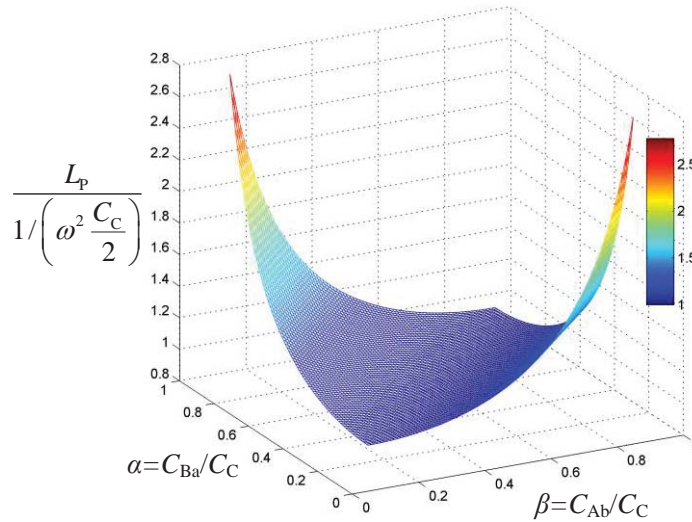
$$Q_1 = \frac{\alpha + \beta - \alpha^2 - \beta^2}{(1 - \alpha - \beta)^2} \left( \frac{2}{Q_s} + 2Q_s \right) + Q_s \quad (4-24)$$

which indicates  $Q_1$  equals  $Q_s$  plus an extra item resulting from misalignment.

Assuming  $Q_s$  is larger than 1, (4-23) can be reduced to:

$$\begin{aligned} L_p &= \frac{1}{\omega^2 \frac{C_c}{2}} \frac{1}{2(\alpha + \beta - \alpha^2 - \beta^2) + (1 - \alpha - \beta)^2} \\ &= \frac{1}{\omega^2 \frac{C_c}{2}} \frac{1}{1 - (\alpha - \beta)^2} \end{aligned} \quad (4-25)$$

Fig. 4-11 shows normalized tuning inductor  $L_p/(1/(\omega^2 C_c/2))$  as a function of misalignment. It indicates that the value of the tuning inductance  $L_p$  required to achieve resonance is affected by the difference between  $\alpha$  and  $\beta$ . Thus, in the cases of symmetrical misalignment ( $\alpha=\beta$ ),  $L_p$  keeps unchanged, which is equal to  $1/(\omega^2 C_c/2)$ . Theoretically, if the absolute value of  $\alpha-\beta$  equals to 1, the inductance required to achieve resonance will become infinity.



**Fig. 4-11: Normalized primary side tuning inductance  $L_p/(1/(\omega^2 C_c/2))$  versus misalignment**

The peak current through the tuning inductor at resonance is:

$$i_{L,peak} = \frac{v_{IN,peak}}{\frac{R_1}{(1+Q_1^2)} + R_{Lp}} \quad (4-26)$$

where  $v_{IN,peak}$  is the peak value of input AC input voltage  $V_{IN}$ .

It is noted that in practical applications,  $Q_1$  should be small for accurately tuning the circuit since large  $Q_1$  will make the system too sensitive.

Considering the losses of the tuning inductor, the output power  $P_{O1}$  can be obtained as

$$\begin{aligned} P_{O1} &= \frac{v_{IN,peak}^2}{2} \frac{1+Q_1^2}{\left(R_1 + (1+Q_1^2)R_{Lp}\right)^2} R_1 \\ &= \frac{v_{IN,peak}^2}{2R} \frac{m}{\left(1 + m \frac{R_{Lp}}{R}\right)^2}, \end{aligned} \quad (4-27)$$

where

$$m = \frac{n_E^2 (1+Q_1^2)}{1+Q_s^2} \quad (4-28)$$

Using (4-26), the input power  $P_{IN1}$  can be easily obtained as:

$$P_{IN1} = \frac{V_{IN}^2}{2} \frac{1+Q_1^2}{R_1 + (1+Q_1^2)R_{Lp}} \quad (4-29)$$

Therefore, efficiency  $\eta_1$  is:

$$\begin{aligned} \eta_1 &= \frac{P_{O1}}{P_{IN1}} = \frac{R_1}{R_1 + (1+Q_1^2)R_{Lp}} \\ &= \frac{1}{1 + \frac{1+Q_1^2}{1+Q_s^2} \frac{R_{Lp}}{R} n_E^2} \end{aligned} \quad (4-30)$$

To evaluate the effect of misalignment on the output power at resonance, ignoring the loss of the tuning inductor,  $P_{O1}$  can be expressed in terms of  $\alpha$  and  $\beta$  by inserting (4-24):

$$\begin{aligned} P_{O1} &= \frac{V_{IN}^2}{2R} \frac{(1-\alpha-\beta)^2}{1+Q_s^2} (1+Q_1^2) \\ &= \frac{V_{IN}^2}{2R} \frac{(1-\alpha-\beta)^2}{1+Q_s^2} \left( 1 + \left( \frac{\alpha+\beta-\alpha^2-\beta^2}{(1-\alpha-\beta)^2} \left( \frac{2}{Q_s} + 2Q_s \right) + Q_s \right)^2 \right) \end{aligned} \quad (4-31)$$

Assuming  $Q_s=6$ , which is a typical value for CPT systems, the normalized output power  $P_{O1}/(V_{IN}^2/(2R))$  with respect to misalignment is shown in Fig. 4-12.  $\alpha$  and  $\beta$  are chosen to be within the range from 0 to 0.4. The reason of the choice of this range is that in practical CPT applications misalignment will be controlled to avoid extreme misalignment yielding very little or no power [67, 87]. The maximum output power after adding tuning inductor increases with misalignment. Although theoretically the power will become very large when  $\alpha$  and  $\beta$  are close to 0.5, the output power of practical systems cannot go to arbitrarily high since the current through the tuning inductor will become quite large leading to significant losses. It can also be seen that the output power at resonance will increase under the condition of insignificant misalignment. Fig. 4-12 shows the normalized output power  $P_{O1}/(v_{IN,peak}^2/(2R))$  versus misalignment including the losses of the tuning inductor when  $R_{Lp}/R=0.2$ . When the inductor losses are taken into account, the output power increases at first and drops with significant misalignment due to the increased inductor losses. It can also be concluded that the increase of misalignment will increase the input capacitance  $C_{IN}$ , resulting a larger  $Q_1$  that leads to bigger voltage boost capability in some sense.

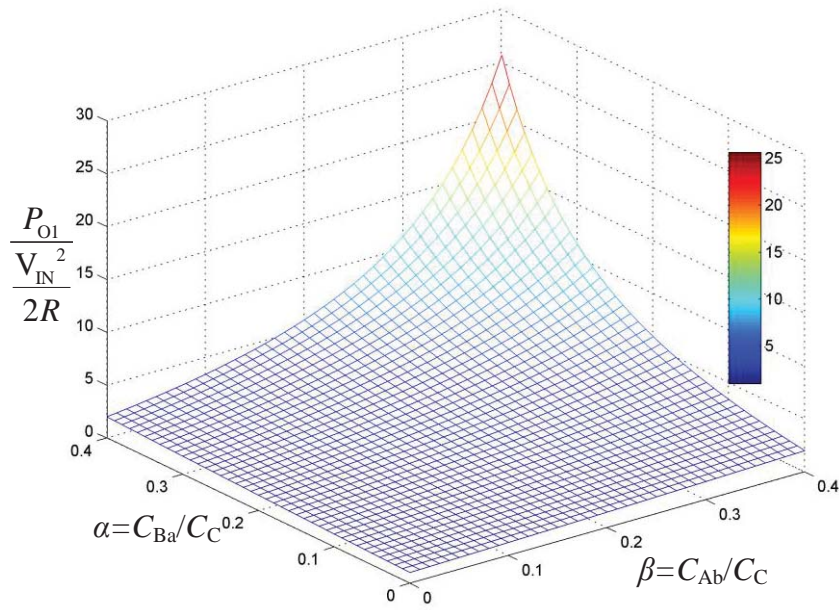
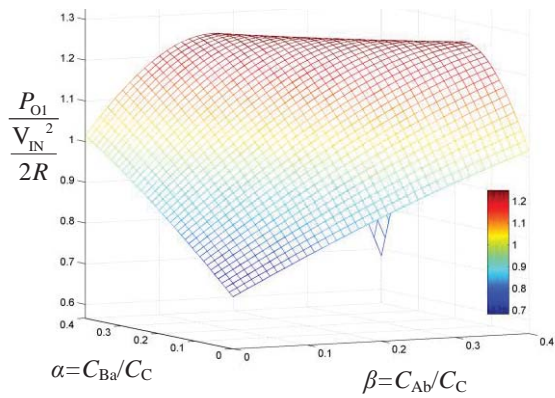
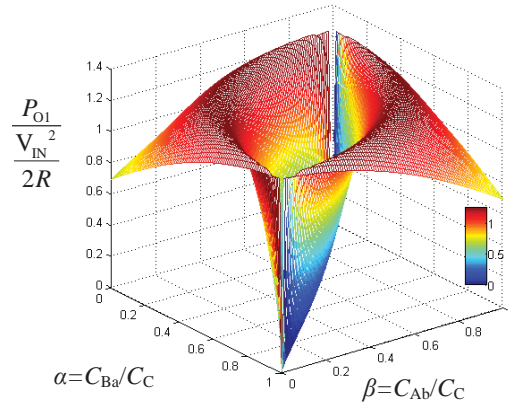


Fig. 4-12: Normalized output power at resonance for primary side tuning versus misalignment.



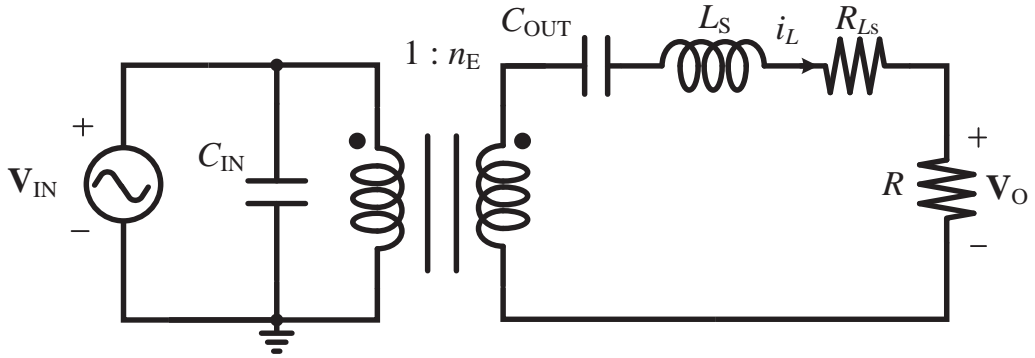
(a)



(b)

Fig. 4-13: Normalized output power  $P_{O1}/(V_{IN,peak}^2/(2R))$  versus misalignment when  $R_{Lp}/R=0.2$ , (a)  $0 < \alpha, \beta < 0.4$ , (b)  $0 < \alpha, \beta < 1$ .

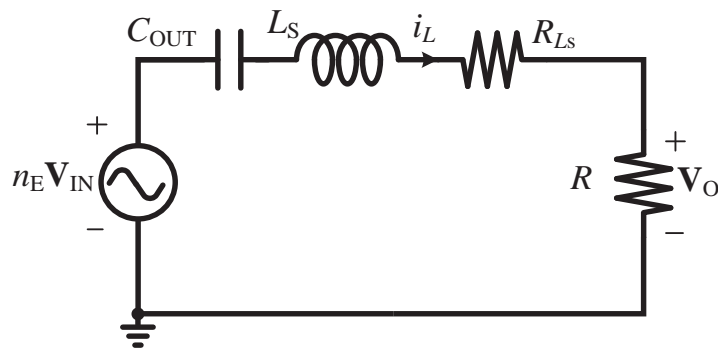
**B) Secondary Side Tuning**



**Fig. 4-14: Secondary side tuning**

Fig. 4-14 shows the CPT system with the series tuning inductor placed on the secondary side. Similarly, the CPT system with secondary side tuning inductor can be simplified using the ideal transformer reflecting the primary side to the secondary side as shown in Fig. 4-15. Different from the primary side tuning, the secondary side inductor is used to compensate for the output capacitance  $C_{OUT}$ . To achieve the maximum power transfer, the secondary side tuning inductor  $L_S$  can be calculated by

$$L_S = \frac{1}{\omega^2 C_{OUT}} \quad (4-32)$$



**Fig. 4-15: Impedance transformation of secondary side tuning**



The peak current through  $L_S$  is

$$i_{L,peak} = \frac{n_E v_{IN,peak}}{R_{L_S} + R} \quad (4-33)$$

Considering the loss of the tuning inductor, the output power  $P_{O2}$  is

$$P_{O2} = \frac{(n_E v_{IN,peak})^2}{2} \frac{R}{(R_{L_S} + R)^2} \quad (4-34)$$

Assuming 100% efficiency, the output power  $P_{O2}$  received by the load  $R$  is

$$P_{O2} = \frac{(n_E v_{IN,peak})^2}{2R} \quad (4-35)$$

### *C) Comparison of output power*

From (4-13), the output power using secondary side tuning  $P_{O2}$  can also be expressed in terms of  $\alpha$  and  $\beta$ :

$$P_{O2} = \frac{v_{IN,peak}^2}{2R} (1 - \alpha - \beta)^2 \quad (4-36)$$

Dividing (4-31) by (4-36), the ratio between the output power with the primary and secondary tuning inductors is defined by  $\gamma$ , which is

$$\gamma = \frac{P_{O1}}{P_{O2}} = \frac{1 + Q_1^2}{1 + Q_S^2} \quad (4-37)$$

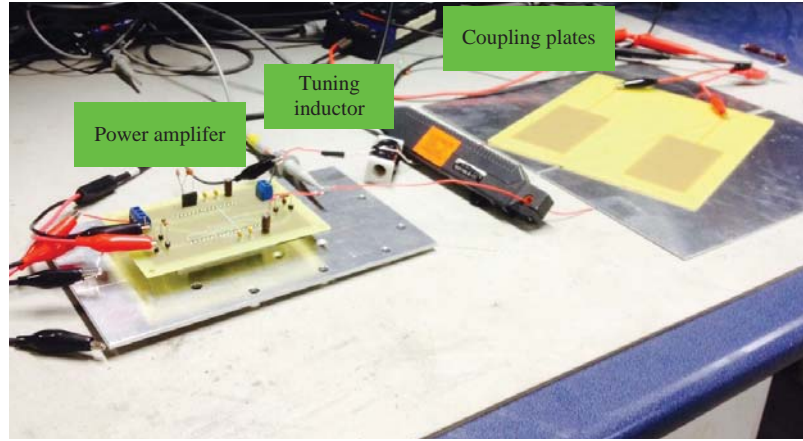
According to (4-18), (4-19), and (4-22),  $Q_1$  can be expressed in terms of  $Q_S$ :

$$Q_1 = \frac{\omega C_{IN} R}{n_E^2} (1 + Q_S^2) + Q_S \quad (4-38)$$

The first term in (4-38) is the effect of misalignment. When no misalignment exists between coupling plates ( $C_{IN}=0$ ),  $Q_1$  is equal to  $Q_S$ . Otherwise,  $Q_1$  is greater than  $Q_S$ , since  $\gamma$  is greater than one. Hence, it is preferred that the series tuning inductor is placed on the primary side if more power is desired.

From Fig. 4-9 it can be seen that the primary side tuning inductor and the input capacitance form a parallel resonant tank, which helps to boost the input voltage and produce more power. While in the secondary side tuning method shown in Fig. 4-14, the series tuning inductor and the output capacitance constitute a series resonant tank. Therefore, the output voltage would be lower than the input voltage since the turns ratio  $n_E$  is less than one. Furthermore, the secondary side tuning is not desirable if a voltage-fed converter is used because the parallel capacitor  $C_{IN}$  will be connected directly with the primary voltage source, generating significant current spikes.

### 4.2.3 Simulations and Experimental Results



**Fig. 4-16: The Prototype CPT system for cross coupling comparison.**

To verify the proposed model in determining the accurate tuning inductances, a prototype CPT system are constructed with four coupling plates intentionally misaligned as shown in Fig. 4-16. Two cases of different misalignment are investigated, referred to as CPT1( $\alpha=\beta=0.2$ ) and CPT2 ( $\alpha=0.2, \beta=0.4$ ). The practical capacitive coupling interface of the prototype CPT system includes two 150mm×300mm aluminium sheets and two 50mm×100mm copper pads (capacitance of one pair of plates  $C_C=500$  pF), which are all coated with a thin layer of polypropylene as the dielectric material, and is driven by a 1MHz sinusoidal voltage source from a power amplifier. Two terminal cross-coupling capacitances ( $C_{AB}$  and  $C_{ab}$ ) are measured with a precision RLC meter (Agilent 4980) when primary and secondary plates are decoupled. Four coupling capacitances ( $C_{Aa}$ ,  $C_{Ba}$ ,  $C_{Ab}$ , and  $C_{Bb}$ ) are calculated based on variations of the overlapping area between the coupling

plates. The parameters of the system are listed in Table 4-1. Both systems use primary side tuning inductors calculated based on proposed model.

Table 4-1: CPT system specification.

Parameter	Value	
	CPT1	CPT2
Peak input voltage, $v_{IN,peak}$	20 V	20 V
Operating frequency, $f$	1 MHz	1 MHz
Equivalent ac load, $R$	100 $\Omega$	100 $\Omega$
Capacitance between plates A and B, $C_{AB}$	15 pF	15 pF
Capacitance between plates a and b, $C_{ab}$	12 pF	12 pF
Capacitance between plates A and a, $C_{Aa}$	400 pF	400 pF
Capacitance between plates B and b, $C_{Bb}$	400 pF	300 pF
Capacitance between plates A and b, $C_{Ab}$	100 pF	200 pF
Capacitance between plates B and a, $C_{Ba}$	100 pF	100 pF
Calculated input capacitance $C_{IN}$	180 pF	217 pF
Calculated output capacitance $C_{OUT}$	265 pF	265 pF
Calculated capacitive turns ratio $n_E$	0.566	0.377
Calculated primary tuning inductance, $L_P$	96.2 $\mu$ H	99.6 $\mu$ H

#### A) Misalignment Variation

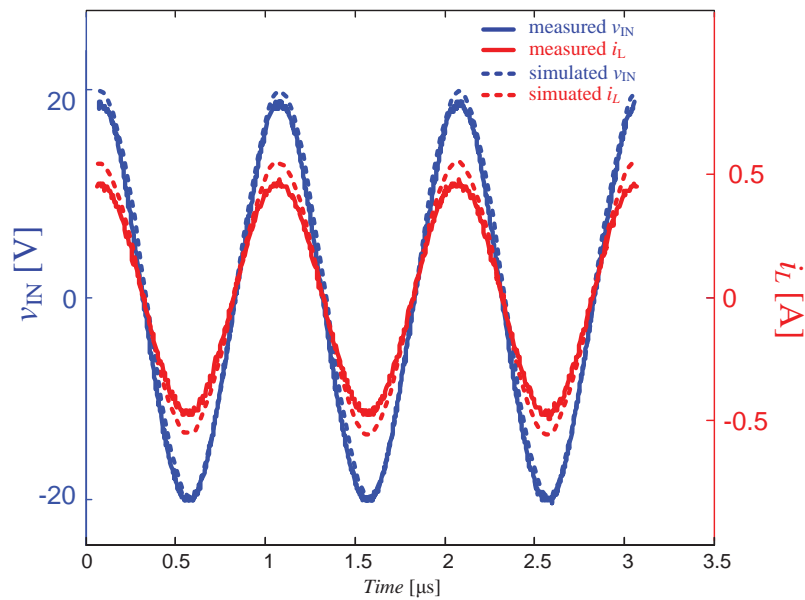
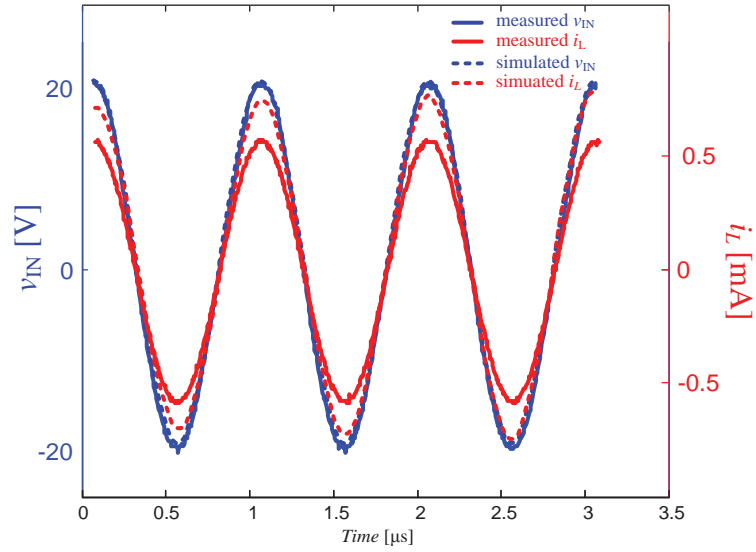
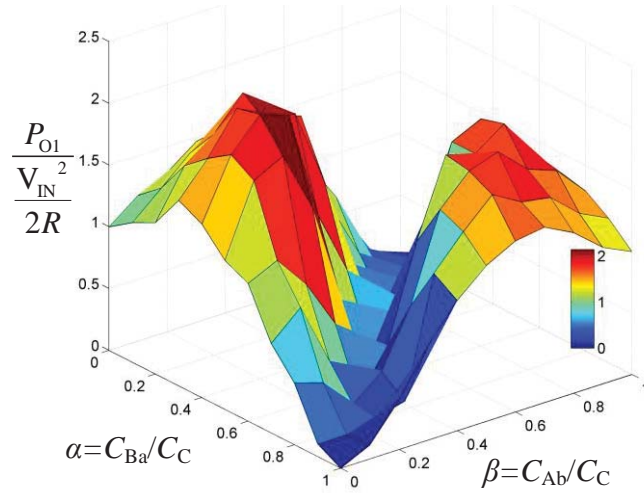


Fig. 4-17: Experimental and simulated data plots of input voltage  $v_{IN}$  and input current  $i_L$  of CPT1.



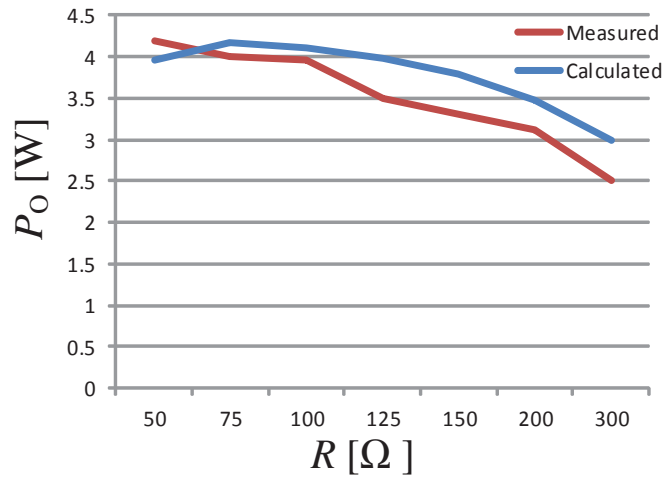
**Fig. 4-18: Experimental and simulated data plots of input voltage  $v_{IN}$  and input current  $i_L$  of CPT2.**

Fig. 4-17 and Fig. 4-18 show simulated and experimental results, which demonstrate that voltage  $v_{AB}$  and current  $i_L$  into the resonant circuit are in phase. The actual values of the inductors in the experiments are 92  $\mu\text{H}$  and 94  $\mu\text{H}$ , which are slightly smaller than calculated values. The parasitic elements such as wire inductance and current loops in the circuits contribute some inductance. It also shows that the current is smaller than the simulated value due to the conduction and core losses of the tuning inductor at high frequency operation. The difference between the experimental and simulated waveforms will be reduced if the inductor is optimized for high frequency operation (using better ferrites and litz wires with low losses at high frequencies). The output powers of CPT1 and CPT2 are measured to be 3.48 W and 3.58 W, respectively. The output power of CPT2 is slightly larger than CPT1 because the misalignment of CPT2 is larger than that of CPT1, which agrees with the prediction from the model. Fig. 4-19 shows the output power as a function of a full range of variation of misalignment, which is in agreement with Fig. 4-13(b) derived from the model except for some extreme conditions. With severe misalignment the inductor current becomes very large at resonance leading to significant losses, so the output power cannot maintain high output power at vicinity of points where  $\alpha=0, \beta=1$  and  $\alpha=1, \beta=0$ .



**Fig. 4-19: Experimental data plots of the normalized output power  $P_{O1}/(v_{IN,peak}^2/(2R))$  versus misalignment ( $v_{IN,peak}^2/(2R) = 2 \text{ W}$ ).**

**B) Load variation**



**Fig. 4-20: Output power versus load  $R$ .**

In order to evaluate the effect of load variation on the output power under the cross coupling conditions, the load of CPT2 system is varied since it can produce more power. Fig. 4-20 shows the output power variations with the load. It shows that the measured

values are in good agreement with calculated values based on the proposed model. At light load, the deviation of the model from the experimental results increases because the larger load resistance yields lower tank quality.

### 4.3 Dynamic Model with State-space Description

An equivalent circuit diagram of a CPT system with cross coupling is illustrated in Fig. 4-21. The tuning inductor is placed on the primary side for the reason given in previous sections.  $v_{ac}$  is the equivalent ac voltage from the output of an power inverter.  $L_C$  is the compensation inductor to cancel the impedance introduced by the capacitive coupling interface.  $C_{Aa}$  and  $C_{Bb}$  represent the main coupling capacitances which is designed to maximise.  $C_{AB}$ ,  $C_{Ab}$ ,  $C_{Ba}$ , and  $C_{ab}$  represent undesired cross coupling capacitances, respectively. The equivalent series resistance (ESR) of all coupling capacitors are not taken into account since they are quite almost negligible at high frequency operation.  $R_e$  is the equivalent resistance reflected from the input port of a rectifier.

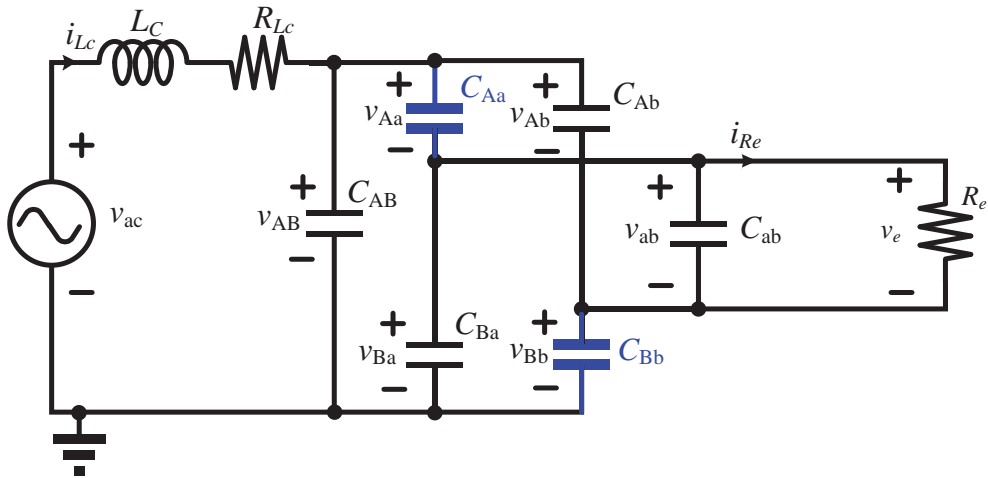


Fig. 4-21: An equivalent circuit of a CPT system with cross coupling.

Four state variables are introduced to establish a state-space model for the CPT system:

$$\begin{aligned} \mathbf{x} &= [x_1 \quad x_2 \quad x_3 \quad x_4]^T \\ &= [i_{Lc} \quad v_{AB} \quad v_{Aa} \quad v_{ab}]^T \end{aligned}$$

where

- $i_{Lc}$  current through the compensation inductor  $L_C$ ;
- $v_{AB}$  voltage at the input port of the capacitive coupling interface;
- $v_{Aa}$  voltage across the cross coupling capacitance  $C_{Aa}$ ;
- $v_{ab}$  voltage at the output port of the capacitive coupling interface.

Input variable is

$$\mathbf{u} = [u] = [v_{ac}]$$

According to Kirchhoff's Voltage Law (KVL) and Kirchhoff's Current Law (KCL) from the circuit theory, four differential equations can be obtained:

$$\left\{ \begin{array}{l} L_C \frac{dx_1}{dt} + R_{Lc} x_1 + x_2 = u \\ x_1 = C_{AB} \frac{dx_2}{dt} + (C_{Aa} + C_{Ab}) \frac{dx_3}{dt} + C_{Ab} \frac{dx_4}{dt} \\ (C_{Aa} + C_{Ba}) \frac{dx_3}{dt} = C_{Ba} \frac{dx_2}{dt} + C_{ab} \frac{dx_4}{dt} + \frac{x_4}{R_e} \\ C_{Bb} \frac{dx_2}{dt} = (C_{Ab} + C_{Bb}) \frac{dx_3}{dt} + (C_{Ab} + C_{Bb} + C_{ab}) \frac{dx_4}{dt} + \frac{x_4}{R_e} \end{array} \right. \quad (4-39)$$

These can be expressed in standard state-space form as follows:

$$\dot{\mathbf{x}} = \mathbf{Ax} + \mathbf{Bu}\dot{\mathbf{x}} \quad (4-40)$$

The system matrix  $A$  is given by

$$A = \begin{bmatrix} -\frac{R_{L_c}}{L_C} & -\frac{1}{L_C} & 0 & 0 \\ \frac{N_1}{D} & 0 & 0 & -\frac{N_2}{DR_e} \\ \frac{N_5}{D} & 0 & 0 & \frac{N_4}{DR_e} \\ \frac{N_2}{D} & 0 & 0 & -\frac{N_3}{DR_e} \end{bmatrix} \quad (4-41)$$

where

$$D = C_{Aa}C_{ab}C_{AB} + C_{Aa}C_{Ab}C_{AB} + C_{ab}C_{Ab}C_{AB} + C_{Aa}C_{ab}C_{Ba} + C_{Aa}C_{Ab}C_{Ba} + C_{ab}C_{Ab}C_{Ba} + \\ C_{ab}C_{AB}C_{Ba} + C_{Ab}C_{AB}C_{Ba} + C_{Aa}C_{ab}C_{Bb} + C_{Aa}C_{Ab}C_{Bb} + C_{ab}C_{Ab}C_{Bb} + C_{Aa}C_{AB}C_{Bb} + \\ C_{ab}C_{AB}C_{Bb} + C_{Aa}C_{Ba}C_{Bb} + C_{Ab}C_{Ba}C_{Bb} + C_{AB}C_{Ba}C_{Bb}$$

$$N_1 = C_{Aa}C_{ab} + C_{Aa}C_{Ab} + C_{Aa}C_{Bb} + C_{Ab}C_{Ba} + C_{Ab}C_{ab} + C_{Ba}C_{Bb} + C_{Ba}C_{ab} + C_{Bb}C_{ab}$$

$$N_2 = C_{Aa}C_{Bb} - C_{Ab}C_{Ba}$$

$$N_3 = C_{Aa}C_{AB} + C_{Ab}C_{AB} + C_{Aa}C_{Ba} + C_{Ab}C_{Ba} + C_{AB}C_{Ba} + C_{Aa}C_{Bb} + C_{Ab}C_{Bb} + C_{AB}C_{Bb}$$

$$N_4 = C_{Ab}C_{AB} + C_{Ab}C_{Ba} + C_{Ab}C_{Bb} + C_{AB}C_{Bb}$$

$$N_5 = C_{ab}C_{Ba} + C_{Ab}C_{Ba} + C_{ab}C_{Bb} + C_{Ba}C_{Bb}$$

The input matrix  $B$  is given by

$$B = b = \begin{bmatrix} \frac{1}{L_C} & 0 & 0 & 0 \end{bmatrix}^T \quad (4-42)$$

Since  $v_{ab}$  is the output, the output matrix  $C$  is given by

$$C = [0 \quad 0 \quad 0 \quad 1] \quad (4-43)$$

As can be seen in (4-41), the matrix  $A$  has a column consisting of all zeros. It can be reduced to a three-order matrix, and the state vector  $\mathbf{x}$  can also be further simplified as



$$\begin{aligned}\mathbf{x} &= [x_1 \quad x_2 \quad x_3]^T \\ &= [i_{L_c} \quad v_{AB} \quad v_{ab}]^T\end{aligned}\tag{4-44}$$

Thus,  $A$ ,  $B$ , and  $C$  can be obtained, respectively.

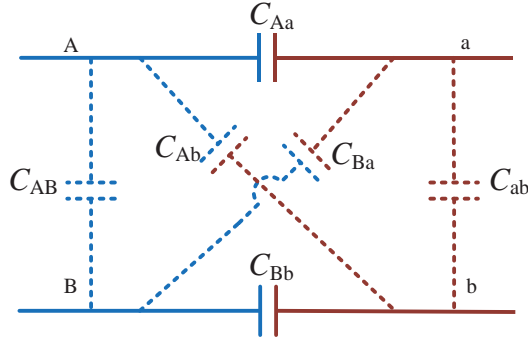
$$A = \begin{bmatrix} -\frac{R_{L_c}}{L_c} & -\frac{1}{L_c} & 0 \\ \frac{N_1}{D} & 0 & -\frac{N_2}{DR_e} \\ \frac{N_2}{D} & 0 & -\frac{N_3}{DR_e} \end{bmatrix}\tag{4-45}$$

$$B = b = \begin{bmatrix} \frac{1}{L_c} & 0 & 0 \end{bmatrix}^T\tag{4-46}$$

$$C = [0 \quad 0 \quad 1]\tag{4-47}$$

#### 4.4 Defining the Mutual Coupling Coefficient

It is well known that the magnetic coupling coefficient has been used to define the mutual magnetic coupling between the coupled coils of an IPT system [18]. However, there is no appropriate term defined for coupling plates of CPT systems, particularly when cross coupling exists. Although a similar coupling coefficient has been defined based on the ratio between the mutual and storage energy of primary and secondary plates [88], it ranges from zero to infinity without giving a clear indication of the coupling degree. Here a new capacitive coupling coefficient  $k_E$  is proposed, with its magnitude ranging from zero to one for quantifying the overall mutual electric coupling between the primary and secondary coupling plates by taking the cross electric field coupling into consideration. For the convenience of demonstration, the capacitive coupling interface with cross coupling is redrawn in Fig. 4-22.



**Fig. 4-22: Capacitive coupling interface with cross coupling.**

A new model is established as shown in Fig. 3 to describe the cross coupling between the primary and secondary coupling plates. Similar to leakage inductances in a transformer model, the two leakage capacitances ( $C_{AB}$  and  $C_{ab}$  in dotted lines) between the plates at the same side are not considered in the calculation of mutual coupling charges since neither of them contributes to the mutual coupling between the primary and secondary plates. They can be analyzed separately at each side if needed.

In Fig. 4-23, the capacitive coupling interface is seen as two equivalent primary and secondary capacitances  $C_P$  and  $C_S$  coupled by a mutual capacitance  $C_M$ . If the voltages at the input and output of the coupling plates are  $V_P$  and  $V_S$  respectively, the charges involved in the mutual coupling (without considering the leakage capacitances) will be:

$$\begin{cases} Q_P = V_P C_P + V_S C_M \\ Q_S = V_S C_S + V_P C_M \end{cases} \quad (4-48)$$

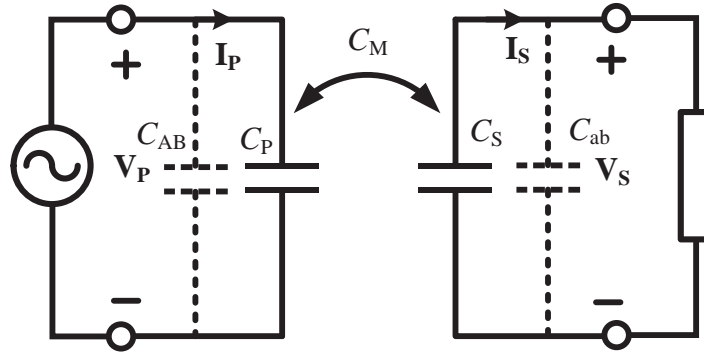


Fig. 4-23: A dual model of the capacitive coupling interface.

$C_P$  can be calculated by setting  $V_S$  to zero (secondary is short-circuited). From (4-48) and Fig. 4-22,  $C_P$  can be expressed as

$$C_P = \frac{Q_P}{V_P} = \frac{(C_{Aa} + C_{Ab})(C_{Ba} + C_{Bb})}{C_{Aa} + C_{Ab} + C_{Ba} + C_{Bb}} \quad (4-49)$$

Similarly,  $C_S$  can be obtained by setting  $V_P$  to zero:

$$C_S = \frac{Q_S}{V_S} = \frac{(C_{Aa} + C_{Ba})(C_{Ab} + C_{Bb})}{C_{Aa} + C_{Ba} + C_{Ab} + C_{Bb}} \quad (4-50)$$

To obtain the mutual capacitance  $C_M$ , the secondary side is made open-circuit, and a current source can be modeled at the secondary side due to the capacitive coupling, as illustrated in Fig. 4-24. Under steady-state conditions, the open circuit output voltage  $V_{SO}$  can be expressed as

$$V_{SO} = j\omega C_M V_P \times \frac{1}{j\omega(C_S + C_{ab})} = \frac{C_M V_P}{C_S + C_{ab}} \quad (4-51)$$

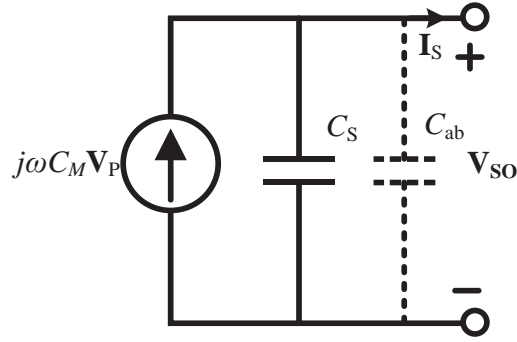


Fig. 4-24: An equivalent model of the secondary side.

Then  $C_M$  can be expressed as

$$C_M = \frac{V_{SO}}{V_P} (C_S + C_{ab}) \quad (4-52)$$

With a given  $V_P$ ,  $V_{SO}$  can also be obtained by analyzing the original circuit shown in Fig. 4-22:

$$V_{SO} = V_P \frac{C_{Aa} C_{Bb} - C_{Ab} C_{Ba}}{C_{ab} (C_{Aa} + C_{Ab} + C_{Ba} + C_{Bb}) + (C_{Aa} + C_{Ba})(C_{Ab} + C_{Bb})} \quad (4-53)$$

Substituting (4-50) and (4-53) for  $C_S$  and  $V_{SO}$  in (4-52) gives

$$C_M = \frac{-C_{Ab} C_{Ba} + C_{Aa} C_{Bb}}{C_{Aa} + C_{Ab} + C_{Ba} + C_{Bb}} \quad (4-54)$$

which shows that  $C_M$  is only determined by the mutual capacitances, and is not affected by the leakage capacitances.

Now similar to the magnetic coupling coefficient between two coils, a new term named capacitive coupling coefficient  $k_E$  can be defined as

$$k_E = \frac{C_M}{\sqrt{C_P C_S}} \quad (4-55)$$

According to (4-49), (4-50), and (4-54),  $k_E$  can be expressed in terms of cross capacitances:

$$k_E = \frac{C_{Aa}C_{Bb} - C_{Ab}C_{Ba}}{\sqrt{(C_{Aa} + C_{Ab})(C_{Aa} + C_{Ba})(C_{Ab} + C_{Bb})(C_{Ba} + C_{Bb})}} \quad (4-56)$$

In a symmetrical coupling situation where  $C_{Aa} = C_{Bb} = C_1$ , and  $C_{Ab} = C_{Ba} = C_2$ ,  $k_E$  can be further simplified as

$$k_E = \frac{C_1 - C_2}{C_1 + C_2} \quad (4-57)$$

According to (4-57), when  $C_2$  is zero, i.e., there is no cross coupling between the primary and secondary plates,  $k_E$  equals one, indicating that only the main capacitances exist between the primary and secondary sides. In this case, the equivalent primary and secondary  $C_P$  and  $C_S$ , as well as the mutual capacitance  $C_M$  are all equal to half of  $C_1$  because the two coupling pairs are in series. When  $C_1$  equals  $C_2$ ,  $k_E$  becomes zero, indicating that cross coupling cancels out the main coupling so the overall mutual coupling between the primary and secondary sides becomes zero. In this case,  $C_P$  and  $C_S$  both equal  $C_1$  due to the contribution of cross coupling, and the mutual capacitance  $C_M$  equals to zero due to the cross coupling cancellation effect. When  $C_2$  is larger than  $C_1$ ,  $k_E$  will be negative, meaning that the coupling plates have changed to such an extent that the crossing coupling becomes larger than the main coupling. In such a case, the coupling pairs may be redefined to make  $k_E$  positive.

In fact, even for the general case defined in (4-56), it can be proven that  $k_E$  falls between -1 and 1, which provides a clear quantitative indication of the overall mutual capacitive coupling between the primary and secondary plates.

Two uncompensated CPT systems (referred to as CPT-1 and CPT-2) with different cross coupling configurations are constructed to compare their capacitive coupling coefficients. The coupling plates of the systems are made of four 100mm × 100mm square aluminum sheets coated with polyethylene as dielectric materials. CPT-1 and CPT-2 have the same main coupling capacitances, but their cross and leakage capacitances are varied by making the distance between the coupled plate pairs of CPT-2 larger. All coupling capacitances shown in Fig. 4-22 are measured using an accurate LCR meter and are shown in Table 4-2. Each parameter is measured independently by eliminating the effect other plates.  $C_P$  and  $C_S$  (see Fig. 4-23) are obtained by measuring the total capacitances when the primary and

secondary plates are shorted respectively, after the leakage capacitances  $C_{AB}$  and  $C_{ab}$  are deducted.  $C_M$  can be determined by (4-52) after a sinusoidal voltage source (with a peak value of 20V at an operating frequency of 1MHz) is applied at the primary side while peak value of the secondary side open-circuit voltage  $V_{SO}$  is measured. When  $C_P$ ,  $C_S$  and  $C_M$  are known,  $k_E$  can be determined by (4-55). The theoretical values of  $C_P$ ,  $C_S$ ,  $C_M$ , and  $k_E$  are also calculated from (4-49), (4-50), and (4-54) also shown in Table 4-2, which are in good agreement with the measured results.

**Table 4-2: Comparison between two CPT systems**

	<i>CPT-1</i>		<i>CPT-2</i>	
$C_{AB}$ (pF)	15		10	
$C_{ab}$ (pF)	15		10	
$C_{Aa}$ (pF)	201		200	
$C_{Bb}$ (pF)	199		201	
$C_{Ab}$ (pF)	43		23	
$C_{Ba}$ (pF)	40		21	
	Measured	Theoretical	Measured	Theoretical
$C_P$ (pF)	116	120	104	111
$C_S$ (pF)	115	120	101	111
$C_M$ (pF)	70	79	77	89
$k_E$	0.60	0.66	0.75	0.80

The primary side is driven by a 1MHz sinusoidal voltage source with a peak value of 20 V, and a purely resistive load of 2 k $\Omega$  is connected at the secondary output. Practical measurements showed that CPT-1 with  $k_E$  of 0.60 produced an output voltage with a peak value of 9.2 V, while CPT-2 with  $k_E$  of 0.75 produced an output voltage of 11.0 V. Clearly the higher output voltage and thus power of CPT-2 is contributed by a stronger overall mutual electric field coupling (reflected by a higher  $k_E$ ) between the primary and secondary plates due to reduced cross coupling effect.

## 4.5 Summary

This chapter presents an accurate steady-state model of the capacitive coupling interface of CPT systems with cross coupling. Effects of misalignment on parameters of the proposed model were analysed in detail. It shows that the input capacitance and the ideal

transformer of the proposed model vary with different coupling conditions while the output capacitance keeps constant. The proposed model was applied to determine the series tuning inductance of a CPT system with cross coupling between the primary and secondary sides to achieve full resonance, and the effect of misalignment on the output power was analysed. Simulations and experimental results have verified the effectiveness of the proposed model. The results of both simulations and experiments show that the calculated primary side tuning inductance can be used to achieve full resonance. With the series resonant compensation, it has demonstrated that misalignment within reasonable range can increase output power at some particular operating points and the relationships of measured output power versus misalignment and load changes agree well with the results predicted by the model. Furthermore, a dynamic model of a CPT system with primary side tuning is provided in the state-space form.

A new term named capacitive coupling coefficient  $k_E$  is also introduced to quantify the overall mutual capacitive coupling between the primary and secondary plates of a CPT system by taking the cross electric field coupling into consideration. The term is derived from a new model based on charge balance, and its physical meaning is explained and demonstrated by experimentally comparing two CPT systems with different cross coupling configurations.

## 5 High Order Compensation Networks for CPT

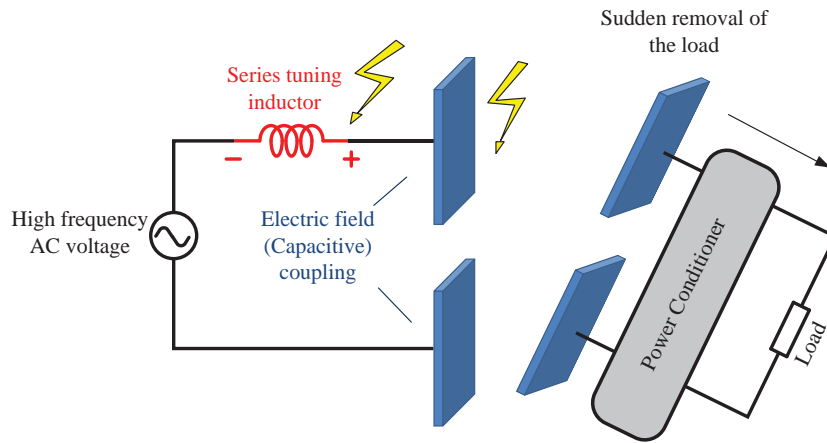
---

### 5.1 Introduction

As discussed in the preceding chapters, the most challenging part in a CPT system is the capacitive coupling interface. It features a small effective capacitance formed by coupling plates. In most CPT applications, the value of the capacitance ranges from a few tens to a few hundreds of picofarads. Thus, compensation networks are required to compensate for the large reactive impedance introduced by the capacitive coupling interface to maximize the power transfer capability. Moreover, the compensation networks and the capacitive coupling interface form a resonant tank that is necessary for resonant converters to achieve soft switching [89-93]. The advantages and disadvantages of existing compensation networks in CPT systems have been discussed in Chapter 2 [55, 56, 62, 64, 67, 85]. The single series tuning inductor is the simplest method to implement and widely used in CPT systems, but this method is vulnerable to open-circuit fault that generates high voltage spikes since the sudden removal of the load together with the secondary side coupling plates interrupts the current flowing through the tuning inductor. Another method uses an impedance transformation network that can “amplify” the load. If the combination of the transformation network and the load presents much larger impedance to the source than the capacitive coupling interface, the load can receive the majority of the power according to the voltage divider principle. However, it requires a very high voltage and extra reactive components on the secondary side to transfer a significant amount of power [52, 55, 56], which presents a safety hazard and increases the size and cost of the CPT system. A negative capacitance concept is proposed to increase the power transfer capability [65, 94,



95]. It is implemented with a capacitor switched by a full-bridge converter, which increases the complexity and cost of the system. The additional switching networks also increase the difficulty in system implementation at high frequency operation. As can be seen, among existing compensation methods, the single series inductor method is the simplest and has been widely used in most CPT systems to increase the power capability. However, it is vulnerable to open-circuit fault due to the ultra-high voltage spikes caused by the sudden removal of the load together with the secondary coupling plates, which is a common scenario for consumer electronics charging applications as shown in Fig. 5-1.



**Fig. 5-1: Demonstration of the sudden removal of the load in a CPT system.**

This chapter presents two new compensation methods. One is to address the open-circuit problem faced by the single series inductor method using a Z-impedance network. The Z-impedance network has been applied in various converters due to its buck-boost functionality and inherent short-circuit immunity [96-98]. Compared with previous work on Z impedance, this Z impedance based compensation focuses on its compensation and voltage boost capability for CPT applications. The basic configuration of the proposed CPT system and its working principle have been described. A mathematic model and underlying equations have been derived to demonstrate the compensating functionality. The effect of the Z-impedance network on the primary converter is also analyzed. Simulations and experimental results have shown the proposed system exhibits open-circuit and short-circuit immunity. The prototype system boosted the input voltage up to 50% with efficiency measured to be over 80%.

The other compensation network is based on a load transformation network. The proposed CPT system is based on the class E topology, which integrates a load transformation network. A state-space model of the system is established, based on which a brief design procedure is provided. Experimental results have demonstrated the load transformation network can increase the ratio of the load current to the tank current, increasing the power transfer capability.

## 5.2 Proposed Z-Impedance Compensation Network for CPT

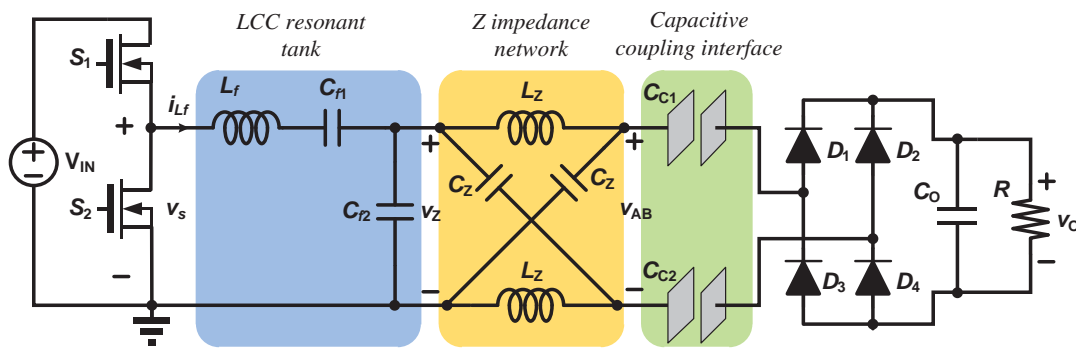


Fig. 5-2: Proposed CPT system with LCC and Z-impedance compensation network.

Fig. 5-2 shows the structure of the proposed CPT system with the Z-impedance compensation network. It includes a half-bridge inverter, a three-order LCC resonant tank, a Z-impedance compensation network, a capacitive coupling interface consisting of two pairs of coupling plates, and a full-bridge rectifier followed by a capacitive filter and a DC load.

### A) LCC resonant network

In Fig. 5-2,  $L_f$ ,  $C_{f1}$ , and  $C_{f2}$  constitute an LCC resonant tank as before the Z-impedance network, and  $C_{f1}$  is placed in series to block the DC offset from the voltage-fed half-bridge inverter. Such an LCC network combines the characteristics of series and parallel LC tanks to achieve high efficiency at light loading conditions, which is desirable for CPT applications with loosely coupled variable loads [99, 100]. Other resonant tanks such as series LC and LCL may also be used. However, a series LC tank has no voltage boost capability and an LCL tank involves one more inductor, which increases the system size

and cost. The capacitor  $C_{f2}$  in parallel with the Z-impedance network contributes to boosting the input voltage  $v_{IN}$ , which helps to increase the power transfer capability of CPT systems. The components of the LCC tank should satisfy the following equations:

$$C_{f1} = C_{f2} \quad (5-1)$$

$$C_f = \frac{C_{f1}C_{f2}}{C_{f1} + C_{f2}} = \frac{C_{f2}}{2} \quad (5-2)$$

$$L_f = \frac{1}{\omega_s^2 C_f} = \frac{2}{\omega_s^2 C_{f2}} \quad (5-3)$$

where  $\omega_s$  is the operating frequency of the half-bridge inverter.

### ***B) Z-impedance compensation network***

The Z-impedance network consists of two identical inductors  $L_Z$  and two identical capacitors  $C_Z$ , exhibiting a symmetrical Z shape structure. As will be explained in the following sections, the Z-impedance network is capable of boosting its input voltage  $v_Z$  and compensating for the capacitive coupling interface. Besides, it is immune to open-circuit and short-circuit faults, which are desirable for CPT applications such as charging portable consumer electronics. When the load together with the secondary coupling plates is suddenly removed, no high voltage spikes will be produced since no inductor current is interrupted, which is a great advantage compared with the conventional compensation method using a single series inductor.

#### **5.2.1 Modelling the Z-impedance Network**

The steady-state characteristics of the Z-impedance compensation network are analyzed using sinusoidal approximation method, assuming that the converter is working in continuous conduction mode and the composite resonant tank has a high Q response at the fundamental frequency of the driving AC voltage. In steady state, the characteristics of the Z-impedance network can be described with a two-port network model. Fig. 5-3 shows the circuit diagram with the voltage across the parallel capacitor  $C_{f2}$  approximated as a sinusoidal AC voltage source  $v_Z$ .  $C_C$  is the effective capacitance of the capacitive coupling interface ( $C_C = C_{C1}C_{C2}/(C_{C1} + C_{C2})$ ), and  $R_e$  is the effective AC resistance presented by the

rectifier with the load, which is equal to  $8R/\pi^2$  when a capacitive filter is used after the rectifier.

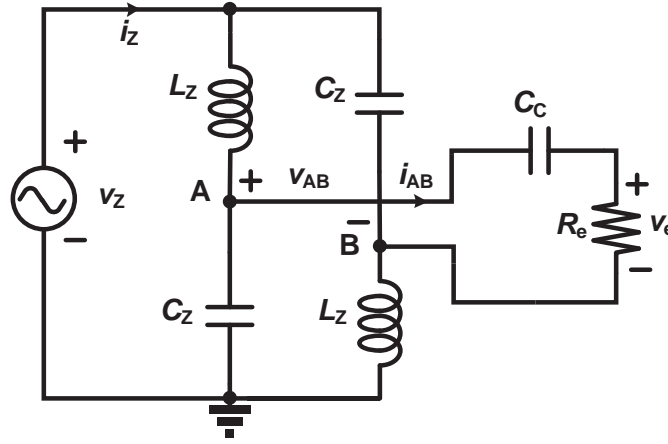


Fig. 5-3: Simplified circuit diagram of the CPT system with Z-impedance network.

The Z-impedance network is modeled using  $g$  parameters, as shown in Fig. 5-4. The terminal voltages and currents can be described as

$$\begin{cases} \mathbf{I}_Z = g_{11} \mathbf{V}_Z + g_{12} \mathbf{I}_{AB} \\ \mathbf{V}_{AB} = g_{21} \mathbf{V}_Z - g_{22} \mathbf{I}_{AB} \end{cases} \quad (5-4)$$

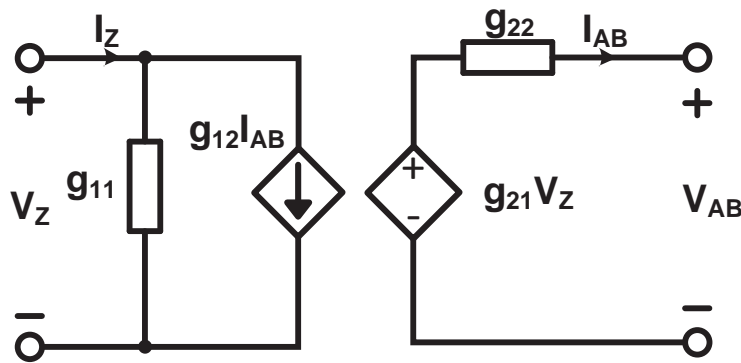


Fig. 5-4: The  $g$ -parameter description of the Z-impedance network.

Referring to Fig. 5-4, the  $g$  parameters can be obtained as

$$\left\{ \begin{array}{l} g_{11} = \frac{2}{j\omega_s L_Z + \frac{1}{j\omega_s C_Z}} = \frac{j2\omega_s C_Z}{1 - \omega_s^2 L_Z C_Z} \\ g_{12} = g_{21} = \frac{-j\omega_s L_Z + \frac{1}{j\omega_s C_Z}}{j\omega_s L_Z + \frac{1}{j\omega_s C_Z}} = \frac{1 + \omega_s^2 L_Z C_Z}{1 - \omega_s^2 L_Z C_Z} \\ g_{22} = \frac{2j\omega_s L_Z \times \frac{1}{j\omega_s C_Z}}{j\omega_s L_Z + \frac{1}{j\omega_s C_Z}} = \frac{j2\omega_s L_Z}{1 - \omega_s^2 L_Z C_Z} \end{array} \right. \quad (5-5)$$

For the convenience of analysis, a resonant frequency of the Z-impedance network  $\omega_Z$  is defined as

$$\omega_Z = \frac{1}{\sqrt{L_Z C_Z}} \quad (5-6)$$

And the normalized operating frequency  $F$  with respect to the resonant frequency of the Z-impedance network can be expressed as

$$F = \frac{\omega_s}{\omega_Z} \quad (5-7)$$

Substituting (5-7) and (5-6) into (5-5) gives

$$\left\{ \begin{array}{l} g_{11} = j\omega_s C_Z \frac{2}{1 - F^2} \\ g_{12} = g_{21} = \frac{1 + F^2}{1 - F^2} \\ g_{22} = j\omega_s L_Z \frac{2}{1 - F^2} \end{array} \right. \quad (5-8)$$

A close examination of (5-8) provides some insight into the Z-impedance network. The first term is an admittance of a capacitor, whose value is  $C_Z$  with a factor of  $2/(1-F^2)$ . The last term is a reactance of an inductor, whose value is  $L_Z$  with the same factor of  $2/(1-F^2)$ . The factor term  $2/(1-F^2)$  is the transformation factor of the Z-impedance network. With an

appropriate choice of the range of  $F$ , the  $g$ -parameter description can be transformed to an equivalent circuit model as illustrated in Fig. 5-5. It consists of an input parallel capacitor  $C_{eq}$  linked with an output series inductor  $L_{eq}$  by an ideal transformer with an effective turns ratio  $n_Z$ . Their values can be directly obtained from  $g$  parameters:

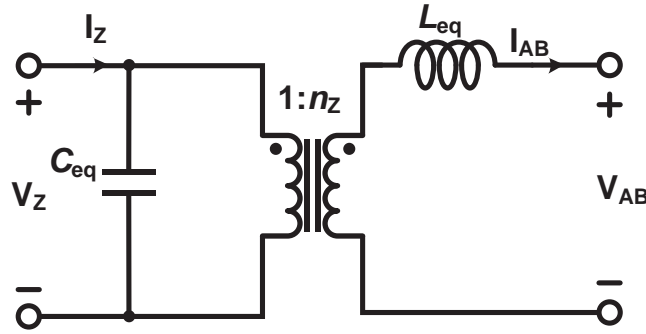


Fig. 5-5: The equivalent circuit model of the Z-impedance network.

$$n_Z = \frac{1 + F^2}{1 - F^2} \quad (5-9)$$

$$C_{eq} = \frac{2}{1 - F^2} C_Z \quad (5-10)$$

$$L_{eq} = \frac{2}{1 - F^2} L_Z \quad (5-11)$$

where  $0 < F < 1$ .

From (5-9), it can be seen that the Z-impedance compensation network has voltage boost capability since the turns ratio of the ideal transformer  $n_Z$  is always larger than one when  $F$  is less than one. The equivalent output inductance  $L_{eq}$  of the Z-impedance network provides the compensation functionality to cancel the impedance of the capacitive coupling interface. It should be noted that the equivalent input capacitance  $C_{eq}$  contributes to the parallel capacitor of the LCC tank, which should be taken into account in the system design procedure. The turns ratio  $n_Z$  and the normalized values of  $L_{eq}/L_Z$  and  $C_{eq}/C_Z$  versus the normalized frequency  $F$  are plotted in Fig. 5-6. They all rise monotonically with the

increase of  $F$ , which means that a high voltage boost ratio  $n_Z$  is achieved when the operating frequency is close to the resonant frequency of the Z-impedance network.

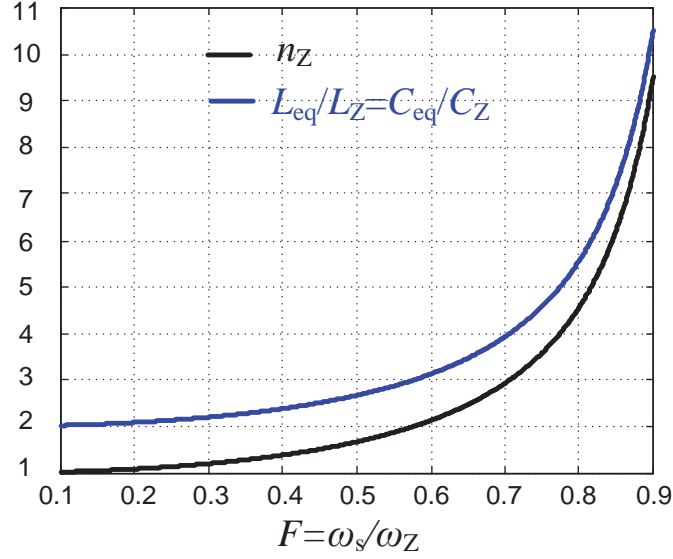


Fig. 5-6: Turns ratio  $n_Z$  and normalized inductance  $L_{eq}/L_Z (=C_{eq}/C_Z)$  versus  $F$ .

For a given value of  $L_Z$ , the required  $F_C$  to compensate for the coupling capacitance  $C_C$  can be calculated from (5-11):

$$F_C = \sqrt{1 - 2\omega_s^2 C_C L_Z} \quad (5-12)$$

which implies that  $L_Z < \frac{1}{2\omega_s^2 C_C}$ .

The required  $C_Z$  can be obtained from the definition of  $F$ :

$$C_Z = \frac{1 - 2\omega_s^2 C_C L_Z}{\omega_s^2 L_Z} \quad (5-13)$$

Therefore, the turns ratio  $n_Z$  is

$$n_Z = \frac{1 - \omega_s^2 C_C L_Z}{\omega_s^2 C_C L_Z} \quad (5-14)$$

In most cases,  $C_C$  can be treated as a fixed value for a certain application. Fig. 5-7 shows the variations of  $n_Z$  and  $C_Z/C_C$  with  $L_Z/(1/(\omega_s^2 C_C))$ . It can be seen that smaller  $L_Z$  yields larger turns ratio  $n_Z$  and  $C_Z$ .

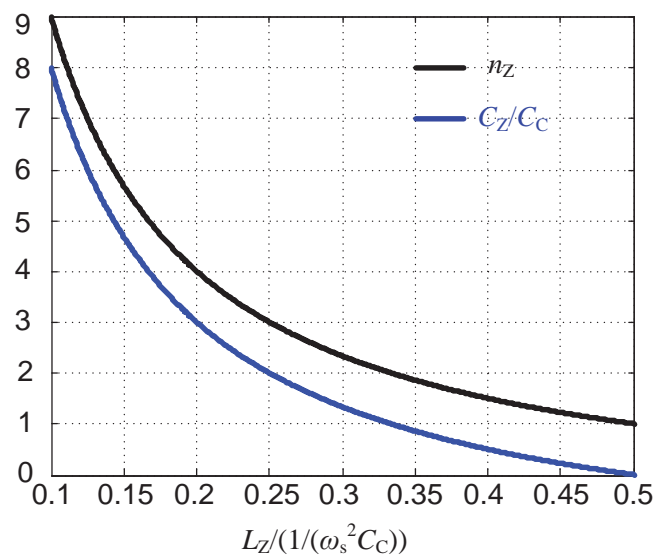


Fig. 5-7: The variations of turns ratio  $n_Z$  and  $C_Z/C_C$  versus  $L_Z/(1/(\omega_s^2 C_C))$ .



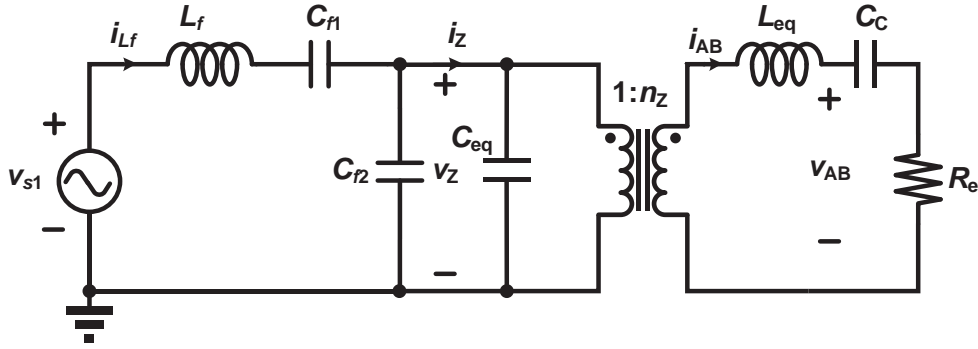


Fig. 5-8: Equivalent circuit of the proposed CPT system.

Using the derived circuit model of the Z-impedance network, an equivalent circuit model of the system is shown in Fig. 5-8.  $v_{s1}$  is the fundamental component of the output voltage of the half-bridge inverter. Referring the secondary side components to the primary side, a simplified equivalent circuit can be obtained in Fig. 5-9. If the equivalent output inductance  $L_{eq}$  fully compensates for the coupling capacitance  $C_c$ , the proposed system can be reduced to a LCC resonant circuit with a larger parallel capacitor ( $C_{f2} + C_{eq}$ ) and a smaller loading resistance ( $R_e/n_z^2$ ). After the parameters of Z-impedance network are determined, the calculation of the actual value of  $C_{f2}$  should take  $C_{eq}$  into consideration, that is

$$C_{f2,actual} = C_{f2,design} - C_{eq} \quad (5-15)$$

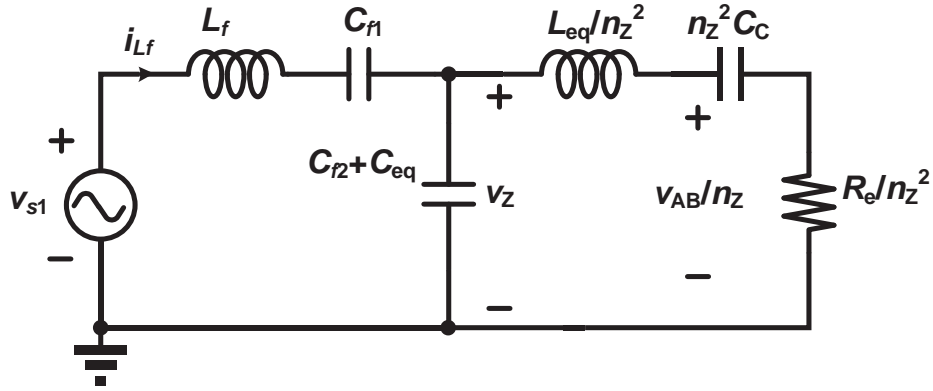


Fig. 5-9: The simplified circuit model of the proposed CPT system by reflecting components to the primary side through the ideal transformer.

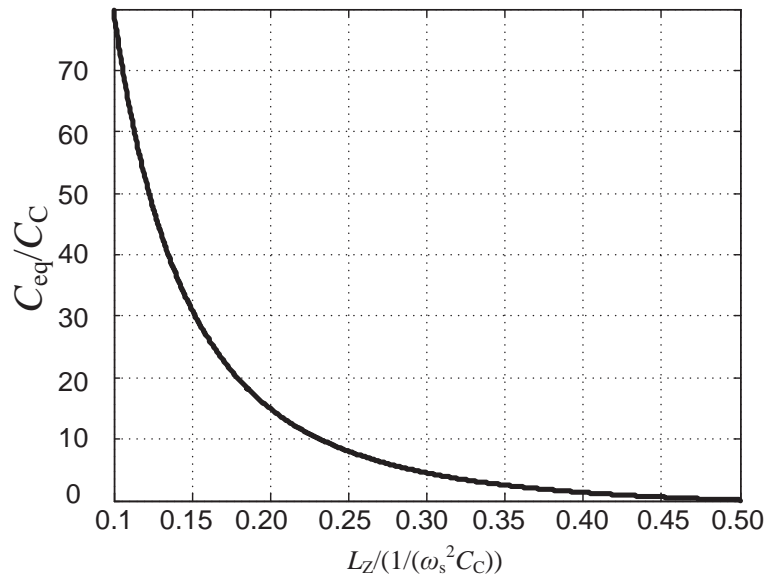


Fig. 5-10: Normalized equivalent input capacitance  $C_{eq}/C_C$  versus  $L_Z/(1/(\omega_s^2 C_C))$ .

In terms of  $L_Z$  and  $C_C$ ,  $C_{eq}$  can be expressed as

$$\frac{C_{eq}}{C_C} = \frac{1 - 2\omega_s^2 C_C L_Z}{(\omega_s^2 C_C L_Z)^2} \quad (5-16)$$

$C_{eq}/C_C$  as a function of  $L_Z/(1/(\omega_s^2 C_C))$  is illustrated in Fig. 5-10. It indicates that smaller  $L_Z$  yields larger equivalent input capacitance  $C_{eq}$ , which is tens of times larger than  $C_C$  if  $L_Z$  is less than one fifth of  $1/(\omega_s^2 C_C)$ .

Referring to Fig. 5-9, the input impedance of the resonant tank seen by the input voltage  $v_{s1}$  can be described as

$$\begin{aligned} \mathbf{Z}_i &= \frac{1}{1+Q_P^2} \frac{R_e}{n_Z^2} + j \left[ \omega_s L_f - \frac{2 + \frac{1}{Q_P^2}}{\omega_s \left( 1 + \frac{1}{Q_P^2} \right) C_{f2}} \right] \\ &= \frac{1}{1+Q_P^2} \frac{R_e}{n_Z^2} + j \frac{1}{\omega_s C_{f2}} \frac{1}{1+Q_P^2} \end{aligned} \quad (5-17)$$

where

$$Q_P = \omega_s C_{f2} \frac{R_e}{n_Z^2} \quad (5-18)$$

The time delay of the zero crossing point of the tank current caused by the inductive impedance is obtained by

$$t_d = \frac{\arctan \frac{n_Z^2}{\omega_s C_{f2} R_e}}{\omega_s} \quad (5-19)$$

The peak value of voltage  $v_Z$  across the Z-impedance network can be expressed as

$$\begin{aligned} v_{Z,peak} &= \frac{v_{S1,peak}}{\|\mathbf{Z}_i\|} \left\| \left( \frac{R_e}{n_Z^2 (1+Q_P^2)} + \frac{Q_P^2}{j \omega_s (1+Q_P^2) C_{f2}} \right) \right\| \\ &= Q_P v_{S1,peak} \end{aligned} \quad (5-20)$$

Ignore all the power losses, the output power  $P_O$  can be expressed as

$$P_O = \frac{2Q_P^2 n_Z^2}{\pi^2 R_e} V_{IN}^2 \quad (5-21)$$

It is noted that the above equations are derived with sinusoidal approximation method, which means the accuracy of the model is dependent on the quality factor of the resonant tank. The LCC tank serves the main purpose of filtering, which affects the performance of Z-impedance compensation network. Therefore, parameters of the LCC tank need to be designed to ensure a high quality factor  $Q_P$ . A tradeoff is needed when choosing a high voltage boost ratio  $n_Z$  and a high quality factor. Although the Z-impedance compensation network provides many benefits such as open-circuit and short-circuit immunity, it also has some downsides including more components counts and larger size. At high operating frequencies, these problems can be mitigated by low cost of the capacitors and modern surface-mount technology (SMT).

A brief design procedure for the CPT system is given as follows:

- 1) Calculate  $R_e$  for a given output power  $P_O$  using (5-21);
- 2) Choose  $L_Z$  for given  $\omega_s$ ,  $C_C$  ( $0.2 < L_Z/(1/(\omega_s^2 C_C)) < 0.5$ ) using (5-12);
- 3) Calculate  $n_Z$ ,  $C_{eq}$ , and  $C_Z$  from  $L_Z$  using (5-13), (5-14), and (5-16);
- 4) Calculate  $L_f$ ,  $C_{f1}$ , and  $C_{f2}$  based on calculated parameters for a given  $Q_P$  using (5-1)-(5-3), and (5-18);

### 5.2.2 Simulations and Experimental Results

A 5 W CPT system is designed based on the analysis in previous sections, aiming to power a consumer electronic device through a capacitive coupling interface of 250 pF. The experimental setup is shown in Fig. 5-11. System parameters for simulations and experiments are listed in Table I. In this design,  $n_Z$  equals 1.53, and  $C_{eq}$  is calculated to be 337 pF, which can be negligible compared with  $C_{f2}$  of 10 nF. The inductor  $L_f$  is slightly larger than calculated value that depends on combinational effects of the deadtime of the half-bridge inverter and the switching transition characteristics of switching devices.

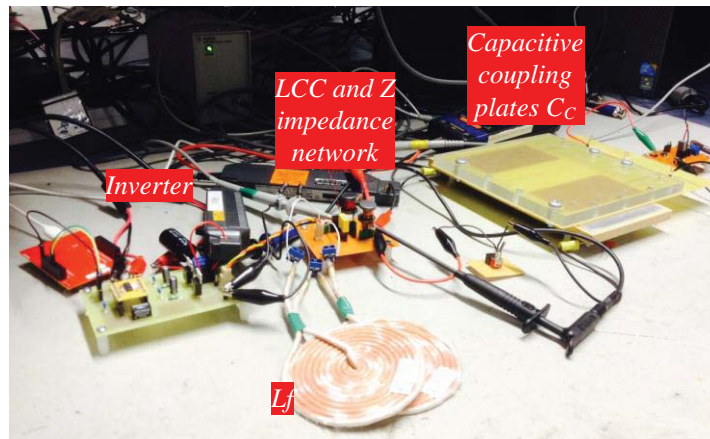


Fig. 5-11: Prototype of the proposed CPT system.

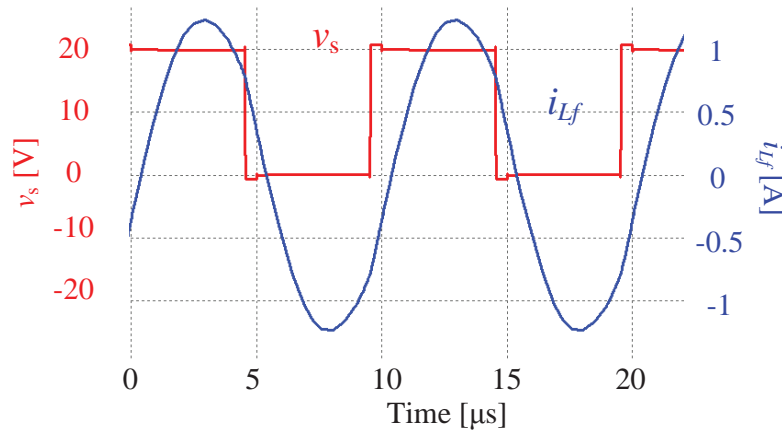
Table 5-1: System parameters for CPT with Z impedance

Parameter	Calculated Value	Experimental Value
Input voltage $V_{IN}$	20 V	20 V
The load $R$	50 $\Omega$	50 $\Omega$
Coupling capacitance $C_C$	250 pF	250 pF
$L_f$	5.1 $\mu$ H	5.5 $\mu$ H, air core, 15 turns
$C_{f1}, C_{f2}$	10 nF	10 nF, film, 630 V
$L_Z$	40 $\mu$ H	41 $\mu$ H, drum core 14 mm $\times$ 15 mm, TN100B, 26 turns
$C_Z$	133 pF	120 pF, ceramic, 1000 V
MOSFETs $S_1$ and $S_2$	FQP4N20	
Diodes $D_1 - D_4$	1N5819	

#### A) Simulated results

The simulate output power is about 4.8 W, which agrees with the desired design specifications. Fig. 5-12 shows the current into the LCC tank lags the output voltage of

the inverter, which means the inverter achieves zero voltage switching (ZVS) condition, thus yielding reduced switching losses. Fig. 5-13 shows the input voltage of the Z-impedance network is in phase with the current into it, indicating the Z-impedance network has completely compensated for the capacitive coupling interface. Fig. 5-14 shows the waveforms of  $v_Z$  and the secondary side voltage which is equal to  $v_Z$  times  $n_Z$ . Because the secondary voltage is a modeled voltage, the voltage across the AC resistive load is used to indicate it (they are equal when  $L_{eq}$  and  $C_C$  are at resonance). It clearly shows that the voltage  $v_Z$  is boosted up to about 1.49 times higher. Fig. 5-15 and Fig. 5-16 demonstrates the short-circuit and open-circuit immunity. When the secondary side plates were shorted, the voltage across the primary side plates and the current through the inductor  $L_f$  settled down after a short transition, and no extreme voltage or current spikes were generated during the transient phase. As shown in Fig. 5-16, the proposed Z-impedance compensation network caused no extreme high voltage spikes suffered by the conventional single series inductor method.



**Fig. 5-12: Simulated waveforms of the output voltage of the inverter and the current into the LCC tank.**

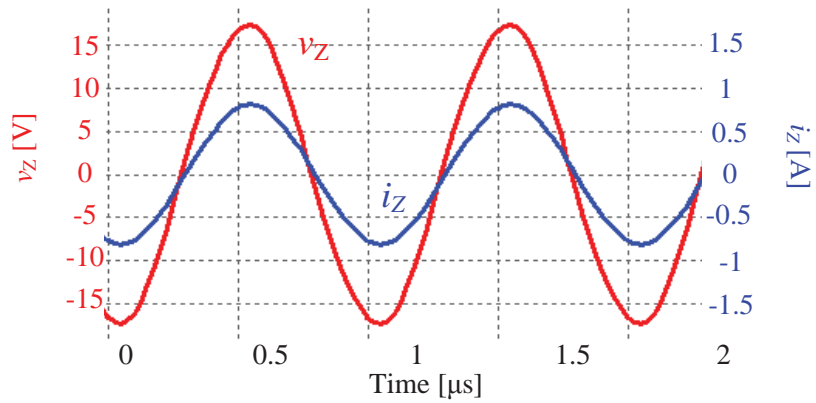


Fig. 5-13: Simulated waveforms of the input voltage of Z-impedance network and the current into it.

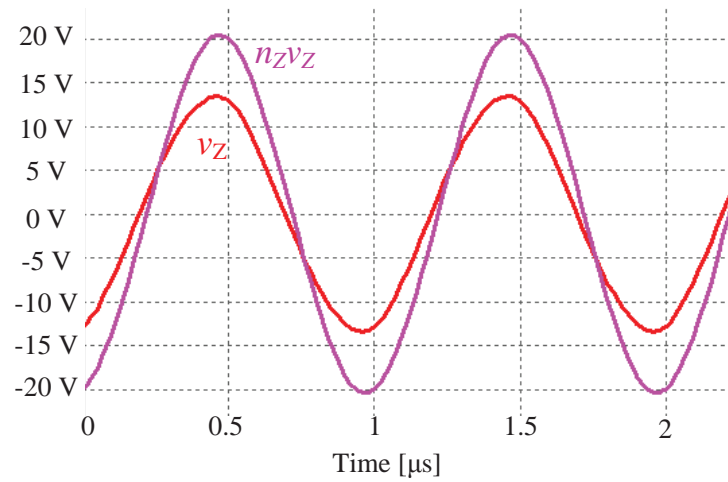
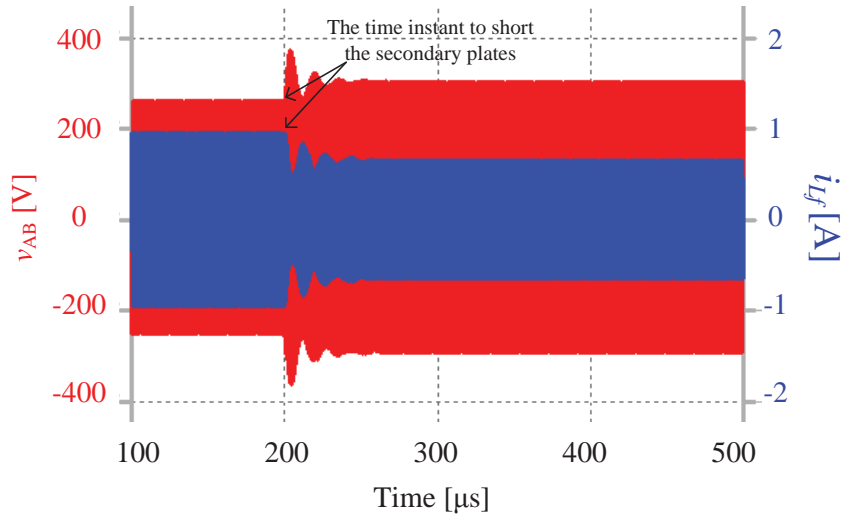
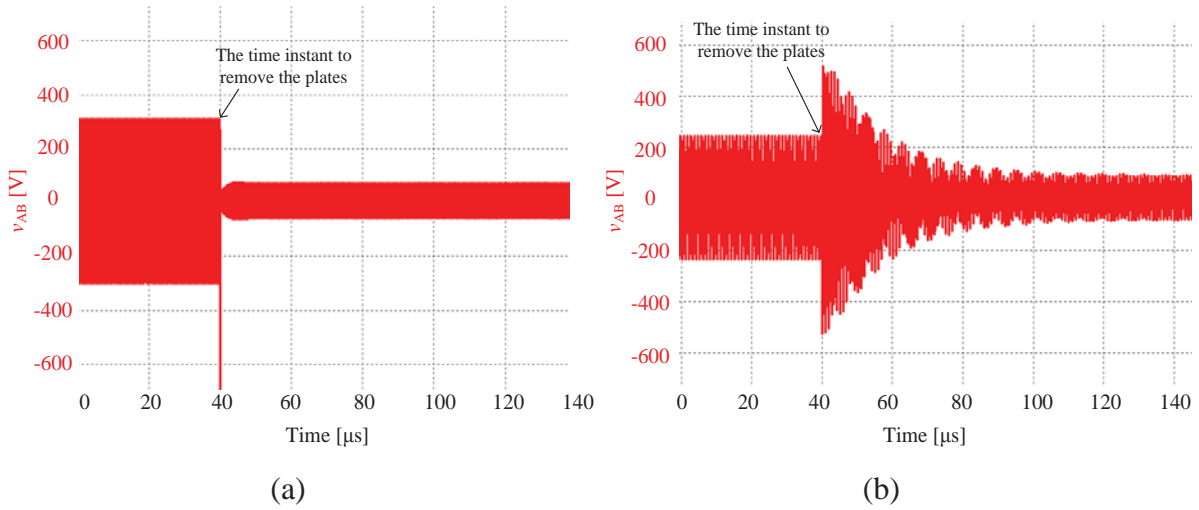


Fig. 5-14: Simulated waveforms of the input voltage of Z-impedance network  $v_Z$  and the secondary side voltage.



**Fig. 5-15: Simulated transient response of the voltage across the primary plates and the current through  $L_f$  after the sudden shorting of the secondary plates.**



**Fig. 5-16: Simulated transient responses of the voltage across the primary plates after the sudden removal of secondary plates of the CPT system with (a) the single series inductor compensation and (b) the proposed Z-impedance compensation.**



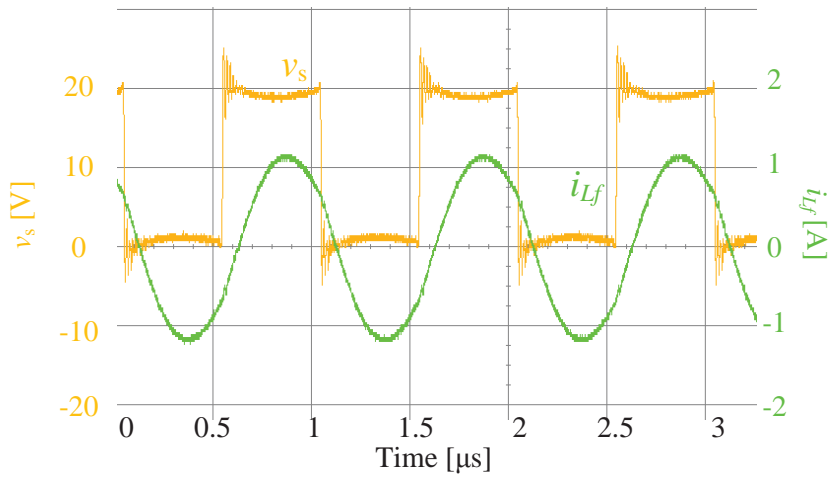
***B) Experimental results***

Experiment was set up based on system parameters listed in Table 5-1. The capacitive coupling interface was made of two pairs of  $100\text{ mm} \times 100\text{ mm}$  square copper pads coated with polypropylene (its dielectric constant is about 2) as the dielectric materials. The size of plates can be made larger or smaller depending on specific applications. For example, a higher operating frequency can make coupling plates smaller. The operating frequency was chosen to be 1 MHz. Switching devices used in the inverter were MOSFET FQP4N20, and the rectifier was composed of four schottky diodes of are 1N5819. Two ceramic capacitors of 120 pF are used in the Z-impedance network, in which the inductors are wound on a drum-shape ferrite core with 0.5 mm wires. Fig. 5-17 and Fig. 5-18 shows the experimental results, indicating the inverter achieved ZVS condition and the Z-impedance network was able to cancel out the reactance of the capacitive coupling interface, thus yielding a pure resistive network. Fig. 5-19 demonstrated the voltage boost capability of the Z-impedance network with  $n_Z$  measured to be around 1.5. Experimental waveforms similar to simulation were depicted in Fig. 5-20. The oscillation period was shorter than simulation due to the damping caused by parasitic resistances. Fig. 5-21 shows when the secondary side plates were removed, no extra high voltage spike was generated, exhibiting open-circuit immunity as desired. As shown clearly, the single series inductor compensation method generated extremely high voltage at the instant of removal of the load, while the voltage overshoot using Z-impedance network is less than 400 V.

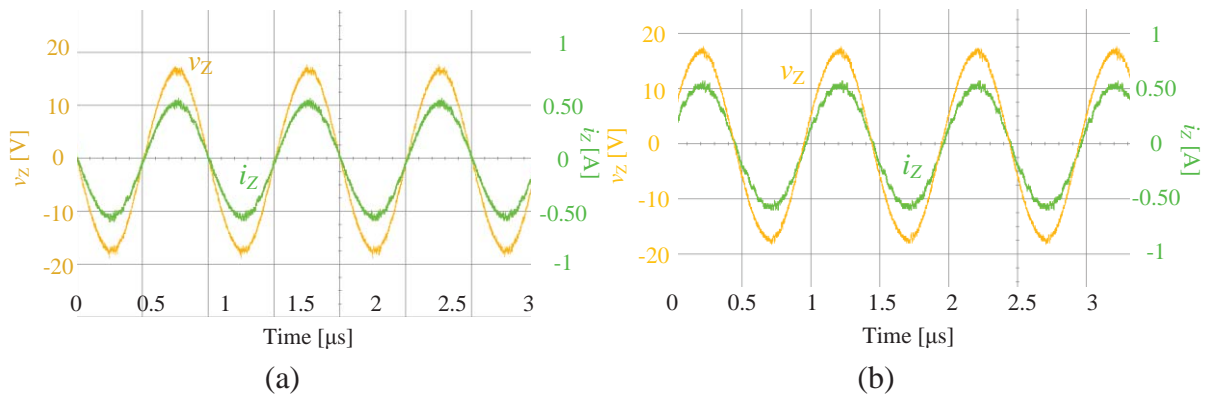
The input DC voltage is 20 V and the input DC current is measured to be 0.2 A. The DC output voltage across the  $50\ \Omega$  load is 12.92 V, yielding power of 3.33 W. Thus, the efficiency of the system is about 83 %. The sources of the losses come from the switching off transition loss of switching devices, conduction loss of the diodes, and losses of inductor including conduction losses and core losses. The MOSFET is modeled as an ideal switch in series with an ON resistance ( $1.4\ \Omega$ ). The diode is modeled as a DC voltage (0.6 V) in series with an ON resistance ( $0.5\ \Omega$ ). The power losses can be estimated by the resistances of components and their distribution is shown in Fig. 5-22.

At high frequency operation, the core loss dominates the losses of the inductor, thus small value inductors are preferred in the design of compensation network. The proposed CPT system uses small inductors and can significantly reduce losses, improving system

efficiency. It was found when  $Q_P$  was chosen to 2.67,  $C_{f2}$  was increased to be 20 nF, and the efficiency dropped to about 50 %. The higher  $Q_P$  leads to better filtering, generating less noise. However, it will increase the inductor current, leading more losses and reduce the efficiency. A trade-off has to be made for  $Q_P$  between higher efficiency and better waveforms. Besides, inductors of the Z impedance network cannot be arbitrary small. It can affect the voltage boost ratio  $n_Z$ , which also relates to the value of  $Q_P$ . Small  $L_Z$  will yield larger  $n_Z$ , thus reducing the quality factor  $Q_P$ .



**Fig. 5-17: Experimental waveforms of the output voltage of the inverter and the current into the LCC tank.**



**Fig. 5-18: Experimental waveforms of the input voltage of Z-impedance network and the current  $i_Z$  into it with (a) 50  $\Omega$  AC load and (b) 50  $\Omega$  DC load.**

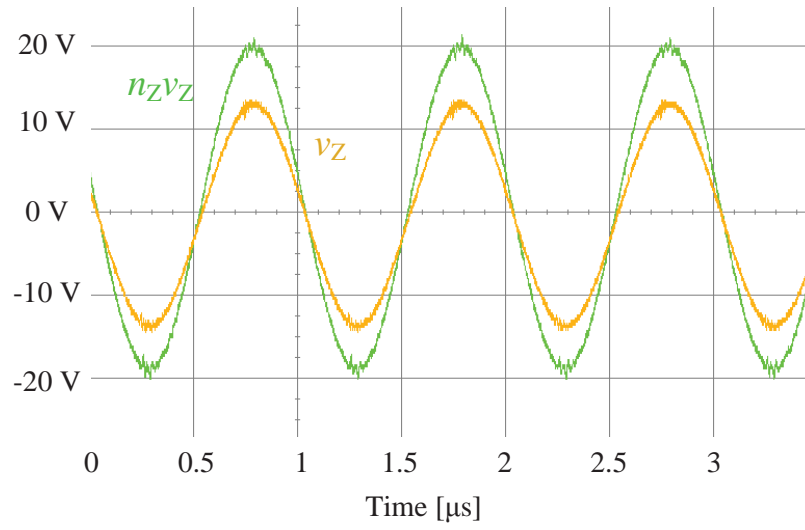


Fig. 5-19: Experimental waveforms of the input voltage of Z-impedance network  $v_Z$  and the secondary side voltage  $n_Z v_Z$ .

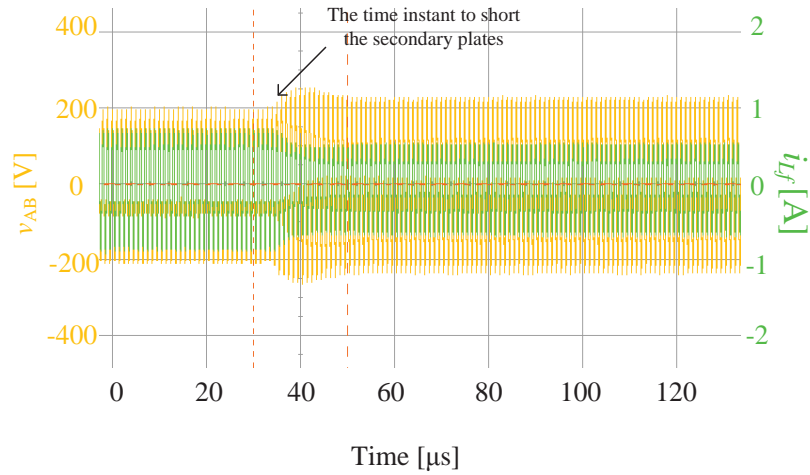
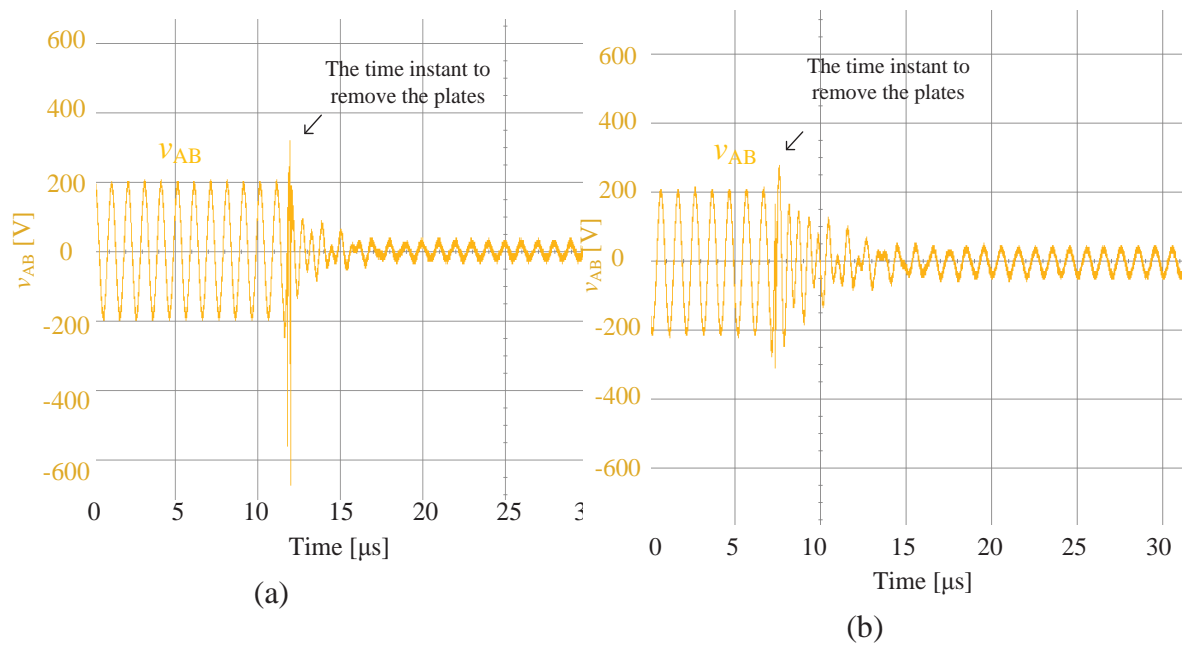
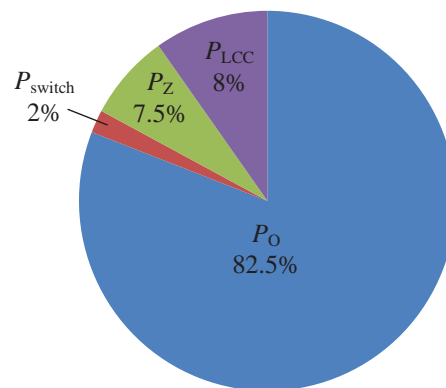


Fig. 5-20: Transient response of the voltage across the primary plates and the current through  $L_f$  after the sudden shorting of the secondary plates.



**Fig. 5-21: Transient responses of the voltage across the primary plates after the sudden removal of secondary plates of the CPT system with (a) the single series inductor compensation and (b) the proposed Z-impedance compensation.**



**Fig. 5-22: Power distribution of the system.**

### 5.3 Modified Class E topology with Load Compensation

#### 5.3.1 Modified Class E Topology and State-space modelling

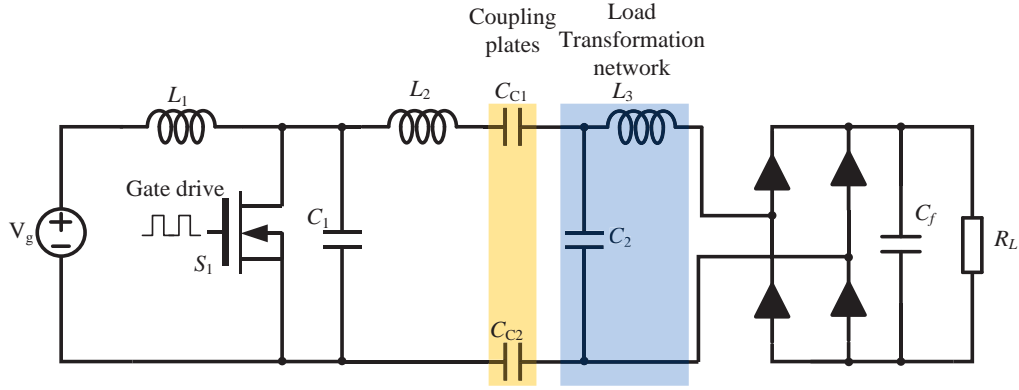


Fig. 5-23: A CPT system based on a modified class E topology.

The proposed CPT system based on a modified class E topology is illustrated in Fig. 5-23. The load transformation network is composed of  $C_2$  and  $L_3$ , which is inserted between the capacitive coupling interface and the rectifier with a capacitive filter. The equivalent circuit model is shown in Fig. 5-24.  $C_C$  is the effective capacitance of the series combination of  $C_{C1}$  and  $C_{C2}$ .  $R_e$  is the equivalent resistance exhibited by the rectifier, which is  $\pi^2/8 \cdot R_L$ . The duty cycle of the switch is fixed to be 0.5 to yield the optimum performance.  $v_e$  is the fundamental component of the input voltage of the rectifier.

As can be seen, the CPT system based on the modified class E topology is a higher order system, which well suits the state-space description. The switch  $S_1$  is modelled as an ideal switch, which can transition between ON and OFF states instantly, and an ON resistance.

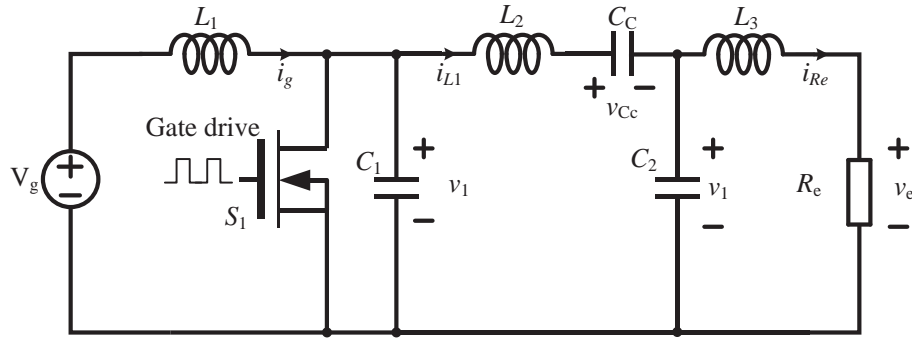


Fig. 5-24: Equivalent circuit of the proposed CPT system.

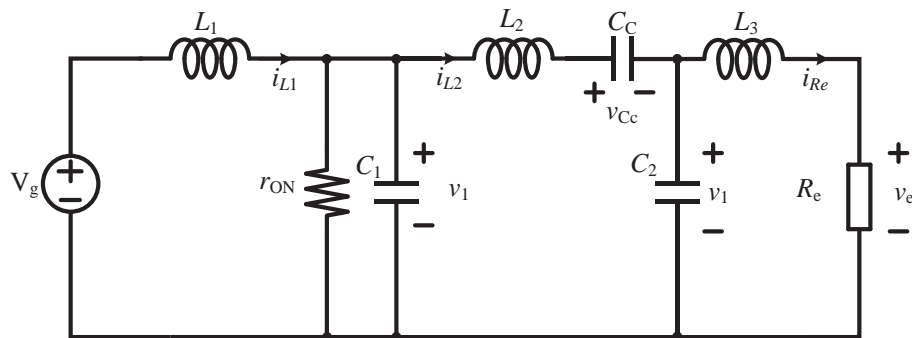
The switching action divides the system into two operation states:

When  $S_1$  turns on, the equivalent circuit can be obtained as shown in Fig. 5-25.  $r_{ON}$  represents the turn-on resistance of the switch. The state variables are chosen to be:

$$\mathbf{x} = [i_{L1} \quad i_{L2} \quad i_{Re} \quad v_{C1} \quad v_{Cc} \quad v_e]^T \quad (5-22)$$

The input variable  $u$  is

$$u = V_g \quad (5-23)$$


 Fig. 5-25: Equivalent circuit when  $S_1$  turns on.

Then the standard form of the state-space equation should be

$$\dot{\mathbf{x}} = \mathbf{A}_1 \mathbf{x} + \mathbf{b}u \quad (5-24)$$

where

$$\mathbf{A}_1 = \begin{bmatrix} 0 & 0 & 0 & -\frac{1}{L_1} & 0 & 0 \\ 0 & 0 & 0 & \frac{1}{L_2} & -\frac{1}{L_2} & -\frac{1}{L_2} \\ 0 & 0 & -\frac{R_e}{L_3} & 0 & 0 & \frac{1}{L_3} \\ \frac{1}{C_1} & -\frac{1}{C_1} & 0 & -\frac{1}{r_{ON}C_1} & 0 & 0 \\ 0 & \frac{1}{C_c} & 0 & 0 & 0 & 0 \\ 0 & \frac{1}{C_2} & -\frac{1}{C_2} & 0 & 0 & 0 \end{bmatrix}$$

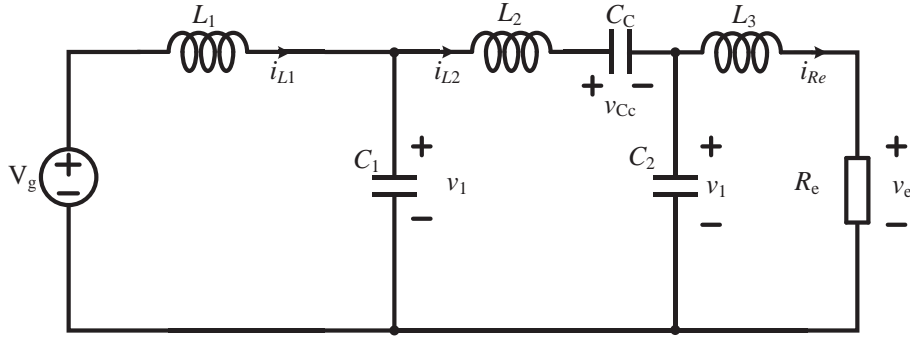
$$\mathbf{b} = \left[ \frac{1}{L_1} \quad 0 \quad 0 \quad 0 \quad 0 \quad 0 \right]^T$$

When  $S_1$  turns on, the equivalent circuit can be obtained as shown in Fig. 5-26. Accordingly, the standard form of the state-space equation is

$$\dot{\mathbf{x}} = \mathbf{A}_2 \mathbf{x} + \mathbf{b}u \quad (5-25)$$

where

$$\mathbf{A}_2 = \begin{bmatrix} 0 & 0 & 0 & -\frac{1}{L_1} & 0 & 0 \\ 0 & 0 & 0 & \frac{1}{L_2} & -\frac{1}{L_2} & -\frac{1}{L_2} \\ 0 & 0 & -\frac{R}{L_3} & 0 & 0 & \frac{1}{L_3} \\ \frac{1}{C_1} & -\frac{1}{C_1} & 0 & 0 & 0 & 0 \\ 0 & \frac{1}{C_c} & 0 & 0 & 0 & 0 \\ 0 & \frac{1}{C_2} & -\frac{1}{C_2} & 0 & 0 & 0 \end{bmatrix}$$


 Fig. 5-26: Equivalent circuit when  $S_1$  turns off.

The analytical solution of (5-24) can be expressed as

$$\mathbf{x}_1(t) = e^{\mathbf{A}_1 t} \mathbf{x}_1(0) + \mathbf{A}_1^{-1} (e^{\mathbf{A}_1 t} - \mathbf{I}) \mathbf{b} \mathbf{u} \quad (5-26)$$

where  $0 \leq t < T/2$ .

Similarly, the analytical solution of (5-25) can be expressed as

$$\mathbf{x}_2(t) = e^{\mathbf{A}_2(t-\frac{T}{2})} \mathbf{x}_1(\frac{T}{2}) + \mathbf{A}_2^{-1} (e^{\mathbf{A}_2(t-\frac{T}{2})} - \mathbf{I}) \mathbf{b} \mathbf{u} \quad (5-27)$$

where  $T/2 \leq t < T$ .

In steady state, the states of the system should satisfy

$$\mathbf{x}_1(0) = \mathbf{x}_2(T) \quad (5-28)$$

Substituting (5-26) and (5-27) into above equation yields

$$\mathbf{x}_1(0) = (1 - e^{\mathbf{A}_2 \frac{T}{2}} e^{\mathbf{A}_1 \frac{T}{2}})^{-1} \left[ e^{\mathbf{A}_2 \frac{T}{2}} \mathbf{A}_1^{-1} (e^{\mathbf{A}_1 \frac{T}{2}} - \mathbf{I}) + \mathbf{A}_2^{-1} (e^{\mathbf{A}_2 \frac{T}{2}} - \mathbf{I}) \right] \mathbf{b} \mathbf{u} \quad (5-29)$$

This result will be used to obtain the optimum values of the system in the design procedure.



### 5.3.2 Design of Load Transformation Network

To provide a circuit-intuitive design guide to determine the components of the load transformation network, the sinusoidal approximation method is used to analyze the system. The voltage  $v_1$  across the capacitor  $C_1$  is approximated using a sinusoidal voltage source, which is the fundamental component of the voltage  $v_1$  at the switching frequency. The equivalent circuit is shown in Fig. 5-27. For the convenience of analysis, the series inductor  $L_2$  is split into two inductors  $L_{2a}$  and  $L_{2b}$ .  $L_{2a}$  is the part of inductance that is at resonance with the coupling capacitance  $C_C$ .  $L_{2b}$  is the part that provides enough remaining inductance to ensure ZVS condition.  $Z_2$  is the impedance exhibited by the load transformation network, which can be expressed as

$$Z_2 = \frac{R_e}{(1 - \omega^2 L_3 C_2)^2 + (\omega R_e C_2)^2} + j \frac{\omega L_3 (1 - R_e^2 C_2 / L_3 - \omega^2 L_3 C_2)}{(1 - \omega^2 L_3 C_2)^2 + (\omega R_e C_2)^2} \quad (5-30)$$

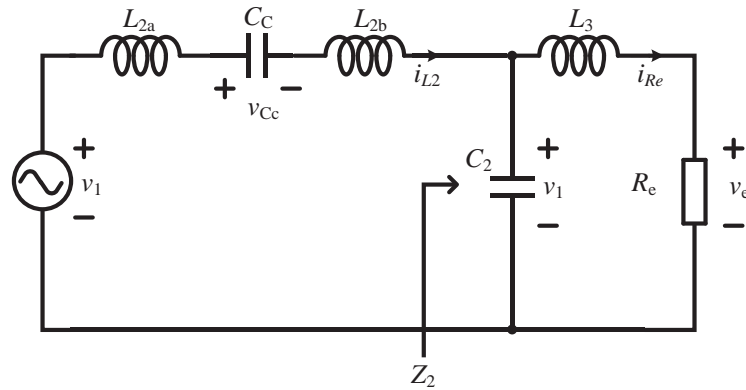


Fig. 5-27: The equivalent circuit of the tank with  $L_2$  represented by two split inductors  $L_{2a}$  and  $L_{2b}$ .

When  $C_2$  and  $L_3$  are at resonance,  $Z_2$  becomes

$$Z_2 = Q_2^2 R_e - j Q_2 R_e \quad (5-31)$$

where

$$Q_2 = \frac{\omega L_3}{R_e} = \frac{1}{\omega C_2 R_e} \quad (5-32)$$

It can be seen that at resonance the impedance presented by the load transformation network includes a capacitive reactance, which can be compensated for by the  $L_{2b}$ .

Ignoring the losses of reactive components in the load transformation network, the following power relationship can be obtained:

$$I_{Re}^2 R_e = I_{L2}^2 Q_2^2 R_e \quad (5-33)$$

where  $I_{Re}$  is the peak value of the current flowing through the equivalent load resistance  $R_e$ ,  $I_{L2}$  is the peak value of the current flowing through the capacitive coupling interface.

From (5-33) the ratio of the current flowing through the load to the current through the capacitive interface is given by

$$\frac{I_{Re}}{I_{L2}} = Q_2 \quad (5-34)$$

The LCL network design is based on the series tank of the class E inverter. After the components of the class E inverter are determined, an iterative algorithm can be used to specify the values of components of the LCL tank. With the initial and ZVS conditions, the parameters of the system can be determined accordingly. The following procedure is proposed for designing the system:

1. Specify the input values for  $P_{in}$ ,  $C_C$ ,  $f$ ,  $R_T$ ,  $Q$ ;
2. Determine the elements values for  $R_{eq}$ ,  $L_{2a}$ ,  $C_1$ ,  $V_{in}$ ,  $I$  and  $\Delta z$  ( $\Delta z$  is the condition for ZVS);
3. Specify initial values of  $Q_2$ ,  $L_{2b}$ ,  $C_2$ ;
4. Find solutions of  $|\mathbf{x}_{1,3}(0)| < |\Delta z|$  by changing values of  $L_3$ ,  $C_2$ ;
5. Obtain the desired results.

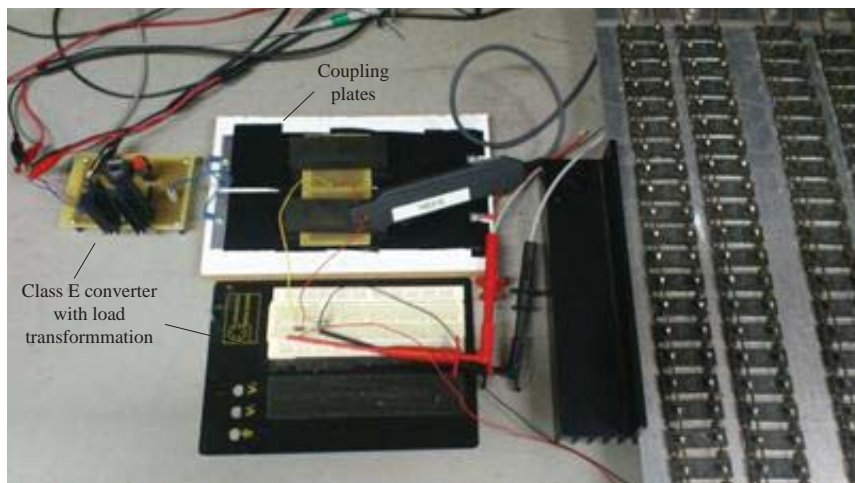
### 5.3.3 Experimental results

A prototype CPT system using the proposed load transformation network is designed and built, which is illustrated in Fig. 5-28. The system parameters are listed in Table 5-2.

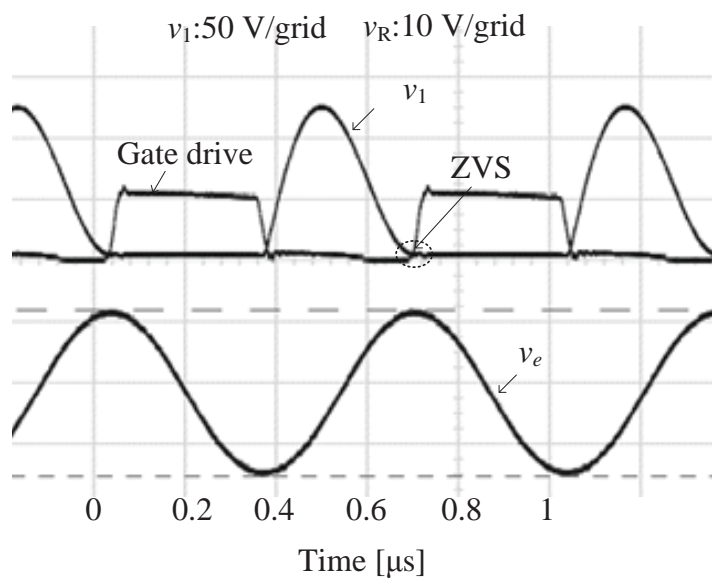
Experimental voltage and current waveforms are shown in Fig. 5-29 and Fig. 5-30. It was observed that the output voltage was of a good quality sinusoidal waveform, which confirmed that the proposed compensation method served as an effective band pass filter. The voltage  $v_1$  across the switch fell to zero before the switch is turned on, demonstrating ZVS condition was achieved. The tank current  $i_{L2}$  was smaller than the load current  $i_{Re}$  as expected. This implies that the system can achieve higher output power without imposing higher voltage stress on the coupling plates. This is one of the significant features of the proposed compensation method based on the load transformation. The efficiency was measured to be about 66%, which is relatively low due to the core losses and conduction losses of the inductor. It can be further improved if better components with low ESRs are used.

**Table 5-2: System parameters of CPT with load transformation**

PARAMETERS	VALUES
Input voltage $V_{in}$	30 V
Operating frequency, $f$	1.5 MHz
Input power $P_{in}$	6 W
Out power $P_{out}$	3.97 W
Load Resistance $R$	4.2 $\Omega$
Duty cycle $D$	0.5
Total coupling capacitance $C_C$	100 pF
Series tank inductor $L_2$	127.5 $\mu$ H
Parallel capacitor $C_1$	182.334 pF
LCL tank capacitor $C_2$	5.6 nF
LCL tank inductor $L_3$	2.5 $\mu$ H



**Fig. 5-28: Prototype of the proposed CPT system with load transformation.**



**Fig. 5-29: The voltage across the switch and gate drive signal demonstrating ZVS.**

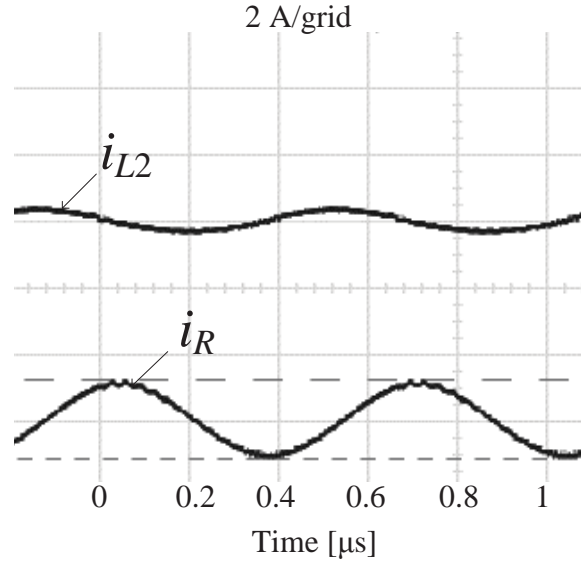


Fig. 5-30: The currents through the capacitive coupling interface and the load.

## 5.4 Summary

This chapter proposes two compensation methods for CPT systems.

The first method is using a Z-impedance network to compensate for the capacitive coupling interface. It can eliminate the extremely high voltage spikes suffered by conventional single series inductor compensation method from open-circuit fault when the secondary side plates are suddenly removed. The proposed Z-impedance compensation network can bring additional advantages such as short-circuit immunity and voltage boost capability. A mathematical model of the Z-impedance network is developed and an equivalent circuit model of the whole system is established to analyze the effects of Z-impedance network on the LCC tank. The equivalent output inductance exhibited by Z-impedance network can be adjusted by changing the normalized frequency. Simulations and experimental results from a 5 W CPT system design demonstrated that the proposed Z-impedance network could effectively compensate for the reactance of the capacitive coupling interface with short-circuit and open-circuit immunity, and boosted the output voltage up to 50% with measured efficiency of over 80%.

The second method is using an LCL resonant network integrated with the class E topology. A dynamic state space model of the system is derived. The conventional class E design method is combined with a computer-based iteration algorithm to determine the parameters of the proposed compensation circuit which gives high power transfer capacity and power efficiency. The experimental results have shown that the proposed method can help increase the load current while maintaining a relatively low current through the coupling plates. Thus, it can improve the power transfer capability of the CPT system with reduced voltage across the coupling places and better filtering of switching harmonics to the load. Experimental results have demonstrated the current through the load was about three times higher than that through the capacitive coupling interface.

## 6 Power Flow Control of CPT Using Switched Capacitors

---

### 6.1 Introduction

In previous chapters, the selection of converters suitable for CPT systems has been discussed. A new steady-state model of the capacitive coupling interface and a quantitative term defining the mutual coupling in the capacitive coupling interface have been provided. A Z-impedance compensation network has been proposed to address the short-circuit problem suffered by the conventional inductor-based compensation method, and a load transformation network has been developed to increase the ratio of the load current to the tank current so as to increase the power transfer capability.

For practical CPT systems, the power flow control is an indispensable part, which regulates the output regardless of circuit parameter variations and load change. The tuning/detuning method using a soft-switched transformer will increase the system size, and extra inductive components are not suitable for high frequency operation due to core losses of magnetic materials. The multiple-period pulse-width method varies the operating frequency, complicating the filter design and introducing EMI problem.

This chapter proposes a novel control scheme by switching a shunt capacitor bank. The CPT system is built based on a class E converter topology. In Chapter 3, the CPT system based on the class E converter topology has demonstrated higher efficiency and higher output power for given input voltages and coupling capacitance. It uses only one single switching device, eliminating the short-through problem suffered by most other converter topologies using multiple switches. Moreover, the design of the gate driver circuitry is also

simple since the source of the MOSFET is connected to the ground. The capacitor bank consists of multiple small capacitors in parallel. The effective capacitance of the switched capacitor bank is determined by the number of the capacitors connected to the circuit.

## 6.2 New Suboptimum Operation of Class E Converter

In the previous analysis, the CPT system based on the class E converter topology is designed to work in the optimum operation mode, which needs to satisfy both zero voltage and zero voltage slope conditions at the turn-on time instant of the switch [75, 76, 101, 102]. However, this optimum operation offers little flexibility of design since all the circuit parameters are all set according to the required lagging phase shift between the tank voltage and current. The suboptimum operation of the class E converter satisfies only the zero voltage condition, which provides a wider range of various system parameters such as shunt capacitors, tank inductors, and operating frequency [103]. However, there exists another suboptimum operation mode for the class E converter. It satisfies the zero voltage condition not only at the turn-on instant of the switch but also maintains zero drain-source voltage for a duration when the body diode of the switching device is conducting current. This feature provides a new way of controlling the output power by changing the resonant frequency of the tank while maintaining high efficiency. The proposed control scheme is based on this new suboptimum operation of the class E converter topology. The effective capacitance of the shunt capacitor bank is controlled by the states of the switches. The circuit parameters need to be redesigned to maintain the sub-optimum operation while changing the shunt capacitance, which is different from previous optimum and sub-optimum operation.

The CPT system based on the class E converter topology is redrawn in Fig. 6-1 for convenience of analysis. The two pairs of coupling plates are represented as a single effective coupling capacitor  $C_C$ . The inductor in the resonant tank  $L_T$  is split into two parts. One part named  $L_{rc}$  is at resonance with  $C_C$ . The other part  $L_{rx}$  provides required inductive impedance to achieve ZVS condition.



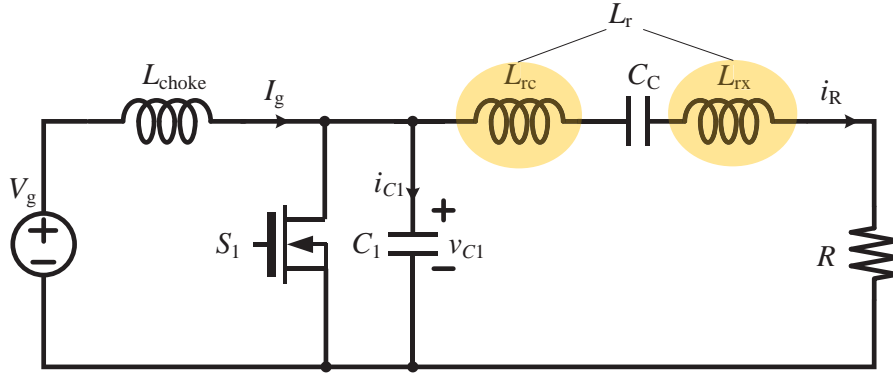


Fig. 6-1: Redrawn diagram of the CPT system based on Class E topology.

Since all the circuit parameters of the class E are interrelated, it is not easy and straightforward to find the effect of the shunt capacitance variation on the voltage across the switch. However, a qualitative analysis can be provided by viewing the class E operation as a combination of two different resonant modes, which can help to determine the maximum and minimum values of the shunt capacitance that can still stay in the sub-optimum operation mode.

When the switch  $S_1$  is open, the voltage  $v_{C1}$  can be seen as the response of a forced second order system consisting of  $L_r$ , a series connection of  $C_C$  and  $C_1$ , and the load  $R$ . The oscillation frequency  $\omega_d$  of  $v_{C1}$  can be expressed as

$$\begin{aligned}\omega_d &= \frac{1}{\sqrt{L_r \frac{C_C C_1}{C_1 + C_C}}} \sqrt{1 - \frac{1}{4Q_L^2}} \\ &= \frac{1}{\sqrt{L_r \frac{C_C}{1 + \frac{C_C}{C_1}}}} \sqrt{1 - \frac{1}{4Q_L^2}}\end{aligned}\tag{6-1}$$

where

$$Q_L = \frac{\omega L_r}{R}$$

If  $Q_L$  is large enough, the period of the voltage  $v_{C1}$  is

$$T_d = \frac{2\pi}{\omega_d} = 2\pi \sqrt{L_r \frac{C_c}{1 + \frac{C_c}{C_1}}} \quad (6-2)$$

As can be seen from (6-2), when the shunt capacitor  $C_1$  increases, the period of oscillation will increase, which indicates that the oscillating waveform  $v_{C1}$  will not drop to zero at the turn-on instant of the switch. The increase of  $C_1$  will delay the zero cross point of the voltage across the switch  $v_{C1}$ , failing to achieve the ZVS condition. Thus, the upper limit of the value of  $C_1$  will cause  $v_{C1}$  to exactly reach zero at the turn-on instant of the switch. The lower limit of the value of  $C_1$  will cause  $v_{C1}$  to drop to zero at a quarter of the operating period. Fig. 6-2 demonstrates the waveforms of  $v_{C1}$  with different values of  $C_1$ . When  $C_1$  is either too small or too large,  $v_{C1}$  will go above zero.

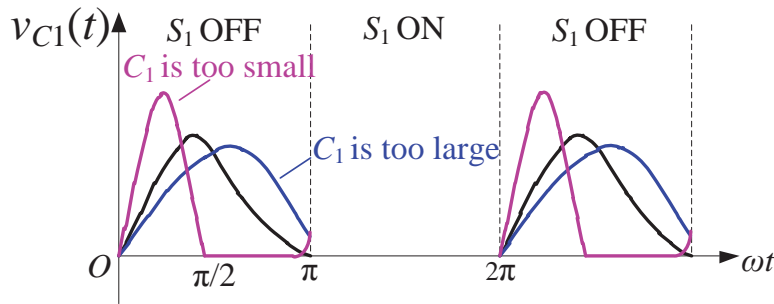


Fig. 6-2: Waveforms of the voltage  $v_{C1}$  across the switch with different values of  $C_1$ .

The voltage  $v_{C1}$  across the shunt capacitor is recited here for convenience:

$$v_{C1}(t) = \frac{1}{\omega C_1} \left[ \omega t I_g - I_R (\cos \varphi - \cos(\omega t + \varphi)) \right] \quad (6-3)$$

Setting  $v_{C1}(T/2) = 0$  gives

$$I_g = \frac{2}{\pi} I_R \cos \varphi \quad (6-4)$$

In this case,  $C_1$  reaches the maximum value that can achieve ZVS condition.

Setting  $v_{C1}(T/4) = 0$  gives

$$I_g = \frac{4}{\pi} I_R \cos \varphi \quad (6-5)$$

In this case,  $C_1$  reaches the minimum value that can ensure ZVS condition.

As can be seen later, when  $C_1$  reaches the minimum value, the output power reaches the maximum. Thus, the system is designed in the case of a minimum  $C_1$ .

Ignoring all the losses of the circuit, the output power is equal to the input power, which gives

$$V_g I_g = \frac{I_R^2 R}{2} \quad (6-6)$$

Substituting (6-5) into (6-6),  $I_R$  can be expressed as

$$I_R = \frac{8V_g}{\pi R} \cos \varphi \quad (6-7)$$

The output power  $P_O$  can be obtained as

$$P_O = \frac{32V_g^2}{\pi^2 R} \cos^2 \varphi \quad (6-8)$$

From (3-14), (6-5) and (6-7),  $C_1$  can be expressed as

$$C_1 = \frac{8}{\omega R \pi} \left( \frac{1 + \cos 2\varphi}{4} - \frac{\sin 2\varphi}{2\pi} \right) \quad (6-9)$$

### 6.3 Power Flow Control Analysis

From (6-8), the output power only depends on the phase angle  $\varphi$  of the tank current when the input voltage and load are given. As discussed in Chapter 3, the operation of Class E converter can be seen as a current pulse driving a resonant tank. For convenience of analysis, the waveforms of the imaginary input current pulse  $i_1(t)$  and tank current  $i_R(t)$  are

redrawn here (as shown in Fig. 6-3). The equivalent circuit of the class E converter is shown in Fig. 6-4. The impedance presented by the tank to the current pulse  $i_1(t)$  is

$$Z_{in} = \frac{R + jX}{1 - \omega C_1 X + j\omega C_1 R} \quad (6-10)$$

where  $X = \omega L_r - 1/(\omega C_c)$ .

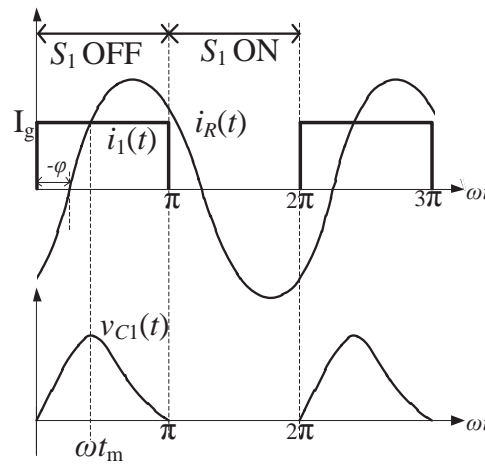


Fig. 6-3: Waveforms of  $i_1(t)$ ,  $i_R(t)$ , and  $v_{C1}(t)$ .

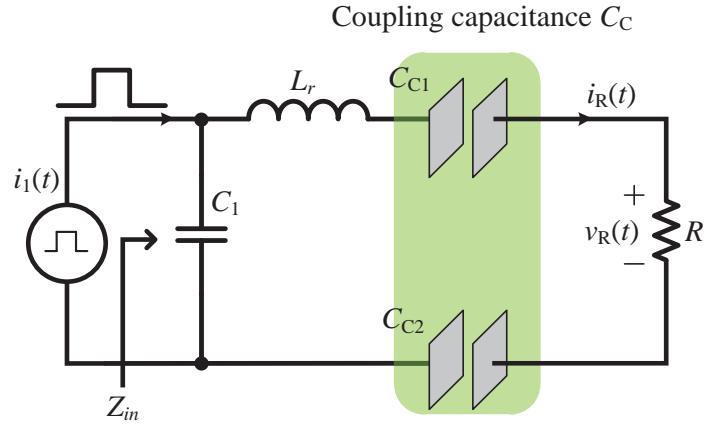


Fig. 6-4: The equivalent circuit of Class E converter using current pulse approximation.

The tank current  $i_R(t)$  in phase form can be expressed as

$$\mathbf{I}_R = \mathbf{I}_1 \frac{1}{1 - \omega C_1 X + j\omega C_1 R} \quad (6-11)$$

Therefore, the phase angle of the tank current can be approximated as

$$\varphi = -\arctan \frac{\omega C_1 R}{1 - \omega C_1 X} \quad (6-12)$$

When  $X$  is fixed, the phase shift  $\varphi$  is the function of  $C_1$ . From (6-12) and (6-8), the output power can be expressed as

$$\begin{aligned} P_o &= \frac{32V_g^2}{\pi^2 R} \frac{1}{1 + \left( \frac{\omega C_1 R}{1 - \omega C_1 X} \right)^2} \\ &= \frac{32V_g^2}{\pi^2 R} \frac{1}{1 + \left( \frac{R}{\frac{1}{\omega C_1} - X} \right)^2} \end{aligned} \quad (6-13)$$

It can be seen when  $C_1$  increases, the output power will decrease.

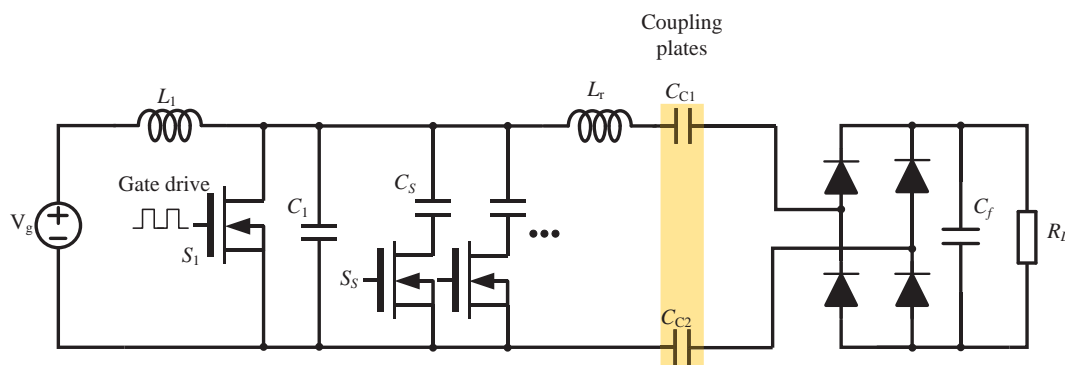


Fig. 6-5: Controlling shunt capacitance with switches.

The variation of the shunt capacitance can be implemented by either a variable capacitor or a shunt capacitor bank. The change of the shunt capacitance is realized by changing the states of switches, which control the connection of each capacitor in the shunt capacitor bank. The ON signal is synchronized with the control signal of  $S_1$ , meaning the control switches in the shunt capacitor bank are all soft switching as long as the system works in the sub-optimum mode.

## 6.4 Simulations and Experimental Study

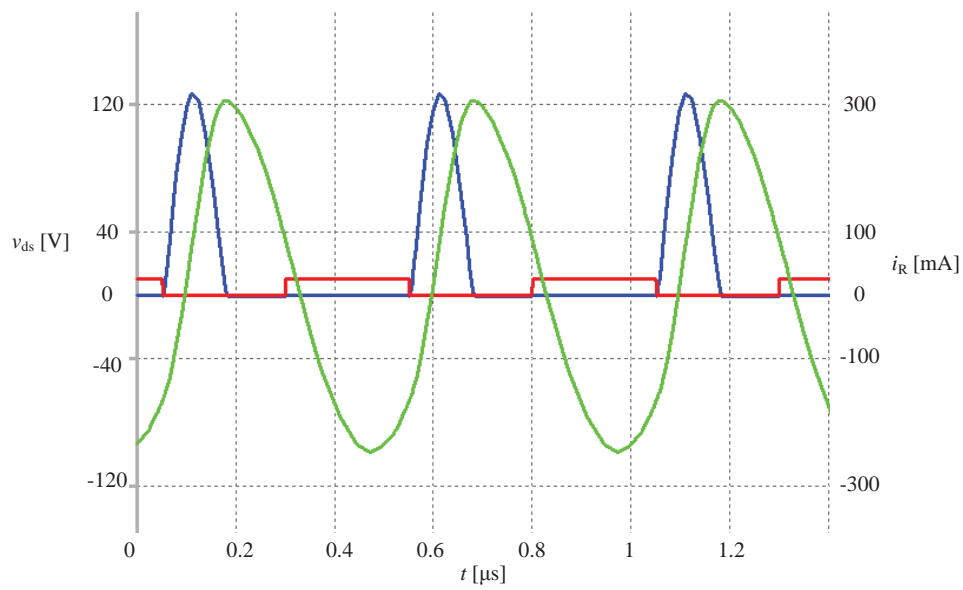
A prototype CPT system based on the class E converter topology is designed and controlled to work in the sub-optimum mode. The system parameters are listed in Table 6-1. Fig. 6-7 shows the output voltage for different shunt capacitances. It has shown the output power decreased linearly with the change of the shunt capacitance. In addition, it was reduced when the shunt capacitance was increased, which agreed well with the previous analysis. The maximum output voltage reached 8.5 V when the capacitance was 50 pF. The output voltage is reduced to 6.5 V when the capacitance was increased to 250 pF, which demonstrated that the output power can be effectively controlled by changing the shunt capacitance.

The capacitive coupling interface was made of two pairs of 100 mm × 100 mm square copper pads coated with polypropylene (its dielectric constant is about 2) as the dielectric materials. The system is operated at 2 MHz, with an input DC voltage of 20 V. When the switch  $S_s$  was open, the output voltage was 15.29 V (as shown in Fig. 6-9). The output

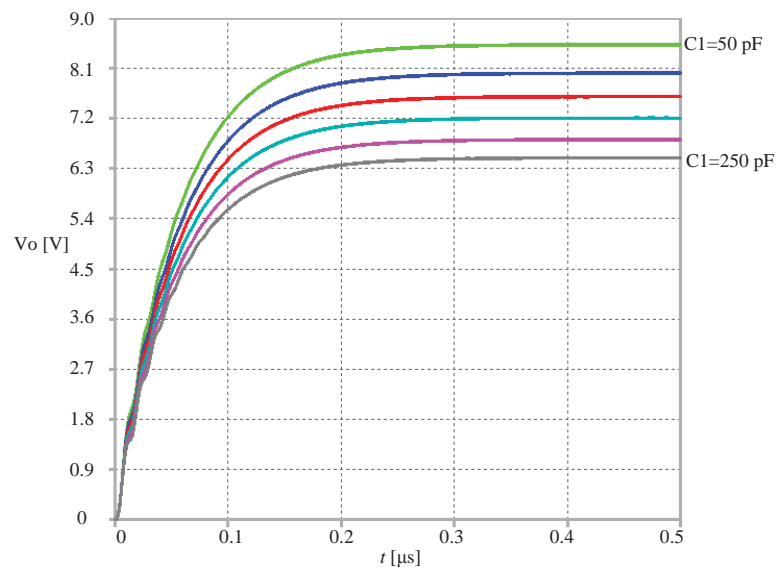
capacitance of the MOSFET serves as the required shunt capacitance, which is around 50 pF according to the output capacitance  $C_{oss}$  curve from the datasheet of FQP4N20. When the switch was closed, the output voltage was 12.45 V (as shown in Fig. 6-10). The control of the output power was implemented under ZVS condition as can be seen from the experimental waveforms. The variation of the effective shunt capacitance can also be made smooth when more small capacitors are connected in parallel controlled by switches. The capacitors and switches can be made very small using surface-mount technology (SMT), which will not increase much volume of the system. The control is easy to implement, which can share the same gate signal for the main switch whose ON/OFF is controlled by NAND gates.

**Table 6-1: System parameters of sub-optimum Class E.**

Parameter	Value
Input voltage $V_{IN}$	20 V
The load $R$	50 $\Omega$
Coupling capacitance $C_C$	250 pF
$L_1$	1 mH, 1410516C
$L_r$	35 $\mu$ H cylindrical core TN100B
$C_S$	100 pF, ceramic, 1000 V
MOSFETs $S_1$ and $S_S$	FQP4N20
Diodes $D_1 - D_4$	1N5819

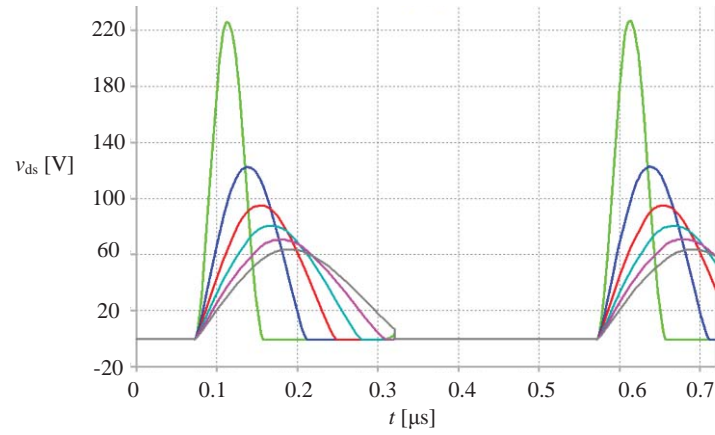


**Fig. 6-6: Waveforms in the CPT in sub-optimum mode: the blue line is the voltage across the switch  $v_{C1}$ , the red line is the gate drive signal, and the green line is tank current  $i_R(t)$ .**

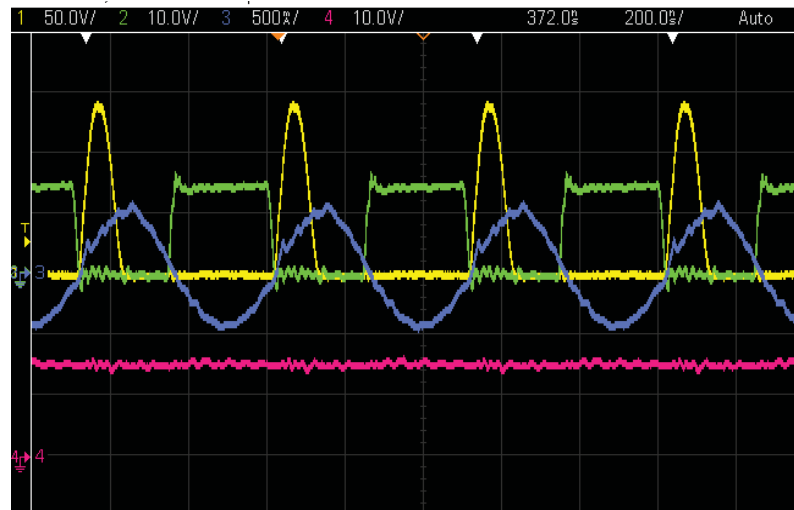


**Fig. 6-7: Output power with different shunt capacitances ranging from 50 pF to 250 pF in simulation.**

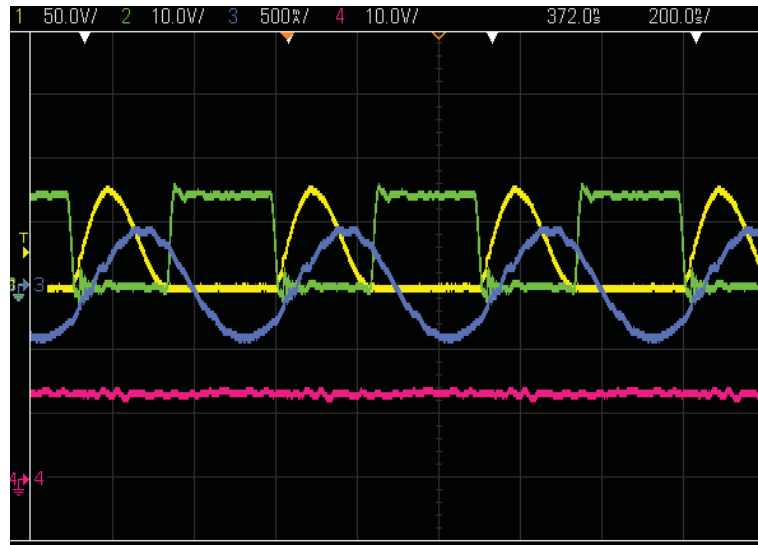




**Fig. 6-8: The voltage across the switch  $v_{C1}(t)$  for different shunt capacitance ranging from 50 pF to 250 pF.**



**Fig. 6-9: Experimental waveform when CPT system works in the proposed sub-optimum mode. The yellow line is  $v_{C1}(t)$ , the green line is gate signal, the blue line is the tank current, and the pink line is the output voltage.**



**Fig. 6-10:** Experimental waveform when the shunt capacitance was increased to 220 pF. The yellow line is  $v_{C1}(t)$ , the green line is gate signal, the blue line is the tank current, and the pink line is the output voltage.

## 6.5 Summary

This chapter proposed a new power flow control method for a CPT system. The output power was controlled by changing the effective shunt capacitance. The system was based on a class E converter topology, which was operated in a new sub-optimum mode. In this new operating mode, the converter of the CPT system can maintain ZVS condition while performing the power flow control, which is the unique feature of the proposed method. The variation of the shunt capacitance was realized by switching on or off the transistor in series with the shunt capacitor. The relationship between the output power and shunt capacitance was derived and equations governing the sub-optimum operation were provided. Simulated and practical results have shown that the proposed control method can effectively vary the output voltage for a given load. The simulated results showed the output voltage rose linearly over the increase of shunt capacitance. The converter can maintain ZVS condition with the shunt capacitance ranging from 50 pF to 250 pF, yielding high efficiency.

## 7 Conclusions and Suggestions for Future Work

---

### 7.1 General Conclusions

This thesis has conducted the research on the compensation networks for the capacitive coupling interface and power flow control methods for CPT systems. It focuses on the following aspects:

- Studying three soft-switching resonant converters suitable for high frequency operation in CPT systems.
- Modelling the capacitive coupling interface with cross coupling taken into consideration.
- Proposing two compensation networks to address the open-circuit problem suffered by conventional single inductor method and to increase the power transfer capability.
- Developing a new power flow control method for a CPT system by changing effective shunt capacitance.

Chapter 1 briefly introduced the development of the wireless/contactless power transfer technology. It has been shown that the wireless power transfer technology has become increasingly popular as it can deliver electric power without direct galvanic connection on some special occasions, such as, charging electric vehicles and powering implanted biomedical devices through skins. Among all the existing wireless power transfer

solutions, IPT is the dominant method. However, due to its working principle based on magnetic coupling, IPT still has some inherent limitations, such as the incapability to transfer power through metal barriers and the limit on the operating frequency imposed by use of ferrites. Using the electric field as the energy transfer medium, CPT has been proposed as an alternative wireless solution, which offers desirable features such as low standing power losses, low EMI, the ability to transfer power through metal barriers, and a preference for high operating frequencies. Moreover, the coupling design of the CPT system is more flexible and easier than the IPT system. The coupling plates can be made from very thin metallic foils or any conductive pads. Despite some fundamental research has been conducted, more advanced compensation networks and power flow control methods are needed to improve the power transfer capability.

An overview of existing compensation and power flow control methods for CPT systems was provided in Chapter 2. The working principles of different compensation and power control methods are summarized, and their advantages and disadvantages are discussed. The single series inductor method is the most widely used compensation network in CPT systems. Despite its simplicity and low cost, this method cannot be used on some occasions where the effective capacitance between the coupling plates is very small. And it also suffers high voltage spikes since it is vulnerable to the open-circuit fault caused by sudden the removal of the secondary side plates. High order compensation networks by increasing both input voltage and load impedance can be employed in the CPT system with very small coupling capacitance. But the capacitors used in these compensation networks have to endure high voltages. An active compensation network using switch-controlled capacitors is also proposed, but it is unsuitable for high frequency operation and involves complicated control circuitry. To achieve the power flow control, various control strategies have been used in CPT system. Some are implemented on the secondary side and the others are placed on the primary side. The voltage regulator is simple but suffers low efficiency. The modified rectifier can control the power with higher efficiency, but it needs to detect the current to achieve soft switching. The primary side control method based on the soft-switched transformer increases the system size and it is also unsuitable for high frequency operation due to extra inductive elements involved. The multi-period method can also regulate the output power, but it requires more complicated filter networks due to the frequency variation.

Chapter 3 studied three selected high frequency switched-mode power converter topologies suitable for CPT systems, which are an autonomous current-fed push-pull converter, a class E converter, and a voltage-fed half-bridge converter. Their working principles are described and key design equations are provided. Three aspects of CPT systems based on the three converter topologies, including the circuit components, the effect of the coupling capacitance variations, and the control scheme, are compared. The autonomous converter topology requires the greatest number of the circuit components, but the efficiency can maintain relatively constant due to its automatic frequency adjusting capability. The class E converter topology can deliver the maximum output power for given coupling capacitance. The half-bridge converter topology has the minimum number of circuit components, which is an ideal cost-effective option for low cost applications. The class E and half-bridge converter topologies can be controlled in multiple ways while the autonomous push-pull topology has limited control options.

Chapter 4 performed theoretical analysis on the capacitive coupling interface. A general model of the capacitive coupling interface has been proposed to analyze the characteristics of the coupling interface, including effects of the cross coupling between primary and secondary plates. The model consists of one input capacitor, one output capacitor, and one ideal transformer with a variable turns ratio affected by coupling condition. Theoretical analysis on the effects of the cross coupling on the model was extensively performed, which has shown the output capacitance keeps constant regardless of coupling variation. The model was used to design a CPT system based on a single series inductor, and simulations and experimental results have shown the proposed model can effectively calculate the required inductance used to achieve full resonance of the circuit. Furthermore, a dynamical model of the capacitive coupling interface with cross coupling was derived and a new term named capacitive coupling coefficient was defined. Two CPT systems with different coupling conditions were evaluated with the new term. Experimental results have shown the capacitive coupling coefficient can provide a useful measure of the coupling condition.

After the theoretical analysis on the new coupling interface, Chapter 5 developed a novel compensation network using a Z-impedance network and a load transformation network. The Z-impedance compensation network can solve the open-circuit problem suffered by the conventional compensation method using a single series inductor. The primary side

converter was based on a half-bridge inverter topology. The LCC tank was placed before the Z-impedance network. A system-level analysis was performed to evaluate the effect of the Z-impedance network on the LCC tank. Design equations governing the performance were also provided. Simulations and practical results have verified that the proposed Z-impedance compensation method can effectively reduce the high voltage spikes. Short-circuit immunity and voltage boost capability were also demonstrated. The load transformation network was integrated into the class E converter topology, which can improve the power transfer performance. A state-space model was used to facilitate the design of the system. The experimental study has shown that the modified CPT system based on the class E converter topology can improve the power transfer capability by increasing the ratio of the load current to the tank current through the coupling plates.

In Chapter 6, by switching on/off the shunt capacitance, a novel power flow control method for CPT systems was proposed. The proposed control method was implemented in a CPT system based on a new-optimum operation mode of a class E converter. In this new operating mode, the converter can maintain ZVS condition with a wider range of components. Design equations governing the sub-optimum operation were provided. Simulated and experimental results have shown the output voltage rose linearly with the increase of the shunt capacitance. The converter can maintain ZVS condition with the shunt capacitance ranging from 50 pF to 250 pF, achieving high efficiency.

## 7.2 Publications from This Research

Three journal papers and three conference papers have been published based on the work of this research:

1. L. Huang, A. P. Hu, A. Swain, and Y. Su, "Z Impedance Compensation for Wireless Power Transfer Based on Electric Field Coupling," in *IEEE Transactions on Power Electronics*, vol. 31, no. 11, pp. 7556-7563, Nov. 2016.
2. L. Huang, A. P. Hu, A. K. Swain, and Y. Su, "Accurate steady-state modeling of capacitive-coupling interface of capacitive power transfer systems with cross-coupling," *Wireless Power Transfer*, 3(1), pp. 53–62.

3. L. Huang and A. P. Hu, "Defining the mutual coupling of capacitive power transfer for wireless power transfer," *Electronics Letters*, vol. 51, pp. 1806-1807, 2015.
4. L. Huang, A. P. Hu, A. Swain, and X. Dai, "Comparison of two high frequency converters for capacitive power transfer," in *Energy Conversion Congress and Exposition (ECCE)*, 2014 IEEE, 2014, pp. 5437-5443.
5. L. Huang, A. P. Hu, and A. Swain, "A resonant compensation method for improving the performance of capacitively coupled power transfer system," in *Energy Conversion Congress and Exposition (ECCE)*, 2014 IEEE, 2014, pp. 870-875.
6. L. Huang, A. P. Hu, A. Swain, S. Kim, and Y. Ren, "An overview of capacitively coupled power transfer: A new contactless power transfer solution," in *Industrial Electronics and Applications (ICIEA)*, 2013 8th IEEE Conference on, 2013, pp. 461-465.

### 7.3 Suggestions for Future Work

This thesis focuses on the development of advanced compensation and power flow control methods for CPT systems. Theoretical analysis, simulations, and practical work have been carried out to accomplish these objectives. Despite successful results of these attempts, more aspects of the CPT system need further investigation, which are suggested as follows:

#### *A) Novel pattern designs of coupling plate*

The coupling plates employed in this research are solid planar pads, which only vary in size and shape. However, new patterns can be applied to the geometric structure of the coupling plates to improve the power transfer performance. For example, multi-loop path pattern can be designed to increase the parasitic inductance of the pads, which can help to reduce the effective capacitive impedance of the coupling capacitive interface. Various patterns of coupling plates could be studied to evaluate their effects on the performance of CPT system.

***B) Control of the effective output inductance of the Z-impedance compensation network***

The proposed Z-impedance compensation network has demonstrated that it can successfully cancel out the effective capacitive reactance of the capacitive coupling. As shown in Chapter 5, the effective output inductance of the Z-impedance compensation network is dependent on the ratio of the resonant frequency of the network to the operating frequency. Since the resonant frequency is determined by both inductors and capacitors of the network, a variable inductor can be obtained either by varying the inductor or the capacitor of the Z-impedance network. A switch-controlled capacitor or inductor can be integrated into the network, which can be controlled to regulate the output power.

***C) Single-plate coupling configuration***

From the experiments conducted in this research, it is found the power can be delivered to the load in a CPT system using only one pair of coupling plates without a return loop. This new phenomenon shows the potential to address the coupling misalignment problem suffered by conventional CPT systems with two pairs of coupling plates. More theoretical and experimental work is needed to further understand this new type of CPT system. New theories and models need to be developed to explain its working principle and the system behaviours since the classical lumped circuit model is unable to provide a satisfactory explanation. Simulation software such as Maxwell and CST would help to analyze the electric field coupling between plates and verify new models which are proposed to describe the coupling.



# Appendix

Appendix A: Experimental data for Fig. 4-19

$P_{O1}$ [W]		$\alpha$										
		0	0.1	0.2	0.3	0.4	0.5	0.6	0.7	0.8	0.9	1
$\beta$	0	2.01	2.26	2.45	3	2.81	2.41	2.23	1.45	1	0.2	0
	0.1	2.36	2.67	3.22	3.53	3.78	3.55	2.45	1.88	0.85	0.2	0.22
	0.2	2.58	3.09	3.58	4.19	4.28	3.8	1.91	0.86	0.35	0.32	0.8
	0.3	2.93	3.31	4.1	3.82	4.11	2.82	1.12	0.11	0.74	0.44	1.53
	0.4	2.74	3.33	3.58	3.8	2.34	1.17	0.23	0.81	1.65	2.36	2.11
	0.5	2.56	3.01	3.42	2.56	1.3	0.2	1.01	2.34	3.05	2.88	2.52
	0.6	2.16	2.32	1.81	1.06	0.32	0.91	1.98	3.59	3.52	3.33	2.77
	0.7	1.56	1.61	0.9	0.32	0.84	2.16	3.46	3.46	3.68	3.06	2.84
	0.8	0.98	0.64	0.26	0.68	1.74	2.96	3.68	3.79	3.25	2.98	2.6
	0.9	0.25	0	0.47	1.44	2.25	2.92	3.27	3.17	3.07	2.57	2.21
	1	0	0.25	0.85	1.61	2.02	2.46	2.74	2.68	2.59	2.34	1.99

## References

- [1] Wikipedia. (2015, Feb 18). *Heinrich Hertz* [Online]. Available: [http://en.wikipedia.org/wiki/Heinrich\\_Hertz](http://en.wikipedia.org/wiki/Heinrich_Hertz)
- [2] W. B. Carlson, *Tesla: Inventor of the electrical age*. Princeton, NJ: Princeton Univ. Press, 2013.
- [3] N. Tesla, "System of transmission of electrical energy," U.S. Patent 645 576, Mar 20, 1900.
- [4] N. Tesla, "Art of transmitting electrical energy through the natural mediums," U.S. Patent 787 412, Apr 18, 1905.
- [5] J. C. Schuder, H. E. Stephenson Jr, and J. F. Townsend, "Energy transfer into a closed chest by means of stationary coupling coils and a portable high-power oscillator," *ASAIO Journal*, vol. 7, pp. 327-331, 1961.
- [6] K. Lashkari, S. E. Shladover, and E. H. Lechner, "Inductive power transfer to an electric vehicle," in *International Electric Vehicle Symposium (8th: 1986: Washington DC)*, 1986.
- [7] E. Lechner and S. Shladover, "Roadway powered electric vehicle: An all-electric hybrid system," in *International Electric Vehicle Symposium (8th)*, 1986.
- [8] A. W. Green and J. T. Boys, "10 kHz inductively coupled power transfer-concept and control," in *Power Electronics and Variable-Speed Drives, 1994. Fifth International Conference on*, 1994, pp. 694-699.
- [9] J. T. Boys, G. A. Covic, and A. W. Green, "Stability and control of inductively coupled power transfer systems," *Electric Power Applications, IEE Proceedings -*, vol. 147, pp. 37-43, 2000.
- [10] A. P. Hu, "Selected resonant converters for IPT power supplies," Ph.D. dissertation, Dept. Elect. Comput. Eng., Univ. Auckland, Auckland, New Zealand, 2001.
- [11] A. K. Swain, S. Devarakonda, and U. K. Madawala, "Modeling, Sensitivity Analysis, and Controller Synthesis of Multipickup Bidirectional Inductive Power Transfer Systems," *Industrial Informatics, IEEE Transactions on*, vol. 10, pp. 1372-1380, 2014.
- [12] A. P. Hu, G. A. Covic, and J. T. Boys, "Direct ZVS start-up of a current-fed resonant inverter," *Power Electronics, IEEE Transactions on*, vol. 21, pp. 809-812, 2006.
- [13] T. D. Dissanayake, A. P. Hu, S. Malpas, L. Bennet, A. Taberner, L. Booth, *et al.*, "Experimental Study of a TET System for Implantable Biomedical Devices," *Biomedical Circuits and Systems, IEEE Transactions on*, vol. 3, pp. 370-378, 2009.

- [14] W. Chwei-Sen, O. H. Stielau, and G. A. Covic, "Design considerations for a contactless electric vehicle battery charger," *Industrial Electronics, IEEE Transactions on*, vol. 52, pp. 1308-1314, 2005.
- [15] W. Chwei-Sen, G. A. Covic, and O. H. Stielau, "Power transfer capability and bifurcation phenomena of loosely coupled inductive power transfer systems," *Industrial Electronics, IEEE Transactions on*, vol. 51, pp. 148-157, 2004.
- [16] W. Chwei-Sen, G. A. Covic, and O. H. Stielau, "Investigating an LCL load resonant inverter for inductive power transfer applications," *Power Electronics, IEEE Transactions on*, vol. 19, pp. 995-1002, 2004.
- [17] J. T. Boys, A. P. Hu, and G. A. Covic, "Critical Q analysis of a current-fed resonant converter for ICPT applications," *Electronics Letters*, vol. 36, pp. 1440-1442, 2000.
- [18] J. T. Boys, G. A. J. Elliott, and G. A. Covic, "An Appropriate Magnetic Coupling Co-Efficient for the Design and Comparison of ICPT Pickups," *Power Electronics, IEEE Transactions on*, vol. 22, pp. 333-335, 2007.
- [19] J. T. Boys, G. A. Covic, and G. A. J. Elliott, "Pick-up transformer for ICPT applications," *Electronics Letters*, vol. 38, pp. 1276-1278, 2002.
- [20] J. Boys and A. Green, "Intelligent road-studs-lighting the paths of the future," 1996.
- [21] A. Abdolkhani and A. P. Hu, "A Contactless Slipring System Based on Axially Traveling Magnetic Field," *Emerging and Selected Topics in Power Electronics, IEEE Journal of*, vol. 3, pp. 280-287, 2015.
- [22] A. P. Hu, J. T. Boys, and G. A. Covic, "ZVS frequency analysis of a current-fed resonant converter," in *Power Electronics Congress, 2000. CIEP 2000. VII IEEE International*, 2000, pp. 217-221.
- [23] A. P. Hu, J. T. Boys, and G. A. Covic, "Frequency analysis and computation of a current-fed resonant converter for ICPT power supplies," in *Power System Technology, 2000. Proceedings. PowerCon 2000. International Conference on*, 2000, pp. 327-332 vol.1.
- [24] G. A. J. Elliott, J. T. Boys, and A. W. Green, "Magnetically coupled systems for power transfer to electric vehicles," in *Power Electronics and Drive Systems, 1995., Proceedings of 1995 International Conference on*, 1995, pp. 797-801 vol.2.
- [25] G. A. Covic, G. Elliott, O. H. Stielau, R. M. Green, and J. T. Boys, "The design of a contact-less energy transfer system for a people mover system," in *Power System Technology, 2000. Proceedings. PowerCon 2000. International Conference on*, 2000, pp. 79-84 vol.1.
- [26] H. W. Secor, "Tesla apparatus and experiments—How to build both large and small Tesla and Oudin coils and how to carry on spectacular experiments with them," *Practical Electrics*, Nov, 1921.

- [27] A. P. Hu, L. Chao, and L. Hao Leo, "A Novel Contactless Battery Charging System for Soccer Playing Robot," in *Mechatronics and Machine Vision in Practice, 2008. M2VIP 2008. 15th International Conference on*, 2008, pp. 646-650.
- [28] L. Chao and A. P. Hu, "Steady state analysis of a capacitively coupled contactless power transfer system," in *Energy Conversion Congress and Exposition, 2009. ECCE 2009. IEEE*, 2009, pp. 3233-3238.
- [29] L. Chao, A. P. Hu, and N. C. Nair, "Coupling study of a rotary Capacitive Power Transfer system," in *Industrial Technology, 2009. ICIT 2009. IEEE International Conference on*, 2009, pp. 1-6.
- [30] L. Ho Fai, B. J. Willis, and A. P. Hu, "Wireless electric power transfer based on Acoustic Energy through conductive media," in *Industrial Electronics and Applications (ICIEA), 2014 IEEE 9th Conference on*, 2014, pp. 1555-1560.
- [31] W. C. Brown, "The History of Power Transmission by Radio Waves," *Microwave Theory and Techniques, IEEE Transactions on*, vol. 32, pp. 1230-1242, 1984.
- [32] A. Wahab, C. Tan Eng, and M. Low Kay, "Wireless pointing device using capacitive coupling," in *Consumer Electronics, 1997. ISCE '97., Proceedings of 1997 IEEE International Symposium on*, 1997, pp. 149-152.
- [33] E. Culurciello and A. G. Andreou, "Capacitive Inter-Chip Data and Power Transfer for 3-D VLSI," *Circuits and Systems II: Express Briefs, IEEE Transactions on*, vol. 53, pp. 1348-1352, 2006.
- [34] K. V. T. Piipponen, R. Sepponen, and P. Eskelinen, "A Biosignal Instrumentation System Using Capacitive Coupling for Power and Signal Isolation," *Biomedical Engineering, IEEE Transactions on*, vol. 54, pp. 1822-1828, 2007.
- [35] D. Salzman, T. Knight, Jr., and P. Franzon, "Application of capacitive coupling to switch fabrics," in *Multi-Chip Module Conference, 1995. MCMC-95, Proceedings., 1995 IEEE*, 1995, pp. 195-199.
- [36] D. C. Ludois, J. Reed, and M. Erickson, "Aerodynamic fluid bearings for capacitive power transfer and rotating machinery," in *Energy Conversion Congress and Exposition (ECCE), 2012 IEEE*, 2012, pp. 1932-1937.
- [37] D. C. Ludois, J. K. Reed, and K. Hanson, "Capacitive Power Transfer for Rotor Field Current in Synchronous Machines," *Power Electronics, IEEE Transactions on*, vol. 27, pp. 4638-4645, 2012.
- [38] L. Huang, A. P. Hu, A. Swain, S. Kim, and Y. Ren, "An overview of capacitively coupled power transfer: A new contactless power transfer solution," in *Industrial Electronics and Applications (ICIEA), 2013 8th IEEE Conference on*, 2013, pp. 461-465.
- [39] J. Chabrol, "Power transfer circuit," U.S. Patent 4 223 313, Sep 16, 1980.

- [40] S. Y. R. Hui and W. C. Ho, "A new generation of universal contactless battery charging platform for portable consumer electronic equipment," in *Power Electronics Specialists Conference, 2004. PESC 04. 2004 IEEE 35th Annual*, 2004, pp. 638-644 Vol.1.
- [41] H. Kurino, K. W. Lee, T. Nakamura, K. Sakuma, K. T. Park, N. Miyakawa, *et al.*, "Intelligent image sensor chip with three dimensional structure," in *Electron Devices Meeting, 1999. IEDM '99. Technical Digest. International*, 1999, pp. 879-882.
- [42] M. Koyanagi, H. Kurino, K. W. Lee, K. Sakuma, N. Miyakawa, and H. Itani, "Future system-on-silicon LSI chips," *Micro, IEEE*, vol. 18, pp. 17-22, 1998.
- [43] A. G. Andreou, Z. K. Kalayjian, A. Apsel, P. Pouliquen, R. Athale, G. Simonis, *et al.*, "Silicon on sapphire CMOS for optoelectronic microsystems," *Circuits and Systems Magazine, IEEE*, vol. 1, pp. 22-30, 2001.
- [44] S. Ping and P. Si, "Wireless power supply for implantable biomedical devices / Ping Si," Thesis (PhD--Electrical and Electronic Engineering)--University of Auckland, 2008. 2008., 2008.
- [45] T. Chun Sen, S. Yue, S. Yu Gang, N. Sing Kiong, and A. P. Hu, "Determining Multiple Steady-State ZCS Operating Points of a Switch-Mode Contactless Power Transfer System," *Power Electronics, IEEE Transactions on*, vol. 24, pp. 416-425, 2009.
- [46] T. D. Dissanayake, D. Budgett, P. Hu, and S. Malpas, "Experimental thermal study of a TET system for implantable biomedical devices," in *2008 IEEE-BIOCAS Biomedical Circuits and Systems Conference, BIOCAS 2008, November 20, 2008 - November 22, 2008*, Baltimore, MD, United states, 2008, pp. 113-116.
- [47] Z. Fei, L. Xiaoyu, S. A. Hackworth, R. J. ScLabassi, and S. Mingui, "In vitro and in vivo studies on wireless powering of medical sensors and implantable devices," in *Life Science Systems and Applications Workshop, 2009. LiSSA 2009. IEEE/NIH*, 2009, pp. 84-87.
- [48] Murata Ltd. (2011, Jan 15). *A mounting example for "AIR VOLTAGE for iPad2"* [Online]. Available: [http://www.murata.com/products/wireless\\_power/index.html](http://www.murata.com/products/wireless_power/index.html)
- [49] Apple Inc. (2016, Feb 22). *Apple watch magnetic charging dock* [Online]. Available: <http://www.apple.com/shop/product/MLDW2AM/A/apple-watch-magnetic-charging-dock?fnode=80>
- [50] D. C. Ludois, K. Hanson, and J. K. Reed, "Capacitive power transfer for slip ring replacement in wound field synchronous machines," in *Energy Conversion Congress and Exposition (ECCE), 2011 IEEE*, 2011, pp. 1664-1669.
- [51] H. Zhang, F. Lu, H. Hofmann, W. Liu, and C. Mi, "A 4-Plate Compact Capacitive Coupler Design and LCL-Compensated Topology for Capacitive Power Transfer in Electric Vehicle Charging Applications," *Power Electronics, IEEE Transactions on*, vol. PP, pp. 1-1, 2016.

- [52] F. Lu, H. Zhang, H. Hofmann, and C. Mi, "An Inductive and Capacitive Combined Wireless Power Transfer System with LC-Compensated Topology," *Power Electronics, IEEE Transactions on*, vol. PP, pp. 1-1, 2016.
- [53] J. Dai and D. C. Ludois, "Wireless electric vehicle charging via capacitive power transfer through a conformal bumper," in *Applied Power Electronics Conference and Exposition (APEC), 2015 IEEE*, 2015, pp. 3307-3313.
- [54] K. Jingook and F. Bien, "Electric field coupling technique of wireless power transfer for electric vehicles," in *TENCON Spring Conference, 2013 IEEE*, 2013, pp. 267-271.
- [55] F. Lu, Z. Hua, H. Hofmann, and C. Mi, "A Double-Sided LCLC Compensated Capacitive Power Transfer System for Electric Vehicle Charging," *Power Electronics, IEEE Transactions on*, vol. 30, pp. 6011-6014, 2015.
- [56] A. Sepahvand, A. Kumar, K. Afridi, and D. Maksimovic, "High power transfer density and high efficiency 100 MHz capacitive wireless power transfer system," in *Control and Modeling for Power Electronics (COMPEL), 2015 IEEE 16th Workshop on*, 2015, pp. 1-4.
- [57] Murata Ltd. (2011, Dec 12). *Wireless power transmission modules* [Online]. Available: [http://www.murata.com/products/wireless\\_power/index.html](http://www.murata.com/products/wireless_power/index.html)
- [58] D. C. Ludois, M. J. Erickson, and J. K. Reed, "Aerodynamic Fluid Bearings for Translational and Rotating Capacitors in Noncontact Capacitive Power Transfer Systems," *IEEE Transactions on Industry Applications*, vol. 50, pp. 1025-1033, 2014.
- [59] H. D. Young and R. A. Freedman, *University Physics*, 10th ed. Boston, MA: Addison-Wesley, 2000.
- [60] B. Ge, D. C. Ludois, and R. Perez, "The use of dielectric coatings in capacitive power transfer systems," in *Energy Conversion Congress and Exposition (ECCE), 2014 IEEE*, 2014, pp. 2193-2199.
- [61] I. Bahl, *Lumped elements for RF and microwave circuits*. Norwood, MA: Artech House, 2003.
- [62] L. Chao, A. P. Hu, G. A. Covic, and N. C. Nair, "Comparative Study of CCPT Systems With Two Different Inductor Tuning Positions," *Power Electronics, IEEE Transactions on*, vol. 27, pp. 294-306, 2012.
- [63] G. Shinji, "Capacitive coupling powers transmission module," *AEI Special Report*, pp. 20-22, Nov. 2012.
- [64] H. Fnato, Y. Chiku, and K. Harakawa, "Wireless power distribution with capacitive coupling excited by switched mode active negative capacitor," in *Electrical Machines and Systems (ICEMS), 2010 International Conference on*, 2010, pp. 117-122.



- [65] T. Kitabayashi, H. Funato, H. Kobayashi, and K. Yamaichi, "Experimental verification of capacitive power transfer using one pulse switching active capacitor for practical use," in *Power Electronics Conference (IPEC-Hiroshima 2014 - ECCE-ASIA), 2014 International*, 2014, pp. 2517-2522.
- [66] C. Liu and A. P. Hu, "Power flow control of a capacitively coupled contactless power transfer system," in *Industrial Electronics, 2009. IECON '09. 35th Annual Conference of IEEE*, 2009, pp. 743-747.
- [67] L. Chao, A. P. Hu, B. Wang, and N. C. Nair, "A Capacitively Coupled Contactless Matrix Charging Platform With Soft Switched Transformer Control," *Industrial Electronics, IEEE Transactions on*, vol. 60, pp. 249-260, 2013.
- [68] K. Young-Sup, Y. Sang-Bong, and H. Dong-seok, "Half-bridge series resonant inverter for induction heating applications with load-adaptive PFM control strategy," in *Applied Power Electronics Conference and Exposition, 1999. APEC '99. Fourteenth Annual*, 1999, pp. 575-581 vol.1.
- [69] W. J. Gu and K. Harada, "A new method to regulate resonant converters," *Power Electronics, IEEE Transactions on*, vol. 3, pp. 430-439, 1988.
- [70] J. James, J. Boys, and G. Covic, "A variable inductor based tuning method for ICPT pickups," in *Power Engineering Conference, 2005. IPEC 2005. The 7th International*, 2005, pp. 1142-1146 Vol. 2.
- [71] J. U. W. Hsu, "Full-range tuning power flow control of IPT power pickups," Ph.D. dissertation, Dept. Elect. & Comput. Eng., Univ. Auckland, Auckland, New Zealand, 2010.
- [72] M. Kline, "Capacitive power transfer," M.S. thesis, Dept. Elect. Eng. & Comput. Sci., Univ. California, Berkeley, USA, 2010.
- [73] M. Kline, I. Izyumin, B. Boser, and S. Sanders, "Capacitive power transfer for contactless charging," in *Applied Power Electronics Conference and Exposition (APEC), 2011 Twenty-Sixth Annual IEEE*, 2011, pp. 1398-1404.
- [74] D. Lohrmann, "Amplifier Has 85 percent Efficiency while Providing up to 10 Watts Power over a Wide Frequency Band," *Electronic Design*, vol. 14, 1966.
- [75] N. O. Sokal and A. D. Sokal, "Class E-A new class of high-efficiency tuned single-ended switching power amplifiers," *Solid-State Circuits, IEEE Journal of*, vol. 10, pp. 168-176, 1975.
- [76] F. H. Raab, "Idealized operation of the class E tuned power amplifier," *Circuits and Systems, IEEE Transactions on*, vol. 24, pp. 725-735, 1977.
- [77] N. Sokal, "Class E high-efficiency switching-mode tuned power amplifier with only one inductor and one capacitor in load network-approximate analysis," *Solid-State Circuits, IEEE Journal of*, vol. 16, pp. 380-384, 1981.

- [78] F. H. Raab, "Class-E, Class-C, and Class-F power amplifiers based upon a finite number of harmonics," *Microwave Theory and Techniques, IEEE Transactions on*, vol. 49, pp. 1462-1468, 2001.
- [79] L. Ray-Lee and C. Feng-Yin, "Self-oscillating push-pull class-E/F converters," in *Circuits and Systems, 2004. Proceedings. The 2004 IEEE Asia-Pacific Conference on*, 2004, pp. 649-652 vol.2.
- [80] M. K. Kazimierczuk, V. G. Krizhanovski, J. V. Rassokhina, and D. V. Chernov, "Class-E MOSFET tuned power oscillator design procedure," *Circuits and Systems I: Regular Papers, IEEE Transactions on*, vol. 52, pp. 1138-1147, 2005.
- [81] K. Fukui and H. Koizumi, "Class E Rectifier With Controlled Shunt Capacitor," *Power Electronics, IEEE Transactions on*, vol. 27, pp. 3704-3713, 2012.
- [82] A. Mediano and N. O. Sokal, "A Class-E RF Power Amplifier With a Flat-Top Transistor-Voltage Waveform," *Power Electronics, IEEE Transactions on*, vol. 28, pp. 5215-5221, 2013.
- [83] F. Raab, "Idealized operation of the class E tuned power amplifier," *Circuits and Systems, IEEE Transactions on*, vol. 24, pp. 725-735, 1977.
- [84] C. Liu, A. P. Hu, and N. K. C. Nair, "Modelling and analysis of a capacitively coupled contactless power transfer system," *Power Electronics, IET*, vol. 4, pp. 808-815, 2011.
- [85] M. P. Theodoridis, "Effective Capacitive Power Transfer," *Power Electronics, IEEE Transactions on*, vol. 27, pp. 4906-4913, 2012.
- [86] A. Kumar, S. Pervaiz, C. Chieh-Kai, S. Korhummel, Z. Popovic, and K. K. Afridi, "Investigation of power transfer density enhancement in large air-gap capacitive wireless power transfer systems," in *Wireless Power Transfer Conference (WPTC), 2015 IEEE*, 2015, pp. 1-4.
- [87] J. Dai and D. C. Ludois, "Biologically inspired coupling pixilation for position independence in capacitive power transfer surfaces," in *Applied Power Electronics Conference and Exposition (APEC), 2015 IEEE*, 2015, pp. 3276-3282.
- [88] L. Chao, A. P. Hu, and M. Budhia, "A generalized coupling model for Capacitive Power Transfer systems," in *IECON 2010 - 36th Annual Conference on IEEE Industrial Electronics Society*, 2010, pp. 274-279.
- [89] R. L. Steigerwald, "High-Frequency Resonant Transistor DC-DC Converters," *Industrial Electronics, IEEE Transactions on*, vol. IE-31, pp. 181-191, 1984.
- [90] V. Vorperian, "Analysis of resonant converters," Ph.D. dissertation, California Institute of Technology, Pasadena, CA, USA, 1984.
- [91] S. Johnson and R. Erickson, "A comparison of resonant topologies in high voltage DC applications," in *Applied Power Electronics Conference and Exposition, 1987 IEEE*, 1987, pp. 145-156.



- [92] S. D. Johnson and R. W. Erickson, "Steady-state analysis and design of the parallel resonant converter," *Power Electronics, IEEE Transactions on*, vol. 3, pp. 93-104, 1988.
- [93] F. C. Lee, "High-Frequency Quasi-Resonant and Multi-Resonant Converter Technologies," in *Industrial Electronics Society, 1988. IECON '88. Proceedings., 14 Annual Conference of*, 1988, pp. 509-521.
- [94] H. Funato, H. Kobayashi, and T. Kitabayashi, "Analysis of transfer power of capacitive power transfer system," in *Power Electronics and Drive Systems (PEDS), 2013 IEEE 10th International Conference on*, 2013, pp. 1015-1020.
- [95] H. Kobayashi, H. Funato, and Y. Chiku, "Enhancement of transfer power of Capacitive Power Transfer system using cascaded One Pulse Switching Active Capacitor(C-OPSAC) with three-level operation," in *Power Electronics and Motion Control Conference (IPEMC), 2012 7th International*, 2012, pp. 884-888.
- [96] S. Miaosen, A. Joseph, W. Jin, F. Z. Peng, and D. J. Adams, "Comparison of traditional inverters and Z-source inverter for fuel cell vehicles," in *Power Electronics in Transportation, 2004*, 2004, pp. 125-132.
- [97] F. Z. Peng, "Z-source inverter," in *Industry Applications Conference, 2002. 37th IAS Annual Meeting. Conference Record of the*, 2002, pp. 775-781 vol.2.
- [98] N. Minh-Khai, J. Young-Gook, and L. Young-cheol, "Single-Phase AC-AC Converter Based on Quasi-Z-Source Topology," *Power Electronics, IEEE Transactions on*, vol. 25, pp. 2200-2210, 2010.
- [99] R. L. Steigerwald, "A comparison of half-bridge resonant converter topologies," *Power Electronics, IEEE Transactions on*, vol. 3, pp. 174-182, 1988.
- [100] M. K. Kazimierczuk, N. Thirunarayan, and S. Wang, "Analysis of series-parallel resonant converter," *Aerospace and Electronic Systems, IEEE Transactions on*, vol. 29, pp. 88-99, 1993.
- [101] M. Kazimierczuk, "Exact analysis of class E tuned power amplifier with only one inductor and one capacitor in load network," *Solid-State Circuits, IEEE Journal of*, vol. 18, pp. 214-221, 1983.
- [102] M. K. Kazimierczuk and K. Puczek, "Exact analysis of class E tuned power amplifier at any Q and switch duty cycle," *Circuits and Systems, IEEE Transactions on*, vol. 34, pp. 149-159, 1987.
- [103] T. Suetsugu and M. K. Kazimierczuk, "Analysis of sub-optimum operation of class E amplifier," in *Circuits and Systems, 2003 IEEE 46th Midwest Symposium on*, 2003, pp. 1071-1074 Vol. 3.